Resonant Oscillations Of Gases And Liquids In Three Dimensions

Daniel David Waterhouse
Jesus College
Oxford

Thesis submitted for the degree of Doctor of Philosophy

Trinity term 1995

Abstract

Although extensive work has been carried out on one-dimensional resonant oscillations of both liquids in a tank (where the free surface varies in only one spatial dimension) and gases in a resonator, little is known about two-dimensional solutions. This thesis aims to unite and extend the knowledge about one-dimensional solutions and also develop a theory for classifying two-dimensional motions and, as a consequence, understand the different types of responses that may be found in tanks and resonators of arbitrary geometry. To do this we focus on (i) the nonlinearity and (ii) the geometry (and, hence, the nature of the spectrum) and ignore dissipation to lowest order although it is, in general, important. However, we can easily include dissipative effects *a posteriori* and its initial absence makes it easier to analyse the new two-dimensional effects. For reasons which will become apparent, we will mainly consider cuboid-shaped geometries and perturb the sidewalls of such tanks and resonators, allowing for the gradual introduction of two-dimensional effects.

The thesis is split into two parts, underlying the differences between the problems that arise when the spectrum of the relevant linear problem is commensurate or non-commensurate. After a general introduction in Chapter 1 and a discussion of the model and governing equations in Chapter 2, the first part, comprising Chapter 3, looks at oscillations in deep water where the response typically consists of a finite number of modes. The second part is more extensive, looking at shallow water sloshing and the analogies of this problem with acoustic oscillations, both of which have a spectrum containing an infinite set of commensurate frequencies and the solution is much more intricate. We develop the problem and its one-dimensional solutions in Chapter 4 and then extend these ideas to two-dimensions in Chapter 5. With all this in mind we then make some general remarks about oscillations in tanks and resonators of arbitrary geometry in Chapter 6.

Acknowledgements

I would like to thank my supervisors Dr John Ockendon and Dr Hilary Ockendon for their guidance and encouragement over the last three years. I would also like to acknowledge Prof. Bill Chester for many informative discussions during the course of my research and Prof. Dima Vasiliev for his help on inverse problems. For financial support I am grateful to the EPSRC for an earmarked award. On a more personal note, I am indebted to both my fiancée, Debbie Lawrance, and my parents for their love and support over the years. Last, but not least, I extend my gratitude to my friends and colleagues who have made my time in Oxford a pleasure. In particular, Linda Cummings, Dale Heron, James Lawry and Giles Richardson have contributed toward a lively and stimulating working environment.

Contents

List of Figures

List of Tables

Chapter 1

Introduction

Who would have thought that liquid sloshing around in containers could be a problem? *New Scientist 20 June 1992*

The theory of oscillations within physical systems is a wide-ranging subject giving rise to extensive mathematical treatments. From simple classroom experiments concerning the motion of a pendulum to more complex systems, oscillatory behaviour exhibits observable phenomenon that are rich in mathematical structure. Little mathematical knowledge is needed to find, for instance, the frequency of the oscillations of a pendulum as long as one essential assumption is made. This is that the amplitude of the oscillation is *small*, as is the case in many physical problems. This key assumption allows a linearisation procedure that forms the first step in any mathematical treatment.

Linear theory, however, has its drawbacks. In particular, when the system, such as a pendulum, is forced near its natural frequency, undamped linear theory predicts an unbounded amplitude. This is the well known phenomenon of *resonance* and the key to understanding the size and form of oscillations near resonance may rely on the *nonlinear* terms which were neglected as a first approximation. Understanding how nonlinearity controls the resonant growth is a central issue of this thesis.

Perhaps the most famous example of this nonlinear behaviour can be seen in Duffing's equation[1] (named after Duffing for his work or circuit theory [24]) which can be written as

$$\ddot{x} + k\dot{x} + (1 + \lambda_0)x + x^3 = \varepsilon \cos t, \tag{1.1}$$

[1]This equation exhibits the same type of response as some of the problems discussed in this thesis.

where λ_0 and $k \geq 0$ measures how close the forcing frequency is to the natural frequency and damping respectively. Away from resonance, $\lambda_0 \sim O(1)$, and for $k = 0$, the nonlinear terms are negligible and $x \sim \varepsilon/\lambda_0 \cos t$. As we approach the resonant frequency, $\lambda_0 \ll 1$, the nonlinearity can then be shown to control the growth of the oscillation and results in an amplitude of $O(\varepsilon^{1/3})$ when $\lambda_0 = \lambda\varepsilon^{2/3}$ ($\lambda \sim O(1)$). Figure 1.1 shows the sort of response[2] that emerges, where $x \sim \varepsilon^{1/3} A \cos t$. Here the response is for a "soft spring" (decreasing amplitude with increasing frequency) as opposed to a "hard spring" (increasing amplitude with increasing frequency). When the damping k is $O(\varepsilon^{1/3})$, the peaks in this response diagram are rounded as illustrated by the dashed part of Figure 1.1. A fuller account of this equation may be found, for example, in Jordan & Smith [34] or Stoker [66].

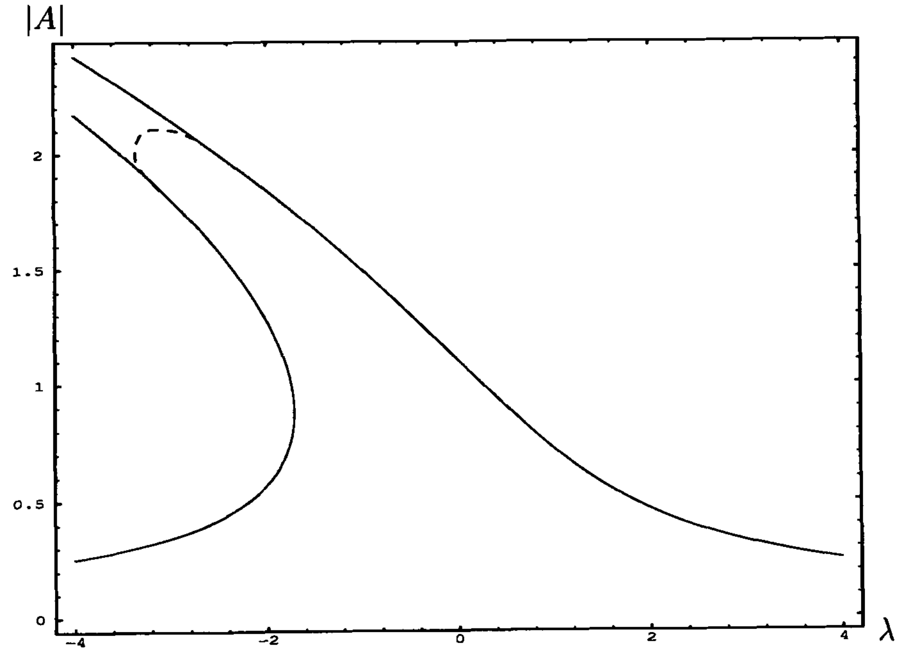

Figure 1.1: Duffing-type response showing amplitude against frequency. The dashed curve shows the effect of damping.

Throughout this thesis we are concerned with two infinite dimensional generalisations of this situation; small amplitude gravity waves in a tank and acoustic oscillations of gas in a resonator of finite dimensions. Forcing the tank or resonator (by rocking from side to side for the tank or placing an oscillatory piston at one

[2] The term "response" is always taken to mean the modulus of the amplitude.

end of the resonator) near one of the natural frequencies[3] causes the associated mode to be resonant. In the case of deep water[4] waves, this is generally the end of the story as the other natural frequencies are *non-commensurate* with the forcing frequency (i.e. the other natural frequencies are not integer multiples of the forcing frequency) and this criterion proves to be of great significance. In this case, third-order effects lead to a balance between the nonlinearity and the forcing in much the same way as for Duffing's equation. However, as the aspect ratio of the tank becomes small, shallow water theory applies and, for rectangular tanks, the natural frequencies become nearly commensurate with the forcing frequency. This is also the case for acoustic oscillations in a resonator with straight sidewalls and rectangular cross-section, and in both cases the type of response is much more complicated. The reason why the commensurability of the spectrum plays such a vital role can be seen from the following simple argument. Forcing either the tank or resonator near to its fundamental frequency causes the $\cos x \sin t$ mode to be excited. The quadratic nonlinearity "doubles" this to create a feedback term $\cos 2x \sin 2t$. Hence if twice the fundamental frequency is also a natural frequency then this mode is also excited. This process continues *ad infinitum* if the whole spectrum is commensurate.

Although we wish to classify the types of response found in tanks or resonators of arbitrary geometry, we will see that taking a tank of rectangular cross-section leads to the most interesting scenario and, in general, we consider this geometry. This is because, as noted above, in the shallow water limit the number of commensurate frequencies becomes infinite. Also, if the ratio of tank breadth to length is rational then there is an infinite set of degenerate eigenfrequencies, i.e. frequencies with more that one associated eigenfunction.

One of the key aims of this thesis is to understand how small variations in the geometry of the tank affect the response. We will see that, for the resonators we will be considering (and probably *only* for them), even weak variations have startling effects, leading to intricate couplings between commensurate modes. By classifying the response for the rectangular tank and then gradually increasing geometrical

[3]In general, we will be concerned with oscillations near the lowest, or fundamental, frequency.
[4]We use the phrase "deep water" to signify that the aspect ratio of the depth to length of the tank is $O(1)$ or greater.

variations (for instance, the curvature of the walls of the tank) we can make general remarks about oscillations in tanks of any shape. We focus on the geometry (determining the linearised eigenfrequencies or causing slight perturbations to these frequencies), nonlinearity and the detuning (the difference between the forcing frequency and the natural frequency) and pay less attention to the damping because its effects can be incorporated *a posteriori* whereas including damping from the start makes it difficult to appreciate the new two-dimensional effects that we are interested in.

Although much of this thesis is concerned with the sloshing problem, we neglect, in general, dispersive effects when considering shallow water oscillations. This dispersion-free model is, of course, applicable to acoustic oscillations. There are, however, a few interesting differences between the two problems.

We next give a review of the literature to see how the problem has evolved, and then present a section outlining the structure of the rest of this thesis.

1.1 Literature review

Mathematical discussions on the oscillations in a tank of fluid considered to be deep really began in earnest with Penny & Prices's [59] work (which developed ideas discussed as early as 1880 by Stokes [68]) on stationary gravity waves. They found expressions, to fifth order, for the possible natural frequencies for fluid of an infinite depth. This work inspired Taylor [71] to carry out experimental work that verified Penny & Price's results and which also considered the resonance problem. This showed, for the first time, the Duffing-like response of the motion (see Figure 1.1). Equivalent results for fluid of a finite depth were found by Tadjbakhsh & Keller [70] (analytically) and Fultz [29] (experimentally). Both works show a change from soft to hard spring behaviour near a critical depth. Further analytical results, determining the nonlinear corrections to the natural frequencies, were given by Concus [19] (for the problem incorporating surface tension) and Verma & Keller [75] (for three-dimensional solutions). The work of Concus was extended by Vanden-Broeck [74] for a special case where the surface tension and depth reach a critical balance. In this case, the motion comprises not one but two resonant modes because the first two natural frequencies are commensurate. Finally, Bridges [9], [10] and Dias &

Bridges [23] have considered more general results when the linear eigenfrequencies are degenerate.

The first analytical work on the resonance problem came from Moiseyev [48] in 1958. He suggested a way in which the nonlinearity contains the resonant growth and predicted the Duffing-type response observed by Taylor and Fultz. Moiseyev's general approach was specialised by Ockendon & Ockendon [54] for the case of a rectangular tank oscillated near its fundamental frequency, and they found the response changed form at a critical depth, in agreement with Tadjbakhsh & Keller. This depth corresponds to a breakdown in the solution procedure and requires terms of fifth order to be included in the analysis. Further results have extended these ideas; Tsai *et al* [73] found the resonant response when the forcing was near the n^{th} natural frequency and Miles [43] derived similar results using a Lagrangian formulation.

There is a large body of literature concerned with the more intricate problems of shallow water sloshing and acoustic oscillations. It is well-known that the shallow water equations can be related to the acoustic equations and, to leading order, both problems satisfy the one-dimensional wave equation. We will see how this analogy applies to the resonance problems considered.

All previous work has been concerned with one-dimensional or quasi-one-dimensional oscillations. The progress of this problem is best given by first considering the development of the acoustic problem.

- In 1964, Chester [14] published his classic paper on one-dimensional (see Figure 1.2(a)) oscillations that provides the starting block for most discussions on resonant acoustic oscillations. By developing a second-order theory, Chester showed that the leading-order velocity was given by $u = g'(t+x) - g'(t-x)$ and that g satisfied

$$\lambda g''(t) + (\gamma + 1)g'(t)g''(t) = -\frac{1}{\pi}\sin t, \tag{1.2}$$

  where $g(t)$ is 2π-periodic and has zero mean over one period, and γ is the ratio of specific heats. The essential ingredient of this equation is the nonlinearity and, for λ close to zero, this equation confirms the shock solutions observed experimentally by Sturtevant [69].

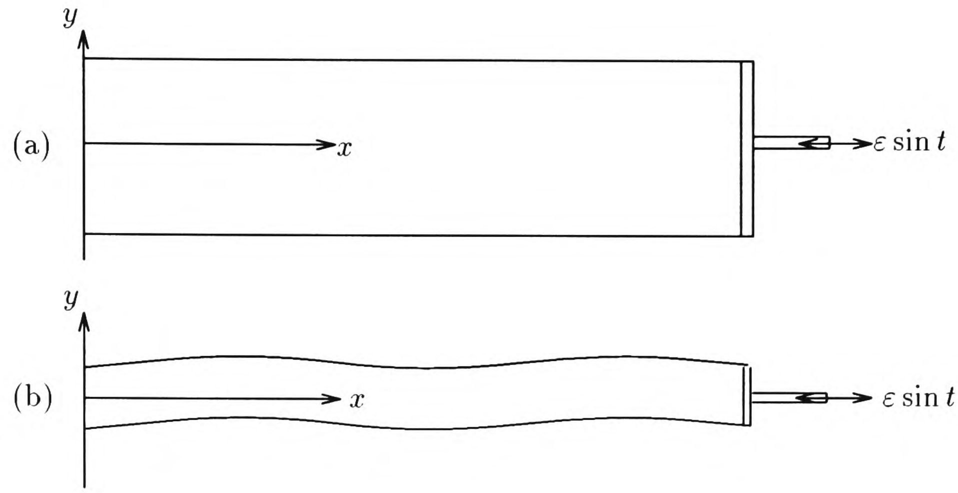

Figure 1.2: Sketches of two types of acoustic resonator with an oscillating piston at one end whose non-dimensional amplitude, ε, is the ratio of the dimensional amplitude to the length of the resonator: (a) resonator with straight sides, (b) thin resonator with slowly varying sides.

- Chester also considered the effect of damping (in the form of a viscous boundary layer) on the shock wave response, showing that its effect is to round off the shock profile. Further work on this aspect has been done by Keller [35].

- In 1977 Keller [36] considered a thin resonator with slowly varying sidewalls (see Figure 1.2(b)) and showed that (1.2) is changed by the introduction in its right-hand side of a convolution term between g and the function determining the geometry of the sidewall. For a very simple form of this geometry, Keller showed how the occurrence of shocks is changed as the amplitude of this geometry is increased.

- Cox & Mortell [21] showed how the periodic solutions considered by Chester evolve from an initial state of rest.

- For acoustic oscillations in a sphere, Chester [17] has shown that a single-mode response arises whose amplitude satisfies a cubic equation, once again similar to the Duffing-type response. The analogue of this problem for oscillations in a cylindrical wedge has been given by Ellermeier [26].

- To bridge the gap between the Duffing-type response and the shock solutions, Peake [58] considered the problem of acoustic oscillations in the annulus between two spheres. By letting the radius of the inner sphere tend to either zero or the radius of the outer sphere he has shown the transition between the two cases. He also considered further the problem of a thin resonator with slowly varying sides as in Keller [36] and his work is summarised in Ockendon *et al* [57]. Taking the area variation across the resonator as $1 + \sigma b(x)$, where σ is small, they show, for the case $b'(x) = 2x$, how the likelihood of the emergence of shocks decreases as σ increases and eventually vanishes for σ large. Their work shows how the commensurability of the spectrum is inextricably linked to the type of response.

For the shallow water problem we must look further back to find the correct parameter regimes before we can begin to solve the problem. The work of Korteweg & de Vries [37] first suggested the scalings leading to a balance between dispersion and nonlinearity, although we must not forget that the work was inspired by Boussinesq [7], as pointed out in Miles' essay on the Korteweg-de Vries equation [44]. These scalings were exploited by Ockendon & Ockendon [54] in deriving an ordinary differential equation similar to (1.2) for the function f (where the velocity potential is given by $\phi \sim f(t + x) + f(t - x)$) but with the inclusion of a higher fourth-order term representing dispersion. This term is slightly different to that suggested by Chester [15] for the same problem but has a similar effect. Miles [46] has also considered a similar problem using a Lagrangian formulation (although this necessitates truncating the Fourier series for the solution).

The introduction of dispersion has several consequences. Ockendon *et al* [56] showed that for small values of dispersion the shock solutions of (1.2) no longer arise and in fact the solution becomes multi-valued with the response diagram having many of the Duffing-like peaks of Figure 1.1 close to the fundamental frequency. Byatt-Smith [11] and Reynolds & Cox [61] have given further analyses of this problem. This non-uniqueness explains why Cox & Mortell [22] predicted that a periodic response does not arise form a state of rest unless damping is included. The inclusion of surface tension does, however, present a way of removing dispersive effects. Johnson [33] showed that when there is a critical balance between surface tension and depth (the "ripple depth") dispersion is negligible and the problems of shallow water theory and acoustic oscillations are comparable.

Both the dispersive and dispersion-free solutions have been demonstrated experimentally by Chester & Bones [16] with good agreement between experiment and theory.

There are two other areas of interest which have been covered in the literature, relevant to both the acoustic and sloshing problems. Firstly there is the problem of high-frequency oscillations. Although we are primarily concerned with the most practically important case of resonance near the fundamental frequency, the problem is more complex for high-frequency oscillations. Seymour & Mortell [63] have presented a theory for this case and a review of this is given in Appendix C.1.1.

Finally, an interesting class of problems arises by considering the following. One of the features of the straight-sided resonator or tank, both of rectangular cross-section, is that the spectrum is commensurate. Now, for an acoustic resonator of varying cross-section (where the sidewalls vary), Keller [36] showed that a special geometry exists where the spectrum is also commensurate. When the geometrical variations in the walls of the tank are large enough, the leading-order problem satisfies a non-constant coefficient wave equation. It is an interesting question to ask for which variations is the spectrum commensurate? This sort of inverse problem has been considered by, for example, Barcilon [2].

1.2 Thesis structure

To study oscillations in tanks or resonators and extend and add to the work discussed above, we first present a framework for such oscillations and the relevant equations governing the motion. This is done in Chapter 2, where we also demonstrate how linear theory predicts the resonant growth when the tank is forced near its lowest (fundamental) frequency and where a non-degenerate eigenmode is excited. This chapter also introduces most of the physical parameters, the most important being the amplitude of the forcing, ε, the detuning, λ_0, and the amplitude of the geometric variations, ν_0. The final important parameter is the shallow water depth κ, introduced in Chapter 4. Because there are so many variables and parameters we have included a table of notation at the end of the thesis.

With these foundations in place, the rest of this thesis is split into two parts; the first part concentrates on oscillations in a nearly rectangular tank whose aspect ratio of depth to length is $O(1)$ or greater. The entirety of work done in this case is given in Chapter 3 and is concerned with the effects of four parameters, namely the depth, the breadth, the strength of the geometric imperfection and, to a limited extent, the surface tension. When the breadth is an integral multiple of the length, geometric variations in one wall of the tank lead to the excitation of a transverse mode (one that is perpendicular to the primary longitudinal motion) whose amplitude is coupled to that of the longitudinal mode. This interesting feature is due to the degeneracy of the spectrum, in which there is more than one mode associated with the fundamental frequency. This degeneracy and the resulting two-dimensional responses have received little attention in the literature and the classification of these responses provides one of the main challenges of this thesis.

After the comparatively straightforward analysis of deep water sloshing, the second part of this thesis is concerned with shallow water sloshing and acoustic oscillations. We split this part into three chapters. In Chapter 4 the shallow water scalings are given and the underlying models are derived. The rest of the chapter is concerned with one-dimensional solutions of both the sloshing and acoustic problems when no transverse motions are generated and the resonator is "thin". An integro-differential equation is derived and we give a review of the effects of different physical parameters on the response. In particular, we extend previous work on the effect of base variations by considering more general forms of the geometry of this variation than those previously considered. Finally, when this variation has an amplitude of the same size as the depth of the fluid, the leading-order solution is shown to satisfy a non-constant coefficient wave equation and solutions of this equation are considered.

In Chapter 5 we tackle the more difficult problem of two-dimensional shallow water sloshing and acoustic oscillations. Concentrating on the case when the breadth and length of a rectangular tank or resonator are equal but one wall is non-planar, we discuss the size and coupling of the doubly-infinite set of modes that are now excited. This leads to a theory which suggests that the motion is well described in terms of sets of longitudinal modes and transverse modes alone and we derive the response for a special form of the geometrical variation in this instance. This chapter also includes two other ways of generating two-dimensional motions; firstly by oscillating the tank at an angle to its sides and secondly by forcing the tank near a different natural frequency.

The second part of this thesis is completed in Chapter 6 where we make some general remarks about oscillations in tanks and resonators of arbitrary shape. We also consider a specially configured acoustic problem where there is an infinite set of commensurate modes but just a finite set of degenerate modes.

Finally, in Chapter 7, we present some conclusions.

1.3 Statement of originality

All the work in Chapter 3 is original. Chapter 4 contains some review material but the derivation of the shallow water model and resulting differential equation in Sections 4.1.2 and 4.3.2 as well as the analysis in Sections 4.4.2, 4.4.3 and 4.5.2 are all original. Finally, all of Chapters 5 and 6 are original work.

Chapter 2

Basic equations

2.1 Fluid sloshing in a tank

The motion considered is that of irrotational, inviscid, constant density fluid in a container with a free surface that has negligible surface tension (although we will discuss the effects of non-zero surface tension in later chapters). We denote the fluids velocity, density and pressure by $\boldsymbol{u}$, ρ and p respectively and take axes such that Z is vertically upwards and X and Y are horizontal so that the free surface is at $Z = \xi$.

The equations of motion for such a flow are just Euler's equations (see, for example, Acheson [1] or Stoker [67])

$$\begin{aligned} \boldsymbol{\nabla}.\boldsymbol{u} &= 0, & (2.1) \\ \frac{\partial \boldsymbol{u}}{\partial \tau} + (\boldsymbol{u}.\boldsymbol{\nabla})\boldsymbol{u} &= -\frac{\nabla p}{\rho} - g\boldsymbol{k}, & (2.2) \end{aligned}$$

where g is gravity, which are the conservation of mass and momentum respectively. As the fluid is irrotational, that is $\boldsymbol{\nabla}_\wedge \boldsymbol{u} = \boldsymbol{0}$, we can find a potential Φ such that $\boldsymbol{u} = \boldsymbol{\nabla}\Phi$ and, from (2.1), we have that

$$\nabla^2 \Phi = 0, \tag{2.3}$$

and (2.2) leads to Bernoulli's equation

$$\frac{\partial \Phi}{\partial \tau} + \frac{1}{2}(\boldsymbol{\nabla}\Phi)^2 + gZ + \frac{p}{\rho} = 0. \tag{2.4}$$

2.1.1 Free surface conditions

At the free surface there will be two conditions. Firstly there is the *dynamic* condition which is just a balance between the pressure in the fluid interface and the ambient pressure above the fluid which we will take to be zero. Hence $p = 0$ on the free surface and (2.4) gives

$$g\xi + \Phi_\tau + \frac{1}{2}(\nabla\Phi)^2 = 0 \quad \text{on} \quad Z = \xi. \tag{2.5}$$

We also have a *kinematic* condition at the free surface which states that particles in the free surface remain there (which is equivalent to the statement that the velocity component of the fluid normal to the free surface is the same as the normal velocity of the surface). If we write

$$F = Z - \xi(X, Y, \tau),$$

so that the free surface is at $F = 0$, then this kinematic condition just says that the convective derivative of F is zero at the free surface, i.e.

$$\frac{\partial F}{\partial \tau} + (\boldsymbol{u}.\nabla)F = 0 \quad \text{on} \quad F = 0,$$

and this can be written in terms of the velocity potential as

$$\Phi_Z = \xi_\tau + \Phi_X\xi_X + \Phi_Y\xi_Y \quad \text{on} \quad Z = \xi. \tag{2.6}$$

2.1.2 Geometry of tank and boundary conditions

We will be concerned with fluid contained in an almost rectangular container. It will be seen that a small change in the geometry can dramatically change the solution in certain cases so the geometry chosen is that shown in Figure 2.1. The depth of the fluid in the tank is taken to be hL, the breadth $b\pi L$ and the length πL. The sidewalls are flat except the back wall which is given by $Y = b\pi L[1 + \nu_{w0}a_w(X/L)]$ and the base which is given by $Z = -hL[1 + \nu_{b0}a_b(X/L)]$, where $\nu_{w0}, \nu_{b0} \ll 1$ and $a_w(X/L), a_b(X/L)$ have $O(1)$ amplitude. Throughout this thesis the parameter ν_0 characterises the amplitude of geometric variations and the function $a(x)$ the shape of the variation. We use the added suffix w to mean the wall variation and b to mean the base variation. For a tank at rest the boundary conditions on the walls

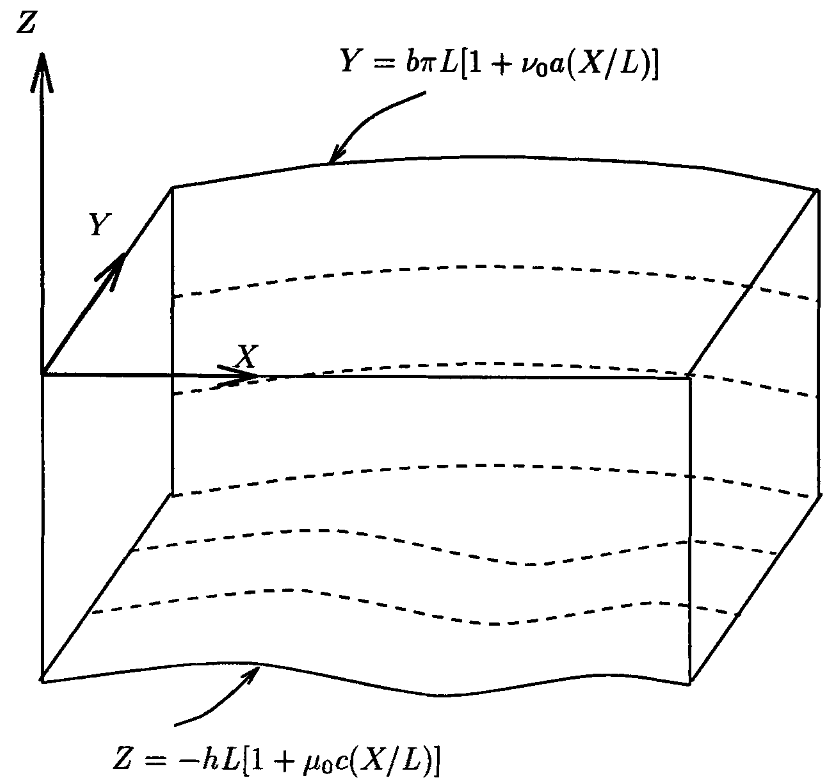

Figure 2.1: The geometry of the tank.

are just that there must be no velocity normal to each wall, i.e. $\boldsymbol{u}.\boldsymbol{n} = 0$ on the fixed walls. In terms of the velocity potential this leads to

$$\Phi_X = 0 \quad \text{on} \quad X = 0, \pi L, \tag{2.7}$$

$$\Phi_Z = -\nu_{b0} h \Phi_X a_b' \left(\frac{X}{L}\right) \quad \text{on} \quad Z = -hL\left[1 + \nu_{b0} a_b \left(\frac{X}{L}\right)\right], \tag{2.8}$$

$$\Phi_Y = 0 \quad \text{on} \quad Y = 0, \tag{2.9}$$

$$\Phi_Y = \nu_{w0} b\pi \Phi_X a_w' \left(\frac{X}{L}\right) \quad \text{on} \quad Y = b\pi L\left[1 + \nu_{w0} a_w \left(\frac{X}{L}\right)\right]. \tag{2.10}$$

2.1.3 Natural frequencies and the effect of forcing

To find the natural frequencies of the tank we consider the linearised form of (2.3), (2.5), (2.6) and (2.7)–(2.10) and neglect the small geometric variations. That is we solve

$$\nabla^2\Phi = 0 \quad , \quad \Phi_X = 0 \quad \text{on} \quad X = 0, \pi L,$$
$$\Phi_Y = 0 \quad \text{on} \quad Y = 0, b\pi L \quad , \quad \Phi_Z = 0 \quad \text{on} \quad Z = -hL,$$
$$\Phi_Z - \xi_\tau = 0 = g\xi + \Phi_\tau \quad \text{on} \quad Z = 0,$$

which leads to

$$\Phi_{n,m} = A_{n,m} \cos \frac{nX}{L} \cos \frac{mY}{bL} \cosh \frac{\lambda_{n,m}}{L}(Z + hL) \sin(\omega_{n,m}\tau + \alpha_{n,m}), \qquad (2.11)$$

where $A_{n,m}$ and $\alpha_{n,m}$ are arbitrary constants and the frequencies $\omega_{n,m}$ are given by

$$\omega_{n,m}^2 = \frac{g}{L}\lambda_{n,m} \tanh(\lambda_{n,m}h) \qquad (2.12)$$

where

$$\lambda_{n,m}^2 = n^2 + \frac{m^2}{b^2}.$$

We will be primarily concerned with the response of the tank near the fundamental frequency $\omega_{1,0}$, so we first consider oscillating the tank in the X-direction, with an amplitude a, so that the walls $X = 0, \pi L$ are displaced to $-a\cos\Omega\tau$ and $\pi L - a\cos\Omega\tau$. We begin by solving the linearised form of (2.3), (2.5), (2.6) and (2.8)–(2.10) with the boundary conditions

$$\Phi_X = a\Omega \sin\Omega\tau \quad \text{on} \quad X = -a\cos\Omega\tau, \pi L - a\cos\Omega\tau, \qquad (2.13)$$

assuming that $a/L = \varepsilon \ll 1$. The solution to this problem is

$$\begin{aligned}\Phi \quad \sim \quad & a\sin\Omega\tau \left(\Omega X + \sum_{n=0}^{\infty} A_{2n+1} \cos\left(\frac{2n+1}{L}\right) X \cosh\left(\frac{2n+1}{L}\right)(Z + hL)\right) \\ & + \sum_{n,m} \Phi_{n,m}, \end{aligned} \qquad (2.14)$$

to leading order, where

$$A_i = \frac{4L\Omega^3}{\pi i^2 \cosh(ih)[\Omega^2 - (gi/L)\tanh(ih)]},$$

so that the solution grows large when

$$\Omega^2 = \omega_{2n+1,0}^2 \quad n = 0, 1, \ldots. \qquad (2.15)$$

As mentioned previously, we will be mainly concerned with the oscillations near the fundamental frequency and so we write

$$\Omega^2 = \omega_{1,0}^2(1 + \lambda_0) = \frac{g}{L}(1 + \lambda_0)\tanh h \qquad (2.16)$$

where λ_0 ($\varepsilon \ll \lambda_0 \ll 1$) is the detuning, and hence $\Omega^2 - \omega_{1,0}^2 \sim O(\lambda_0)$ and $\Phi \sim O(\varepsilon/\lambda_0)$. To see how the nonlinear terms can grow to stop this infinite growth at resonance we now non-dimensionalise the equations.

2.1.4 Non-dimensional equations

Typical length and time-scales for the problem are L and $1/\Omega$ respectively so we write

$$\boldsymbol{X} = L\boldsymbol{x} \quad , \quad a = L\varepsilon \quad , \quad \tau = \frac{t}{\Omega},$$
$$\Phi = \Omega L^2\phi \quad , \quad \xi = L\eta.$$

Equations (2.3), (2.5), (2.6), (2.8)–(2.10) and (2.13) are now

$$\begin{aligned}
\nabla^2\phi &= 0, && (2.17)\\
\phi_x &= \varepsilon\sin t \quad \text{on} \quad x = -\varepsilon\cos t, \pi - \varepsilon\cos t, && (2.18)\\
\phi_z &= -\nu_{b0}h\phi_x a_b'(x) \quad \text{on} \quad z = -h[1 + \nu_{b0}a_b(x)], && (2.19)\\
\phi_y &= 0 \quad \text{on} \quad y = 0, && (2.20)\\
\phi_y &= \nu_{w0}b\pi\phi_x a_w'(x) \quad \text{on} \quad y = b\pi\left[1 + \nu_{w0}a_w(x)\right], && (2.21)
\end{aligned}$$

and, on $z = \eta$,

$$\begin{aligned}
\phi_z &= \eta_t + (\phi_x\eta_x + \phi_y\eta_y), && (2.22)\\
\eta &+ (1+\lambda_0)\tanh h\left[\phi_t + \frac{1}{2}\left({\phi_x}^2 + {\phi_y}^2 + {\phi_z}^2\right)\right] = 0. && (2.23)
\end{aligned}$$

In the undisturbed state, the free surface is at $z = 0$ and so, by conservation of mass, (2.17) and (2.22), η has zero mean, i.e.

$$\int_0^{b\pi}\int_0^{\pi} \eta \mathrm{d}x\mathrm{d}y = 0. \qquad (2.24)$$

Finally, we seek solutions that have the same period as the forcing because any damping will automatically act least on this lowest frequency mode whereas modes with a higher frequency will be rapidly damped down. Hence we require

$$\boldsymbol{\nabla}\phi(\boldsymbol{x}, t) = \boldsymbol{\nabla}\phi(\boldsymbol{x}, t + 2\pi), \qquad (2.25)$$

and this can be integrated to give

$$\phi(\boldsymbol{x}, t) = \phi(\boldsymbol{x}, t + 2\pi) + \phi_p(t). \qquad (2.26)$$

Notice that $\boldsymbol{\nabla}\phi$ is taken to be periodic and not ϕ, as taking ϕ to be periodic contradicts with the statement that η has zero mean. This can be seen by integrating (2.23) over x and y, using (2.24) and noting that, in general, the term $|\boldsymbol{\nabla}\phi|^2$

does not integrate to zero, whereas the ϕ_t term only gives a non-zero term when $\phi_p(t) \neq 0$.

The equations (2.17)–(2.25) provide the basic model for resonant sloshing. However, we can make rescalings of these equations depending on the depth. We see from (2.14) that the linearised form of these equations gives

$$\phi \sim \frac{\varepsilon}{\lambda_0} A \cos x \cosh(z+h) \sin t, \tag{2.27}$$

for $\lambda_0 \gg \varepsilon$. It is clear, however, that as $\lambda_0 \to 0$ the linearisation breaks down. The controlling mechanism is the nonlinear terms that were initially neglected. To understand how these terms grow to balance with the leading-order term we consider (2.23) which shows that the nonlinear terms feedback a term

$$\frac{\varepsilon^2}{\lambda_0^2} A^2 \cos 2x \cosh 2(z+h) \sin 2t \tag{2.28}$$

in to the solution. It is at this stage that we see the distinction between deep and shallow water problems. As already remarked, the eigenvalues are nearly commensurate when $h \ll 1$ and (2.28) forces the second mode to be resonated and hence (2.27) is modified to comprise the sum of the first two modes. This process continues (as discussed in the introduction) so that all the modes are resonated and the nonlinear terms of $O(\varepsilon^2/\lambda_0^2)$ then balance with the detuning term in (2.23) of $O(\lambda_0 \phi) = O(\varepsilon)$ when $\lambda_0 \sim O(\varepsilon^{1/2})$ with ϕ growing to $O(\varepsilon^{1/2})$. We will return to this parameter regime in the next section as well as in the shallow water work of Section 4.1.

However, for deep water ($h \geq O(1)$), the second mode is not resonant and (2.28) will not balance with the detuning term. Hence, we look to third-order nonlinear effects when (2.27) interacts with (2.28) to give a $(\varepsilon^3/\lambda_0^3)A^3 \cos x \cosh(z+h) \sin t$ term. This balances with the detuning term when $\lambda_0 \sim O(\varepsilon^{2/3})$ and ϕ and η grow to $O(\varepsilon^{1/3})$. Thus, for deep water, we rescale by

$$\phi = \varepsilon^{1/3} \phi_d \quad , \quad \eta = \varepsilon^{1/3} \eta_d \quad , \quad \lambda_0 = \varepsilon^{2/3} \lambda_d, \tag{2.29}$$

where $\lambda_d \sim O(1)$ and the suffix d is always used to denote deep water. These are the scalings originally suggested by Moiseyev [48]. Waterhouse [76] demonstrated that, for deep water, variations in the base of the tank provide no interesting features so, in the deep water model, we take $\nu_{b0} = 0$ and choose ν_{w0} so the wall variations have an effect that balances with the detuning, i.e.

$$\nu_{w0} = \varepsilon^{2/3}\nu_{wd} \quad , \quad \nu_{wd} \sim O(1). \tag{2.30}$$

Hence, substituting these scalings into (2.17)–(2.25), we now have our deep water model,

$$\begin{aligned}
\nabla^2\phi_d &= 0, && (2.31)\\
(\phi_d)_x &= \varepsilon^{2/3}\sin t \quad \text{on} \quad x = -\varepsilon\cos t, \pi - \varepsilon\cos t, && (2.32)\\
(\phi_d)_z &= 0 \quad \text{on} \quad z = -h, && (2.33)\\
(\phi_d)_y &= 0 \quad \text{on} \quad y = 0, && (2.34)\\
(\phi_d)_y &= \nu_{wd}\varepsilon^{2/3} b\pi(\phi_d)_x a_w'(x) \quad \text{on} \quad y = b\pi\left[1+\nu_{wd}\varepsilon^{2/3}a_w(x)\right], && (2.35)\\
\int_0^{b\pi}\int_0^{\pi}\eta_d \mathrm{d}x\mathrm{d}y &= 0, && (2.36)\\
\nabla\phi_d(\boldsymbol{x},t) &= \nabla\phi_d(\boldsymbol{x},t+2\pi), && (2.37)
\end{aligned}$$

and, on $z = \varepsilon^{1/3}\eta_d$,

$$\begin{aligned}
(\phi_d)_z &= (\eta_d)_t + \varepsilon^{1/3}\left[(\phi_d)_x(\eta_d)_x + (\phi_d)_y(\eta_d)_y\right], && (2.38)\\
\eta_d &+ (1+\varepsilon^{2/3}\lambda_d)\tanh h\left[(\phi_d)_t + \frac{1}{2}\varepsilon^{1/3}\left((\phi_d)_x^2 + (\phi_d)_y^2 + (\phi_d)_z^2\right)\right] = 0. && (2.39)
\end{aligned}$$

2.2 Acoustic resonators

The motion of gas in a nearly rectangular resonator that has a piston oscillating at one end has much in common with the shallow water limit of the equations just derived, as discussed in the introduction. For this reason we will recount the equations governing acoustic oscillations so that we can compare the solution of this problem with that of the fluid problem. We will use a similar configuration to Ockendon *et al* [57] to describe the motion of the gas in a resonator such as that illustrated in Figure 2.2. In this configuration the sidewalls are given by $Z = 0$ and $Z = h_0[1 + \nu_{b0}a_b(X/L)]$, the front by $Y = 0$ and the back wall[1] by $Y = \pi L[1 + \nu_{w0}a_w(x/L)]$, using the same notation for the geometrical imperfections as in the last section.

[1] The reason for varying the geometry in both the back wall and top will become clear in Chapter 6, and for one-dimensional considerations (see Chapter 4) we just set ν_{w0}=0.

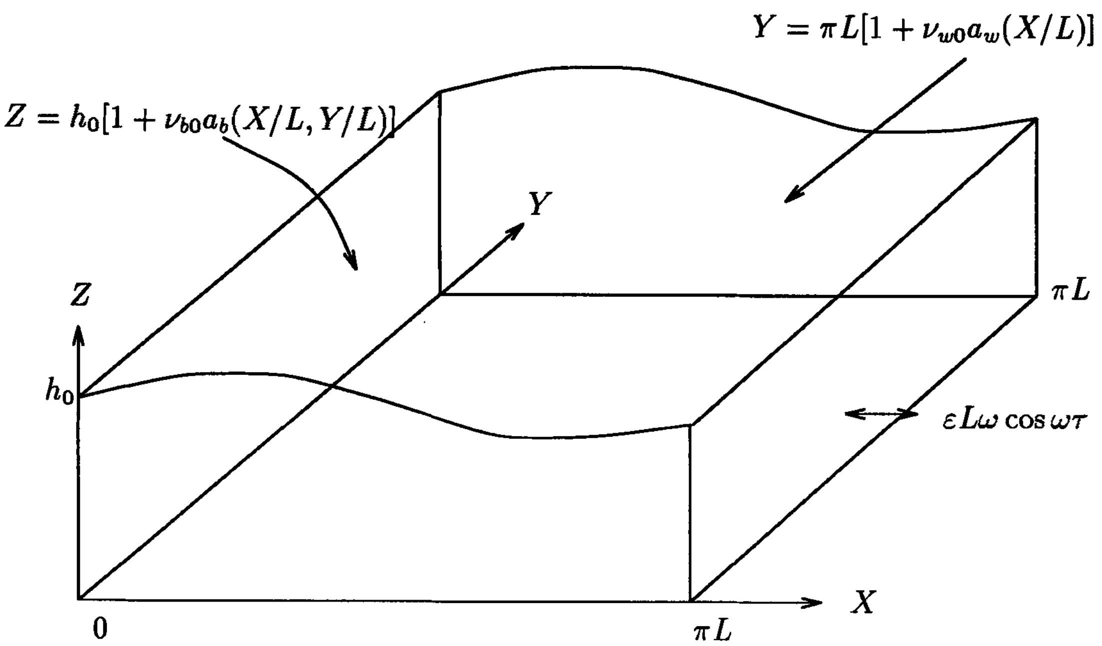

Figure 2.2: Oscillations of a piston at one end of an acoustic resonator.

The gas is taken to be compressible and we assume it is inviscid. Also, if we assume that the gas is initially irrotational and homentropic then, in the subsequent motion, the flow remains homentropic in the absence of shocks. In the problems considered in this thesis all shocks that occur are weak and result in third-order changes in the entropy (see Appendix A.1.1) which are negligible within the general framework considered here. Hence the flow always remains homentropic and then, using Kelvin's circulation theorem, we have that the flow remains irrotational. The governing equations are then given by the conservation of mass, momentum and energy,

$$\rho_\tau + \boldsymbol{\nabla}.(\rho \boldsymbol{u}) = 0, \tag{2.40}$$

$$\rho(\boldsymbol{u}_\tau + (\boldsymbol{u}.\boldsymbol{\nabla}\boldsymbol{u})) + \boldsymbol{\nabla} p = \boldsymbol{0}, \tag{2.41}$$

$$\frac{p}{p_0} = \left(\frac{\rho}{\rho_0}\right)^\gamma, \tag{2.42}$$

where $\rho, \boldsymbol{u}, p$ and γ denote the gases density, velocity, pressure and ratio of specific heats respectively and p_0 and ρ_0 are the values of pressure and density in the undisturbed gas. If we introduce the velocity potential defined by $\boldsymbol{u} = \boldsymbol{\nabla}\Phi$ then p and ρ can be eliminated to give (see, for instance, Ockendon & Tayler [55])

$$[a^2-(\Phi_X)^2]\Phi_{XX}+[a^2-(\Phi_Y)^2]\Phi_{YY}+[a^2-(\Phi_Z)^2]\Phi_{ZZ}-2\Phi_X\Phi_Y\Phi_{XY}$$
$$-2\Phi_X\Phi_Z\Phi_{XZ}-2\Phi_Y\Phi_Z\Phi_{YZ}=\frac{\partial}{\partial\tau}(\Phi_\tau+|\nabla\Phi|^2), \quad (2.43)$$

where

$$a^2=\{a_0^2-(\gamma-1)(\Phi_\tau+\tfrac{1}{2}|\nabla\Phi|^2)\}, \quad (2.44)$$

and $a_0^2=\gamma p_0/\rho_0$. The boundary conditions for the resonator illustrated in Figure 2.2 are then

$$\Phi_X = 0 \quad \text{on} \quad X=0, \quad (2.45)$$
$$\Phi_X = \varepsilon L\omega\sin\omega\tau \quad \text{on} \quad X=\pi L-\varepsilon L\cos\omega\tau, \quad (2.46)$$
$$\Phi_Y = 0 \quad \text{on} \quad Y=0, \quad (2.47)$$
$$\Phi_Y = \nu_{w0}\pi\Phi_X a_w'\left(\frac{X}{L}\right) \quad \text{on} \quad Y=\pi L\left[1+\nu_{w0}a_w\left(\frac{X}{L}\right)\right], \quad (2.48)$$
$$\Phi_Z = 0 \quad \text{on} \quad Z=0, \quad (2.49)$$
$$\Phi_Z = h_0\nu_{b0}\left[(a_b)_X\Phi_X\left(\frac{X}{L},\frac{Y}{L}\right)+(a_b)_Y\Phi_Y\left(\frac{X}{L},\frac{Y}{L}\right)\right]$$
$$\text{on} \quad Z=h_0\left[1+\nu_{b0}a_b\left(\frac{X}{L},\frac{Y}{L}\right)\right]. \quad (2.50)$$

The natural frequencies found by linearising (2.43)–(2.50) are

$$\omega_{n,m,k}^2=\frac{a_0^2}{L^2}\left(n^2+m^2+\frac{k^2L^2}{h_0^2}\right), \quad (2.51)$$

so there is an infinite set of frequencies commensurate with the fundamental $\omega_{1,0,0}$.

The arguments at the end of the last section reveal that second-order nonlinear effects will contain the resonant growth associated with forcing the resonator close to its fundamental frequency. Hence, when we take ω to be within $O(\varepsilon^{1/2})$ of the fundamental by writing

$$\omega^2=\frac{a_0^2}{L^2}(1+\varepsilon^{1/2}\lambda), \quad (2.52)$$

where $\lambda\sim O(1)$, we find $\Phi\sim O(\varepsilon^{1/2})$ and hence we nondimensionalise with

$$\Phi=\varepsilon^{1/2}L^2\omega\bar{\varphi} \quad , \quad \omega\tau=t \quad , \quad X=Lx \quad , \quad Y=Ly \quad , \quad Z=h_0z. \quad (2.53)$$

Equations (2.43)–(2.50) are now

$$\frac{L^2}{h_0^2}\bar{\varphi}_{zz}+\bar{\varphi}_{xx}+\bar{\varphi}_{yy}-\bar{\varphi}_{tt}=\varepsilon^{1/2}(\lambda\bar{\varphi}_{tt}+2\bar{\varphi}_x\bar{\varphi}_{xt}+2\bar{\varphi}_y\bar{\varphi}_{yt}$$
$$+\frac{2L^2}{h_0^2}\bar{\varphi}_z\bar{\varphi}_{zt}+(\gamma-1)\bar{\varphi}_t(\bar{\varphi}_{xx}\bar{\varphi}_{yy}+\frac{L^2}{h_0^2}\bar{\varphi}_{zz}))+O(\varepsilon), \quad (2.54)$$

and

$$\bar{\varphi}_x = 0 \quad \text{on} \quad x = 0 \quad , \quad \bar{\varphi}_x = \varepsilon^{1/2} \sin t \quad \text{on} \quad x = \pi + O(\varepsilon),$$
$$\bar{\varphi}_y = 0 \quad \text{on} \quad y = 0 \quad , \quad \bar{\varphi}_z = 0 \quad \text{on} \quad z = 0, \tag{2.55}$$
$$\bar{\varphi}_y = \nu_{w0}\pi\bar{\varphi}_x a_w'(x) \quad \text{on} \quad y = \pi[1 + \nu_{w0}a_w(x)],$$
$$\bar{\varphi}_z = \nu_{b0}\frac{h_0^2}{L^2}((a_b)_x\bar{\varphi}_x + (a_b)_y\bar{\varphi}_y) \quad \text{on} \quad z = 1 + \nu_{b0}a_b(x,y).$$

Following Ockendon *et al* [57], we note that the boundary condition on the top, $z = 1 + \nu_{b0}a_b(x,y)$, implies that $\bar{\varphi}_z \sim O(\nu_{b0}h_0^2\varphi/L^2)$, so we write

$$\bar{\varphi} = \varphi(x,y,t) + \nu_{b0}\frac{h_0^2}{L^2}\hat{\varphi}(x,y,z,t),$$

where we take

$$\int_0^{1+\nu_{b0}a_b(x,y)} \hat{\varphi}\mathrm{d}z = 0$$

without loss of generality (by absorbing the integral of $\hat{\varphi}$ over z into φ). Then, under the assumption that $\nu_{b0}h_0^2/L^2 \ll \varepsilon^{1/2}$ (so the resonator is "thin"), equations (2.54)–(2.55) can be integrated from $z = 0$ to $z = 1 + \nu_{b0}a_b(x,y)$ to give, correct to $O(\varepsilon^{1/2})$, our fundamental nondimensional wave equation

$$[A_b(x,y)\varphi_x]_x + [A_b(x,y)\varphi_y]_y - A_b(x,y)\varphi_{tt} = \varepsilon^{1/2}[A_b(x,y)\{\lambda\varphi_{tt} + 2\varphi_x\varphi_{xt}$$
$$+2\varphi_y\varphi_{yt}\} + (\gamma-1)\varphi_t\{[A_b(x,y)\varphi_x]_x + [A_b(x,y)\varphi_y]_y\}], \tag{2.56}$$

together with

$$\varphi_x = 0 \quad \text{on} \quad x = 0, \tag{2.57}$$
$$\varphi_x = \varepsilon^{1/2}\sin t \quad \text{on} \quad x = \pi, \tag{2.58}$$
$$\varphi_y = 0 \quad \text{on} \quad y = 0, \tag{2.59}$$
$$\varphi_y = \nu_{w0}\pi\varphi_x a_w'(x) \quad \text{on} \quad y = \pi[1 + \nu_{w0}a_w(x)], \tag{2.60}$$

where

$$A_b(x,y) = 1 + \nu_{b0}a_b(x,y).$$

Again, we look for solutions that are synchronous with the forcing so that

$$\nabla\varphi(x,y,t) = \nabla\varphi(x,y,t+2\pi). \tag{2.61}$$

Equations (2.56)–(2.61) describe the basic model for non-dispersive resonance that we will study in Part II.

Part I

Resonant Oscillations In Deep Water

Chapter 3

Deep water sloshing, $h \geq O(1)$

The theory of water waves in a rectangular tank where the ratio of the depth to the length is of $O(1)$ or greater has been widely studied. Many authors have been interested in the lowest frequency of a standing wave in such a tank and the effects of nonlinearity, depth and surface tension on the frequency predicted by linear theory. A discussion on the development of this problem was given in the introduction. In particular, we refer to the work by Penny & Price [59] and Tadjbakhsh & Keller [70] who calculated the possible frequencies for fluid of infinite and finite depths respectively. All the theoretical results were concerned with the lowest eigenfrequency.

We consider the problem of oscillating such a tank, as outlined in the last chapter, and in such a way that the response is described by the fundamental eigenmode. This will only happen if the other eigenfrequencies are non-commensurate (and hence do not have period 2π), i.e. if

$$\frac{\lambda_{n,m}\tanh(\lambda_{n,m}h)}{\tanh h} \neq k^2 \quad \forall \quad (n,m) \neq (1,0), \tag{3.1}$$

where k is an integer, which will clearly almost certainly hold. We will see in Section 3.4 that introducing surface tension makes it easier for the second or third modes to be commensurate. For zero surface tension, Concus [20] has remarked that, for (n,m) large, (3.1) breaks down, but in this regime damping will cause this high-frequency mode to die down. Hence, in almost all cases in this chapter, it will be assumed that only the fundamental eigenmode (or modes if the fundamental frequency is degenerate) is excited to leading order.

The main part of this chapter is concerned with the effect on this response of small geometric variations in the tank. Throughout, as we remarked at the end of Section 2.1, we concentrate on variations in the back wall of the tank and take a flat base (so $\nu_{b0} = 0$) because any base variations were shown by Waterhouse [76] to have no novel effect for $h \geq O(1)$.

Hence we start in Section 3.1 with the linear solution showing how the solution changes form dramatically as the breadth approaches some integral multiple of the length, and to illustrate this change we concentrate on the case of a tank with a square horizontal cross-section. In Section 3.2 we then study how the nonlinearity alters this solution when $\lambda_0 \sim O(\varepsilon^{2/3})$.

These two sections stress the importance of the possible degeneracy of the fundamental frequency. However, as an aside, we consider in Section 3.3 a special case that arises in the two-dimensional problem when the depth approaches a critical value and the deep water model, (2.31)–(2.37), breaks down.

Finally, in Section 3.4, we present a summary of the above situations and also remark on the effects of surface tension. In particular, we see that the possibility of the second or third modes being commensurate with the fundamental can change the leading-order solution. These special cases are useful in bridging the gap between the single mode responses considered in this chapter and the infinite mode responses of future chapters.

3.1 Linear theory

When $\lambda_0 \gg \varepsilon^{2/3}$ we are away from the regime discussed at the end of Section 2.1 where the nonlinear effects are important. Hence we can consider the model (2.17)–(2.25) with the nonlinear terms being neglected. In the absence of any geometrical variations ($\nu_{b0} = \nu_{w0} = 0$), Ockendon & Ockendon [54] used this model and, by applying the Fredholm Alternative at second order, found that the leading-order solution was the eigensolution

$$\phi \sim \frac{4\varepsilon}{\lambda_0 \pi \cosh h} \cos x \cosh(z+h) \sin t, \tag{3.2}$$

which breaks down as $\lambda_0 \to 0$.

In this section we consider how wall variations ($\nu_{w0} \neq 0$) alter this linear response and shift the resonant frequency. The leading-order response is $O(\varepsilon/\lambda_0)$ so we expand ϕ and η in terms of λ_0,

$$
\begin{aligned}
\phi &= \frac{\varepsilon}{\lambda_0}\phi_0 + \varepsilon\phi_1 + \cdots, \\
\eta &= \frac{\varepsilon}{\lambda_0}\eta_0 + \varepsilon\eta_1 + \cdots,
\end{aligned}
$$

and, for the geometrical variation to have a second-order effect, we take $\nu_{w0} \sim O(\lambda_0)$. Substituting these expansions into equations (2.17)–(2.25) gives, to first order,

$$
\begin{aligned}
\nabla^2\phi_0 &= 0, && (3.3)\\
\phi_{0x} &= 0 \quad \text{on} \quad x = 0, \pi, && (3.4)\\
\phi_{0y} &= 0 \quad \text{on} \quad y = 0, b\pi, && (3.5)\\
\phi_{0z} &= 0 \quad \text{on} \quad z = -h, && (3.6)\\
\phi_{0z} + \tanh h\, \phi_{0tt} &= 0 \quad \text{on} \quad z = 0, && (3.7)\\
\boldsymbol{\nabla}\phi_0(\boldsymbol{x}, t + 2\pi) &= \boldsymbol{\nabla}\phi_0(\boldsymbol{x}, t). && (3.8)
\end{aligned}
$$

The boundary condition on $y = b\pi$ and the conditions (3.7) and (3.8) mean that the form of the solution will depend on whether or not b is an integer. When $b \neq l$ ($l \in \mathbf{N}$) these two conditions can only be satisfied if ϕ_0 is independent of y. If $b = l$ the situation is very different and we have a degenerate eigenfrequency because $\omega_{1,0} = \omega_{0,l}$, so that restriction (3.1) does not hold in the case $(n, m) = (0, l)$. We thus work with the new parameter b_0, defined by

$$
b = 1 + \lambda_0 b_0, \tag{3.9}
$$

so that, by setting $b_0 = 0$, we get the problem of a tank with a square horizontal cross-section[1] and, by letting $b_0 \to \infty$, we arrive at the solution away from $b = 1$. Using (3.9) the leading-order solution is simply

$$
\begin{aligned}
\phi_0 &= A\cos x \cosh(z+h)\sin(t+\alpha_1) &+& \quad B\cos y\cosh(z+h)\sin(t+\beta_1), \\
&= \qquad\qquad \phi_{01} &+& \qquad\qquad \phi_{02}
\end{aligned} \tag{3.10}
$$

[1]This is qualitatively the same as the cases $b = l$ so we will only consider the $b = 1$ case.

where ϕ_{01} is a longitudinal wave and ϕ_{02} a transverse wave and $A, B > 0$ and α_1, β_1 are the unknown amplitudes and phases. The free surface profile can then be found from (2.23) to be

$$\eta_0 = -\sinh h[A \cos x \cos(t + \alpha_1) + B \cos y \cos(t + \beta_1)].$$

We find the unknown constants by considering the $O(\varepsilon)$ terms in (2.17)–(2.25) which are

$$\begin{aligned}
\nabla^2 \phi_1 &= 0, && (3.11)\\
\phi_{1x} &= \sin t \quad \text{on} \quad x = 0, \pi, && (3.12)\\
\phi_{1y} &= 0 \quad \text{on} \quad y = 0, && (3.13)\\
\phi_{1y} &= \pi \frac{\nu_{w0}}{\lambda_0} a_w'(x) \phi_{0x} - \pi[b_0 + \frac{\nu_{w0}}{\lambda_0} a_w(x)] \phi_{0yy} \quad \text{on} \quad y = \pi, && (3.14)\\
\phi_{1z} &= 0 \quad \text{on} \quad z = -h, && (3.15)\\
\phi_{1z} + \tanh h \phi_{1tt} &= -\tanh h \phi_{0tt} \quad \text{on} \quad z = 0, && (3.16)\\
\boldsymbol{\nabla}\phi_1(\boldsymbol{x}, t + 2\pi) &= \boldsymbol{\nabla}\phi_1(\boldsymbol{x}, t). && (3.17)
\end{aligned}$$

The idea now is to find a solvability condition on the ϕ_1 problem to determine A and B. We do this by using the Fredholm Alternative — we multiply (3.11) by all the solutions to the homogeneous problem (3.3)–(3.8) and then integrate over the whole domain; in other words we consider

$$\int_0^{2\pi} \int_0^{\pi} \int_{-h}^{0} \int_0^{\pi} \nabla^2 \phi_1 \cos x \cosh(z + h) \left\{ \begin{array}{c} \sin t \\ \cos t \end{array} \right\} \mathrm{d}x \mathrm{d}z \mathrm{d}y \mathrm{d}t = 0. \qquad (3.18)$$

Integration by parts and the use of (3.10) and (3.11)–(3.17) finally yields $\sin \alpha_1 = \sin \beta_1 = 0$ and

$$\begin{aligned}
\frac{4 \cos \alpha_1}{\pi \cosh h} A^{-1} &= 1 + \frac{\nu_{w0}}{\lambda_0 \pi} G(h) \int_0^{\pi} a_w(x) \cos 2x \mathrm{d}x \\
&- \frac{\nu_{w0}^2}{\lambda_0^2 \pi} G(h) \frac{\sinh h + h\operatorname{sech} h}{\pi[\sinh h + b_0(\sinh h + h\operatorname{sech} h)]} \left(\int_0^{\pi} a_w(x) \cos x \mathrm{d}x \right)^2, \qquad (3.19)
\end{aligned}$$

$$B \cos \beta_1 = \frac{A \cos \alpha_1 \nu_{w0}(\sinh h + h\operatorname{sech} h)}{\lambda_0 \pi[\sinh h + b_0(\sinh h + h\operatorname{sech} h)]} \int_0^{\pi} a_w(x) \cos x \mathrm{d}x, \qquad (3.20)$$

where

$$G(h) = \frac{h\operatorname{sech} h + \sinh h}{\sinh h}$$

Hence α_1 and β_1 are either 0 or π and are chosen so that A and B are always positive. The response (3.10), where A and B satisfy (3.19) and (3.20), is always similar to a generalised simple harmonic motion, i.e. $\phi \sim f(x,y)\sin t/\lambda_0$ for some function f.

We now consider the two limiting cases individually and write $a_w(x)$ as a Fourier series,

$$a_w(x) = \sum_{n=1}^{\infty} \gamma_{wn} \cos nx, \tag{3.21}$$

where, because we use (3.9), we have taken $\gamma_{w0} = 0$.

3.1.1 Solution away from degeneracy

The solution away from $b = 1$ is found by letting $b_0 \to \infty$ in (3.19) and (3.20) which yields

$$B = 0 \quad , \quad \frac{4\cos\alpha_1}{\pi A} = \cosh h + \frac{\nu_{w0}}{2\lambda_0}(\cosh h + h\mathrm{cosech} h)\gamma_{w2} \quad , \quad \sin\alpha_1 = 0. \tag{3.22}$$

This is just the same linear response as when $a_w(x)$ is constant except that the resonant frequency is shifted from $\lambda_0 = 0$ to where

$$\lambda_0 \cosh h + \frac{\nu_{w0}}{2}(\cosh h + h\mathrm{cosech} h)\gamma_{w2} = 0, \tag{3.23}$$

so, unless $b \simeq l$, any change in the geometry is equivalent to a shift in the fundamental frequency by $O(\lambda_0)$.

3.1.2 Close to a square horizontal cross-section

For $b_0 \sim O(1)$, the leading-order solution consists of a longitudinal and a transverse mode of comparable amplitude. We take as a measure of the overall amplitude $\tilde{A} = (A + B)/\lambda_0$ and this is illustrated in the case $b_0 = 0$ in Figure 3.1 for $h = 1.5$ and $a_w'(x) = 2x$. We see from (3.19) that the resonant growth in the figure is close to the spectral lines

$$\frac{4\lambda_0}{\nu_{w0} G(h)} = -\gamma_{w2} \pm (\gamma_{w2}^2 + 4\gamma_{w1}^2)^{1/2}, \tag{3.24}$$

and we note that this is independent of the choice of amplitude. For $b_0 \neq 0$, we can picture the response in the following way. If we consider viewing the response in

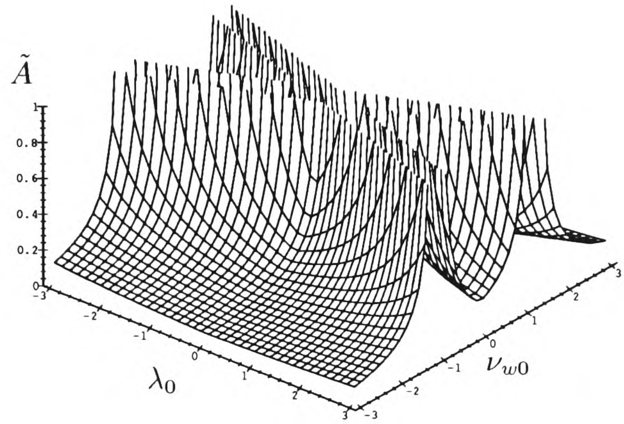

Figure 3.1: Plot of $\tilde{A}$ against λ_0 and ν_{w0} showing the linear response when $b = 1$.

Figure 3.1 from above we see an X-shape which we can think of as the combination of a left- and right-hand wedge. As b_0 increases from zero the left-hand wedge moves away and the right-hand one starts to open out. Finally the left-hand wedge totally disappears, leaving the right-hand wedge perfectly straight, corresponding to the response (3.22). This is shown graphically in Waterhouse [76]. The lines of resonance can also be seen, from (3.19), to shift from (3.24) to (3.23) as b_0 increases.

The degeneracy of the spectra thus adds the novel feature that the resonant frequency shifts form one value ($\lambda_0 = 0$) to *two* values for ν_{w0} non-zero. This result could have been anticipated if we had considered the perturbation to the linearised natural frequencies, (2.12), caused by the wall variations which would have given us a picture similar to Figure 3.2. This shows that all the natural frequencies split into two values as ν_{w0} increases from zero. Note that the change in the value of each natural frequency and the slope of the lines in Figure 3.2 are dependent on the coefficients γ_{wn}. We can use as a paradigm for this phenomenon a pair of coupled Duffing-like oscillators and we will say more about this in Section 3.2.3.

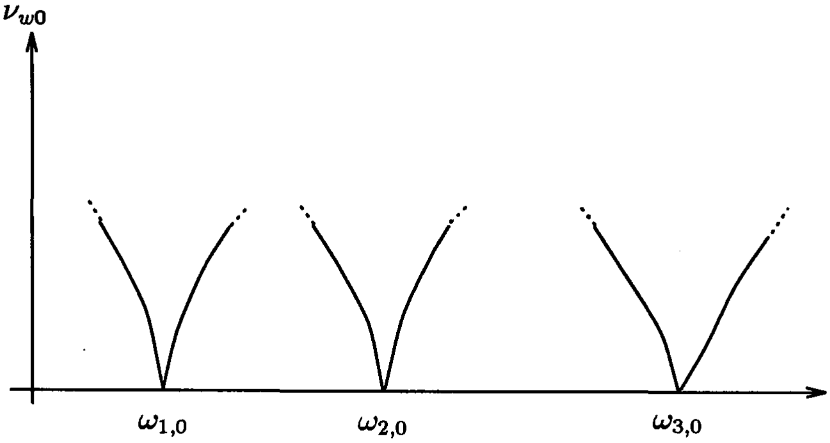

Figure 3.2: Change in the values of the natural frequencies of a tank of nearly-square cross-section as ν_{w0} increases.

3.2 Nonlinear response

As $\lambda_0 \to O(\varepsilon^{2/3})$ we found in Section 2.1 that the nonlinear terms contain the resonant growth witnessed in the last section. In this regime we use the model (2.31)–(2.39) and now expand the velocity potential and free surface height in powers of $\varepsilon^{1/3}$,

$$\phi_d = \phi_0 + \varepsilon^{1/3}\phi_1 + \varepsilon^{2/3}\phi_2 + \cdots, \tag{3.25}$$

$$\eta_d = \eta_0 + \varepsilon^{1/3}\eta_1 + \varepsilon^{2/3}\eta_2 + \cdots. \tag{3.26}$$

Substituting these expansions into (2.31)–(2.39) we again find that, to leading order, ϕ_0 satisfies equations (3.3)–(3.8). To bridge the gap between tanks of square and non-square cross-section, we this time write

$$b = 1 + \varepsilon^{2/3} b_d,$$

(so, from (3.9), $b_d = \lambda_d b_0$) and so we again take $\gamma_{w0} = 0$.

Hence, as before,

$$\phi_0 = [A\cos x \sin(t+\alpha_1) + B\cos y \sin(t+\beta_1)]\cosh(z+h), \tag{3.27}$$

$$\eta_0 = -\sinh h[A\cos x\cos(t+\alpha_1) + B\cos y\cos(t+\beta_1)], \tag{3.28}$$

where $A, B > 0$, but when we now proceed to $O(\varepsilon^{1/3})$, we have the *homogeneous* problem

$$
\begin{aligned}
\nabla^2\phi_1 &= 0, && (3.29)\\
\phi_{1x} &= 0 \quad \text{on} \quad x = 0, \pi, && (3.30)\\
\phi_{1y} &= 0 \quad \text{on} \quad y = 0, \pi, && (3.31)\\
\phi_{1z} &= 0 \quad \text{on} \quad z = -h, && (3.32)\\
\int_0^\pi \int_0^\pi \eta_1 \mathrm{d}x\mathrm{d}y &= 0, && (3.33)\\
\nabla\phi_1(\boldsymbol{x}, t + 2\pi) &= \nabla\phi_1(\boldsymbol{x}, t), && (3.34)
\end{aligned}
$$

together with

$$
\begin{aligned}
\phi_{1z} &= \eta_{1t} + \phi_{0x}\eta_{0x} + \phi_{0y}\eta_{0y} - \eta_0\phi_{0zz},\\
\eta_1 + \tanh h\phi_{1t} &= -\tanh h(\eta_0\phi_{0tz} + \tfrac{1}{2}{\phi_{0x}}^2 + \tfrac{1}{2}{\phi_{0y}}^2 + \tfrac{1}{2}{\phi_{0z}}^2), \qquad (3.35)
\end{aligned}
$$

on $z = 0$. This has solution

$$
\begin{aligned}
\phi_1 = {} & [C\cos x \sin(t + \alpha_2) + D\cos y \sin(t + \beta_2)]\cosh(z + h)\\
& + [A_1 \cos 2x \cosh 2(z + h) + A_3]\sin 2(t + \alpha_1)\\
& + [A_2 \cos 2y \cosh 2(z + h) + A_4]\sin 2(t + \beta_1)\\
& + A_5 \cos x \cos y \cosh\sqrt{2}(z + h)[\sin(t + \alpha_1)\cos(t + \beta_1)\\
& + \sin(t + \beta_1)\cos(t + \alpha_1)] + \beta_0 t,
\end{aligned}
$$

where

$$
A_1 = \frac{-3A^2}{16\sinh^2 h}, \quad A_2 = \frac{-3B^2}{16\sinh^2 h}, \quad A_3 = \frac{A^2}{16}(1 + 4\sinh^2 h),
$$
$$
A_4 = \frac{B^2}{16}(1 + 4\sinh^2 h), \quad A_5 = \frac{AB\sinh h(1 - 2\sinh^2 h)}{\sqrt{2}\sinh\sqrt{2}h\cosh h - 4\cosh\sqrt{2}h\sinh h},
$$

C, D, α_2 and β_2 are arbitrary constants, η_1 can be determined from (3.35) and condition (3.33) implies that

$$
\beta_0 = -\frac{1}{8}(A^2 + B^2).
$$

Examining the $O(\varepsilon^{2/3})$ terms leads to the *inhomogeneous* problem

$$\begin{aligned}
\nabla^2\phi_2 &= 0, \\
\phi_{2x} &= \sin t \quad \text{on} \quad x = 0, \pi, \\
\phi_{2y} &= 0 \quad \text{on} \quad y = 0, \\
\phi_{2y} &= \pi\nu_{wd}a'_w(x)\phi_{0x} - \pi[b_d + \nu_{wd}a_w(x)]\phi_{0yy} \quad \text{on} \quad y = \pi, \qquad (3.36) \\
\phi_{2z} &= 0 \quad \text{on} \quad z = -h, \\
\boldsymbol{\nabla}\phi_2(\boldsymbol{x}, t + 2\pi) &= \boldsymbol{\nabla}\phi_2(\boldsymbol{x}, t),
\end{aligned}$$

and, on the linearised free surface $z = 0$,

$$\begin{aligned}
\phi_{2z} &= \eta_{2t} + \eta_0\phi_{0xz}\eta_{0x} + \eta_0\phi_{0yz}\eta_{0y} + \phi_{0x}\eta_{1x} + \phi_{1x}\eta_{0x} \\
&\quad + \phi_{0y}\eta_{1y} + \phi_{1y}\eta_{0y} - \eta_1\phi_0 - \tfrac{1}{2}\eta_0^2\phi_{0z} - \eta_0\phi_{1zz}, \\
\eta_2 + \tanh h\phi_{2t} &= -\tanh h(\eta_1\phi_{0tz} + \tfrac{1}{2}\eta_0^2\phi_{0t} + \eta_0\phi_{1tz} + \eta_0\phi_{0x}\phi_{0xz} \\
&\quad + \phi_{0x}\phi_{1x} + \eta_0\phi_{0y}\phi_{0yz} + \phi_{0y}\phi_{1y} + \eta_0\phi_0\phi_{0z} + \phi_{0z}\phi_{1z} + \lambda_d\phi_{0t}).
\end{aligned}$$

We again employ the Fredholm Alternative on this problem and find $\sin\alpha_1 = \sin\beta_1 = 0$ and

$$\begin{aligned}
\frac{4}{\pi}\tanh h &= [\nu_{wd}L(h)A + \lambda_d A\sinh h + H(h)A^3 + J(h)AB^2]\cos\alpha_1 \\
&\quad + \nu_{wd}K(h)B\cos\beta_1, \qquad (3.37) \\
0 &= [b_d M(h)B + \lambda_d B\sinh h + H(h)B^3 + J(h)BA^2]\cos\beta_1 \\
&\quad + \nu_{wd}K(h)A\cos\alpha_1, \qquad (3.38)
\end{aligned}$$

where

$$\begin{aligned}
H(h) &= \frac{-1}{32}\mathrm{sech}^2 h\,\mathrm{cosech} h(9 + 15\sinh^2 h - 8\sinh^6 h), \\
K(h) &= -\frac{M(h)}{2}\gamma_{w1}, \\
L(h) &= \frac{M(h)}{2}\gamma_{w2}, \\
M(h) &= \sinh h + h\,\mathrm{sech} h, \\
J(h) &= \frac{1}{8}\frac{\tilde{J}(h)}{(\sqrt{2}\cosh h\sinh\sqrt{2}h - 4\sinh h\cosh\sqrt{2}h)\sinh h\cosh^3 h},
\end{aligned}$$

$$\begin{aligned}\tilde{J}(h) &= -29\sqrt{2}\cosh^5 h \sinh\sqrt{2}h + 52\cosh^4 h\cosh\sqrt{2}h\sinh h \\ &\quad +9\sqrt{2}\cosh^7 h\sinh\sqrt{2}h - 40\cosh\sqrt{2}h\cosh^2 h\sinh h \\ &\quad -20\sinh h\cosh^6 h\cosh\sqrt{2}h + 31\sqrt{2}\sinh\sqrt{2}h\cosh^3 h \\ &\quad +8\cosh\sqrt{2}h\sinh h - 11\sqrt{2}\cosh h\sinh\sqrt{2}h,\end{aligned}$$

and we again have α_1 and β_1 equal 0 or π where the phase is determined by the requirement that $A, B > 0$. We now consider the two limiting cases separately.

3.2.1 Solution away from degeneracy

Letting $b_d \to \infty$ we find that $\sin\alpha_1 = 0$ and

$$A\left[\lambda_d \sinh h + \frac{\nu_{wd}}{2}(\sinh h + h\mathrm{sech}h)\gamma_{w2}\right] + H(h)A^3 = \frac{4}{\pi}\tanh h\cos\alpha_1. \quad (3.39)$$

In two dimensions, with $\nu_{wd} = 0$, this equation becomes

$$\frac{4}{\pi}\tanh h\cos\alpha_1 = \lambda_d A\sinh h + H(h)A^3, \quad (3.40)$$

which is the result found by Ockendon & Ockendon [54], and this response is of the same form as the response of the undamped Duffing equation, (1.1) with $k = 0$. The most notable feature of (3.39) is that $H(h)$ changes sign at a certain depth ($h \simeq 1.06$), so the response looks like a hard spring when $H < 0$ and a soft spring when $H > 0$. This is shown in Figure 3.3 for the simplified response (3.40). A discussion of what happens when $H(h) \equiv 0$ will be given in Section 3.3.

The response (3.39) can be visualised by plotting A against λ_d and ν_{wd} as in Figure 3.4 where we have again taken $h = 1.5$ and $a_w'(x) = 2x$.

The stability of the branches in Figures 3.3 and 3.4 can be found by introducing a slow time-scale (in the same way as Cox & Mortell [22] did for shallow water) and seeing how small perturbations to the original response behave. It is easiest to consider the stability of the two-dimensional response (3.40) as the details for the stability of (3.39) will be the same but more convoluted. Hence we introduce the slow time-scale $\tau = \varepsilon^{2/3}t$ and consider a multiple time-scale solution of (2.31)–(2.39) with $a_w(x) = 0$ and using the expansions (3.25) and (3.26). The leading-order problem is the same as before and the solution is now

$$\phi_0 = (\mathcal{A}(\tau)e^{it} + \bar{\mathcal{A}}(\tau)e^{-it})\cos x\cosh(z+h),$$

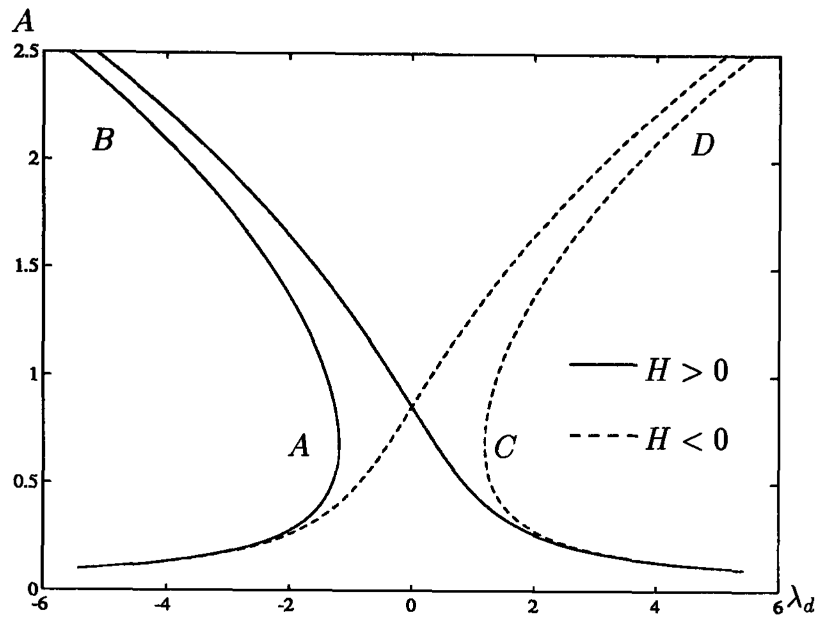

Figure 3.3: Classic Duffing-like response for (3.40).

(so that when $\mathcal{A}$ is independent of τ we have $\mathcal{A} = \frac{1}{2}A(\cos\alpha_1 - i\sin\alpha_1)$). The second-order problem is again the same so the details will not be repeated and the third-order terms this time yield a solvability condition which is an evolution equation for A in terms of the slow time-scale τ. The details of the calculation are the same as before and the result is

$$\lambda_d \mathcal{A} \sinh h - 2i\frac{\mathrm{d}\mathcal{A}}{\mathrm{d}\tau}\sinh h + 4H(h)\mathcal{A}^2\bar{\mathcal{A}} = \frac{2}{\pi}\tanh h, \tag{3.41}$$

which is the same as (3.40) when $\mathcal{A} = \frac{1}{2}A(\cos\alpha_1 - i\sin\alpha_1)$. To see whether solutions of (3.40) are stable we write $\mathcal{A} = \frac{1}{2}A(\cos\alpha_1 - i\sin\alpha_1) + \tilde{\delta}\mathcal{A}_1 + O(\tilde{\delta}^2)$ ($\tilde{\delta} \ll 1$) where A satisfies (3.40) and this results (to $O(\tilde{\delta})$) in

$$2i\frac{d\mathcal{A}_1}{d\tau} = \lambda_d\mathcal{A}_1 + \frac{H(h)}{\sinh h}A^2(\bar{\mathcal{A}}_1 + 2\mathcal{A}_1).$$

This has growing solutions when

$$-3 < \frac{\lambda_d \sinh h}{H(h)A^2} < -1. \tag{3.42}$$

Hence the portions AB and CD in Figure 3.3 are unstable. The corresponding instability in the response when geometrical effects are included will be along the

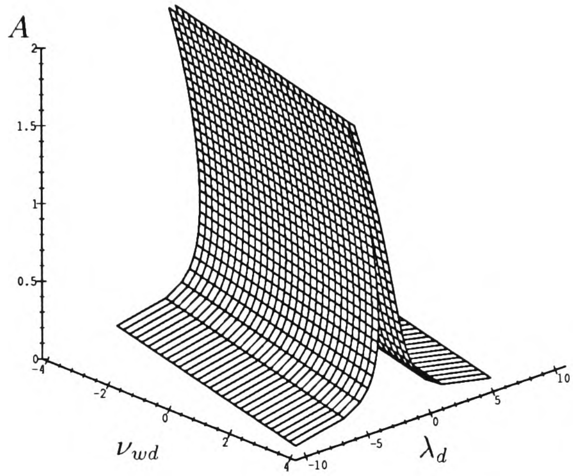

Figure 3.4: Nonlinear response when $b \neq l$, showing how A varies with λ_d and ν_{wd}, given by (3.39).

underside of the branch in Figure 3.4. This instability is also seen experimentally in the work of Fultz [29] where the only experimental responses seen are the ones excluding portions AB and CD of Figure 3.3.

3.2.2 Close to a square horizontal-cross section

If we consider (3.37) and (3.38) with $b_d = 0$ then the response is not as easy to plot. As an example we consider the case $\lambda_d = 0$ and plot the response, $A + B$, against ν_{wd} for the case $a'_w(x) = 2x$ and $h = 1.5$ as shown Figure 3.5(a), where we have indicated the values of the phases α_1 and β_1 in this case. There are now two Duffing-like branches associated with the two 'planes' of Figure 3.1. The nonlinearity has the same effect as in the one-mode case, bending over the response close to the resonant frequency. The general response for any λ_d and ν_{wd} can hence be thought of as Figure 3.1 with each plane bending over on itself. Therefore, as $\lambda_d \to \infty$, the two branches of Figure 3.5 move away but, as $\lambda_d \to -\infty$, they pass through each other and then move apart. Alternatively, we could fix ν_{wd} and plot the amplitude against λ_d, and this is illustrated in Figure 3.5(b) for $\nu_{wd} = 2$ where we again indicate the values of the phases. Again we can see the transition between the response when $b = 1$ and $b \neq 1$ by varying b_d. Considering Figure 3.5(a), as b_d

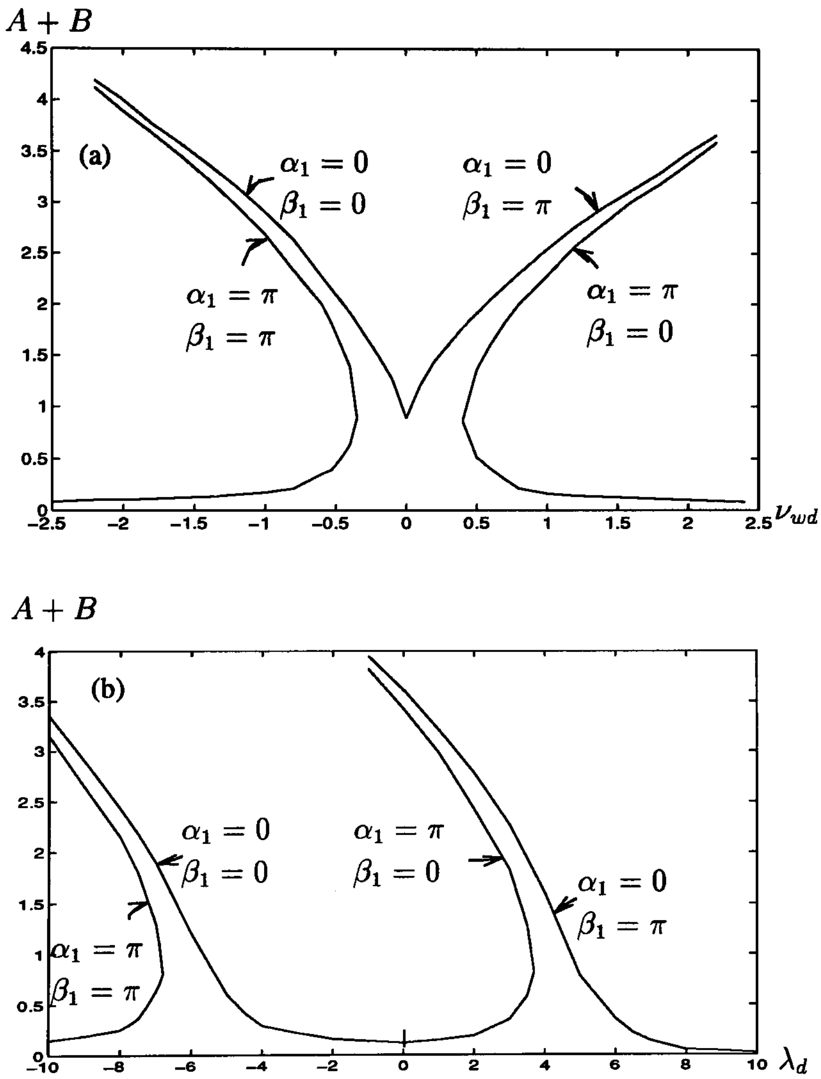

Figure 3.5: Response diagram for the nonlinear solution in a tank with a nearly square horizontal cross section: (a) amplitude against ν_{wd} when $\lambda_d = 0$ and (b) amplitude against λ_d when $\nu_{wd} = 2$

increases it is clear that the right-hand branch moves off and eventually disappears leaving the standard Duffing response of Figure 3.4. This can be seen graphically in Waterhouse [76].

To understand how the geometry causes a transverse wave in this case (and in a similar way in the linear problem of Section 3.1.2) we notice that the forcing in the horizontal direction of strength $O(\varepsilon)$ causes a resonant wave of amplitude $O(\varepsilon^{1/3})$ in the x-direction. This then interacts with the first Fourier component of $a_w(x)$. The geometric coupling is $O(\varepsilon^{2/3})$ which, coupled with the $O(\varepsilon^{1/3})$ longitudinal wave, provides an $O(\varepsilon)$ strength forcing term in the transverse direction. Thus, when $b = 1$, both the transverse wave and longitudinal wave are excited and both with the same forcing strength.

Of course, this excitation of a transverse mode could simply have been induced by taking a tank with no geometrical variations and forcing it in the y-direction as well as in the x-direction. However, the interaction between the modes will not be noticeable in the linear case and we would lose the resonant structure of Figure 3.1 where there are two lines of resonance. In the nonlinear case, if we took the forcing in each direction to have the same amplitude and phase, the solution would be

$$\begin{aligned}\lambda_d A \sinh h + H(h)A^3 + J(h)AB^2 &= \frac{4}{\pi}\tanh h,\\ \lambda_d B \sinh h + H(h)B^3 + J(h)BA^2 &= \frac{4}{\pi}\tanh h.\end{aligned}$$

However, we note that as $h \to 0$, $J(h)/\sinh h \to -1/4$ whereas $H(h)/\sinh h \to -9/(32h^2)$ so that the nonlinear interaction between the two modes is negligible compared to the other terms[2]. The geometric variation, $a_w(x)$, provides a subtle way of exciting a transverse mode which is coupled non-trivially to the longitudinal wave, and this coupling remains in the shallow water limit as we shall see in Chapter 5.

[2]The observation that it takes a cubic (as opposed to quadratic) nonlinearity to couple two modes that have a different direction will turn out to be crucial in our shallow water discussions of Chapter 5 where the nonlinearity is quadratic and these modes do not interact through the nonlinearity but through the geometric variation.

3.2.3 A pair of coupled oscillators as a paradigm for degenerate deep water sloshing

When we are away from degeneracy, Duffing's equation, (1.1), acts as a paradigm model for the interactions between the detuning, nonlinearity and forcing that arise in deep water. Close to degeneracy, the simplest model that illustrates the results we have found are the pair of oscillators,

$$\begin{aligned} \ddot{x} + (1+\lambda_0)x + \nu_{w0}y + x^3 &= \varepsilon \cos t, \\ \ddot{y} + (1+\lambda_0)y + \nu_{w0}x + y^3 &= 0, \end{aligned}$$

which could be written as one fourth-order equation in either x or y and have natural frequencies $1+\lambda_0 \pm \nu_{w0}$, indicating the degeneracy of the system for non-zero ν_{w0}. This pair exhibit the types of responses found in Sections 3.1.2 and 3.2.2 in the regimes $\lambda_0, \nu_{w0} \gg \varepsilon^{2/3}$ $(x, y \sim O(\varepsilon/\lambda_0))$ and $\lambda_0, \nu_{w0} \sim \varepsilon^{2/3}$ $(x, y \sim O(\varepsilon^{1/3}))$ respectively. We can now distinguish between the non-degenerate and degenerate scenarios by taking $\nu_{w0} = 0$ and ν_{w0} non-zero respectively. Figure 3.6 summarises the possible responses of this system for free (dark lines) and forced (normal lines) oscillations in the linear and nonlinear regimes.

This picture helps to confirm the essential feature of the degenerate case which is the splitting of the resonant frequency into two distinct values as ν_{w0} increases. The other features of the response mirror those of the non-degenerate case with the linear free and forced oscillations being bent over by the nonlinearity.

3.2.4 Resonance of higher modes

It is fairly straightforward to adapt the theory presented here to describe the excitation of modes higher than the fundamental. To do this (2.16) would have to be changed to $\Omega^2 = (1+\lambda_0)\omega_{n,m}^2$ in order to elicit the (n,m)-mode and the equations would need to be rescaled. We could then generate the motion using a wavemaker at each end of the tank (see Section 5.3.2). However, the analysis presented for the fundamental mode will be qualitatively the same as for these other modes. Recalling Figure 3.2, we can see that when the frequency we are forcing close to is non-degenerate (or, equivalently, when $\nu_{w0} = 0$), there is a single Duffing-type branch whereas for a degenerate frequency we expect to see two branches as in the

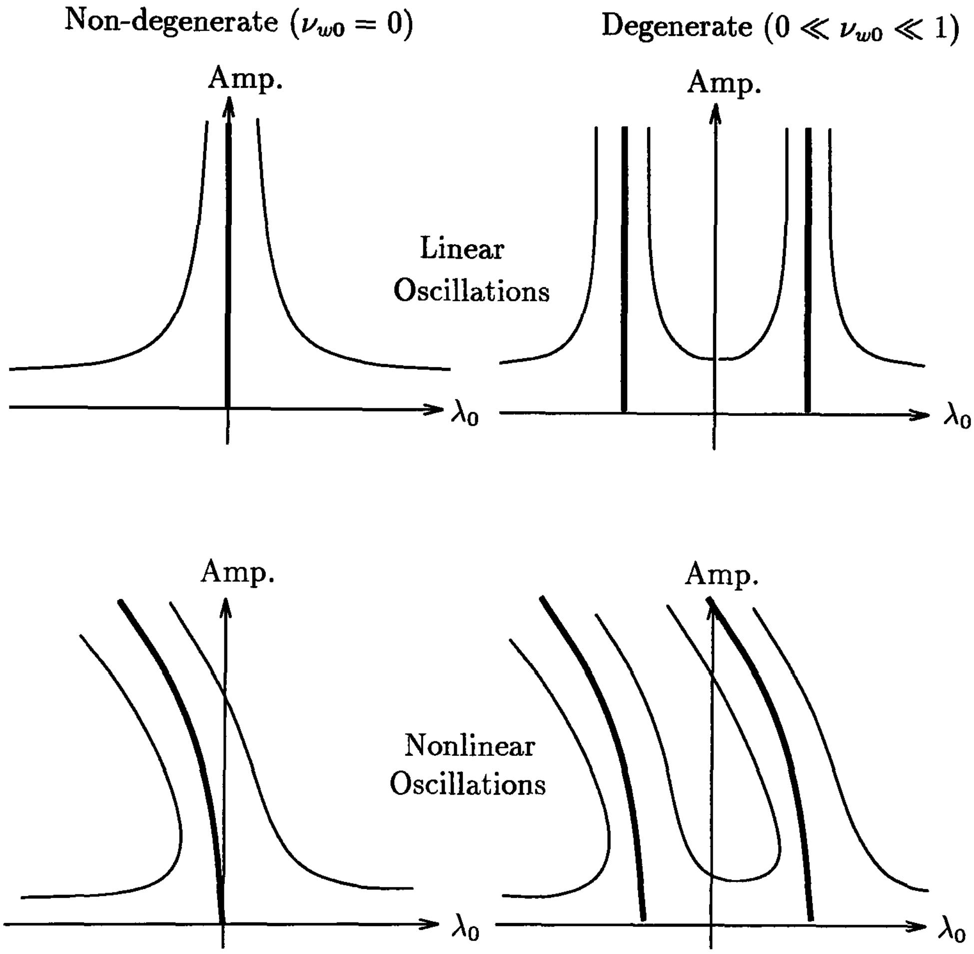

Figure 3.6: Linear and nonlinear responses for non-degenerate and degenerate responses. The dark lines represent free oscillations and the normal lines forced oscillations.

above analysis. This has been seen for free, non-degenerate oscillations by Verma & Keller [75] (for $b = 1$ and $(n, m) = (1, 1)$) and by Bridges [10]. Also Tsai *et al* [73] provided the solution for a forced tank in the special case of two-dimensional motions.

3.3 Solution near a critical depth

The solution (3.39) breaks down when $H(h) = 0$ (which occurs at $h = h_0 = 1.058$) and as $\lambda_d \to 0$. For simplicity we take $\nu_{wd} = 0$, as in Waterhouse [77], and concentrate on the effect of nonlinearity in this case. As h gets closer to h_0 it is necessary to re-scale the variables and pose new expansions for ϕ and η. To deduce the correct scalings in this case, we put

$$h = h_0 + \varepsilon^{\alpha} h_1, \tag{3.43}$$

where α is a positive constant to be found. Substituting this into (3.40) means that $A^3\varepsilon^{\alpha} \sim O(1)$ together with $\lambda_0 \varepsilon^{-2/3} A \sim O(1)$ for all the terms to balance. Hence $A = \varepsilon^{-\alpha/3}\bar{A}$ and $\lambda_0 \sim O(\varepsilon^{(\alpha+2)/3})$ so that

$$\phi \sim \varepsilon^{(1-\alpha)/3} \bar{A} \cos x \cosh(z + h) \sin(t + \alpha_1). \tag{3.44}$$

For any expansion of ϕ and η it is necessary that the nonlinear terms generate $\cos x \sin t$ terms at $O(1)$ so that the boundary conditions (2.18) can be accommodated. This means that the $O(1)$ problem must involve *odd* powers of ϕ_0, in other words the first term in an expansion for ϕ must be of the form $\varepsilon^{1/(2n+1)}$ $(n = 0, 1, 2, \ldots)$. Coupling this with (3.44) shows that we must take $(1-\alpha)/3 = 1/5$ or $\alpha = 2/5$. Hence the scalings are

$$h = h_0 + \varepsilon^{2/5} h_1 \quad \text{and} \quad \lambda_0 \varepsilon^{-4/5} \sim O(1), \tag{3.45}$$

where h_1 is $O(1)$, together with the expansions

$$\phi = \varepsilon^{1/5}\phi_0 + \varepsilon^{2/5}\phi_1 + \varepsilon^{3/5}\phi_2 + \varepsilon^{4/5}\phi_3 + \varepsilon\phi_4 + \cdots \tag{3.46}$$

and

$$\eta = \varepsilon^{1/5}\eta_0 + \varepsilon^{2/5}\eta_1 + \varepsilon^{3/5}\eta_2 + \varepsilon^{4/5}\eta_3 + \varepsilon\eta_4 + \cdots, \tag{3.47}$$

so that near h_0 the amplitude of the response grows from $O(\varepsilon^{1/3})$ to $O(\varepsilon^{1/5})$. Substituting (3.45), (3.46) and (3.47) into equations (2.17)–(2.25) and comparing $O(\varepsilon^{1/5})$ terms leads to the same first-order problem as before, and so the leading-order solutions are

$$\begin{aligned}\phi_0 &= \bar{A}\cos x\cosh{(z+h)}\sin{(t+\alpha_1)}, && (3.48)\\ \eta_0 &= -\bar{A}\sinh h\cos x\cos{(t+\alpha_1)}, && (3.49)\end{aligned}$$

but now to determine $\bar{A}$ it is necessary to find a solvability condition on the problem for ϕ_4 and η_4. We omit the problems for ϕ_1, ϕ_2 and ϕ_3 and just give the results which are

$$\begin{aligned}\phi_1 &= BC_1\sin{(t+\alpha_2)} + \bar{A}^2(0.46-0.12C_2)\sin 2(t+\alpha_1) - (\bar{A}^2/8)t,\\ \phi_2 &= CC_1\sin{(t+\alpha_3)} + \bar{A}B(0.93-0.23C_2)\sin 2(t+\alpha_1)\\ &\quad +\bar{A}^3(-0.59C_1+0.004C_3)\sin 3(t+\alpha_1) + 0.01\bar{A}^3C_3\sin{(t+\alpha_1)}\\ &\quad -(\bar{A}B/4)t + \bar{A}h_1\cos x\sinh(z+h_0)\sin{(t+\alpha_1)},\\ \phi_3 &= DC_1\sin{(t+\alpha_4)} + ([0.26\bar{A}^4 - 0.23\bar{A}C + 0.30h_1\bar{A}^2 - 0.12B^2]C_2\\ &\quad +0.004\bar{A}^4C_4 + [1.02h_1\bar{A}^2 + 0.46B^2 + 0.60\bar{A}^4 + 0.93\bar{A}C])\sin 2(t+\alpha_1)\\ &\quad +\bar{A}^2B(-1.76C_1+0.01C_3)\sin 3(t+\alpha_1) + \bar{A}^4(0.001C_4+0.15C_2\\ &\quad +0.13)\sin 4(t+\alpha_1) + 0.03\bar{A}^2BC_3\sin{(t+\alpha_1)}\\ &\quad +Bh_1\cos x\sinh(z+h_0)\sin{(t+\alpha_1)}\\ &\quad -0.23h_1\cos 2x\sinh 2(z+h_0)\sin 2(t+\alpha_1),\end{aligned}$$

where $B, C, D, \alpha_2, \alpha_3$ and α_4 are arbitrary constants and

$$C_n = \cos nx\cosh n(z+h_0) \quad n = 1,2,3,4.$$

The η_i $(i = 1,2,3)$ can then be found from equation (2.22). Next, considering the $O(1)$ terms from (2.17)–(2.25), it is found that

$$\begin{aligned}\nabla^2\phi_4 &= 0, && (3.50)\\ \phi_{4x} &= \sin t \quad \text{on} \quad x = 0,\pi, && (3.51)\\ \phi_{4z} &= h_1\phi_{2zz} \quad \text{on} \quad z = -h_0, && (3.52)\\ \phi_{4z} + \tanh h_0\phi_{4tt} &= F(x,t) \quad \text{on} \quad z = 0, && (3.53)\\ \nabla\phi_4(x,z,t) &= \nabla\phi_4(x,z,t+2\pi), && (3.54)\end{aligned}$$

where F is a combination of ϕ_i and η_i $(i = 0, 1, 2, 3)$ given by

$$
\begin{aligned}
F(x,t) &= F_1(x,0,t) - \tanh h_0 \frac{\partial}{\partial t} F_2(x,0,t) \\
&\quad + h_1(\tanh^2 h_0 - 1)\frac{\partial}{\partial t} F_3(x,0,t) \\
&\quad - \tanh h_0[\lambda_0 \varepsilon^{-4/5} + h_1^2(\tanh^2 h_0 - 1)]\frac{\partial^2 \phi_0}{\partial t^2}(x,0,t),
\end{aligned}
$$

and

$$
\begin{aligned}
F_1(x,z,t) &= \eta_2\phi_{0xz}\eta_{0x} + \eta_0\eta_1\phi_{0x}\eta_{0x} + \tfrac{1}{6}\eta_0^3\phi_{0xz}\eta_{0x} + \eta_1\phi_{0xz}\eta_{1x} + \eta_1\phi_{1xz}\eta_{0x} \\
&\quad + \tfrac{1}{2}\eta_0^2\phi_{0x}\eta_{1x} + \tfrac{1}{2}\eta_0^2\phi_{1xzz}\eta_{0x} + \eta_0\phi_{0xz}\eta_{2x} + \eta_0\phi_{2xz}\eta_{0x} + \eta_0\phi_{1xz}\eta_{1x} \\
&\quad + \phi_{3x}\eta_{0x} + \phi_{0x}\eta_{3x} + \phi_{1x}\eta_{2x} + \phi_{2x}\eta_{1x} - \eta_3\phi_0 - \eta_0\eta_2\phi_{0z} - \tfrac{1}{2}\eta_1^2\phi_{0z} \\
&\quad - \tfrac{1}{2}\eta_0^2\eta_1\phi_0 - \tfrac{1}{24}\eta_0^4\phi_{0z} - \eta_2\phi_{1zz} - \eta_0\eta_1\phi_{1zzz} - \tfrac{1}{6}\eta_0^3\phi_{1zzzz} \\
&\quad - \eta_1\phi_{2zz} - \tfrac{1}{2}\eta_0^2\phi_{2zzz} - \eta_0\phi_{3zz}, \\
F_2(x,z,t) &= \eta_3\phi_{0tz} + \eta_0\eta_2\phi_{0t} + \tfrac{1}{2}\eta_1^2\phi_{0t} + \tfrac{1}{2}\eta_0^2\eta_1\phi_{0tz} + \tfrac{1}{24}\eta_0^4\phi_{0t} + \eta_2\phi_{1tz} \\
&\quad \eta_0\eta_1\phi_{1tzz} + \tfrac{1}{6}\eta_0^3\phi_{1tzzz} + \eta_1\phi_{2tz} + \tfrac{1}{2}\eta_0^2\phi_{2tzz} + \eta_0\phi_{3tz} \\
&\quad + \eta_2\phi_{0x}\phi_{0xz} + \eta_0\eta_1\phi_{0xz}^2 + \eta_0\eta_1\phi_{0x}^2 + \tfrac{2}{3}\eta_0^3\phi_{0xz}\phi_{0x} \\
&\quad + \eta_1\phi_{0xz}\phi_{1x} + \eta_1\phi_{0x}\phi_{1xz} + \tfrac{1}{2}\eta_0^2\phi_{0x}\phi_{1x} + \eta_0^2\phi_{0xz}\phi_{1xz} \\
&\quad + \tfrac{1}{2}\eta_0^2\phi_{0x}\phi_{1xzz} + \eta_0\phi_{1x}\phi_{1xz} + \eta_0\phi_{0xz}\phi_{2x} + \eta_0\phi_{0x}\phi_{2xz} + \phi_{0x}\phi_{3x} \\
&\quad + \phi_{1x}\phi_{2x} + \eta_2\phi_{0z}\phi_0 + \eta_0\eta_1\phi_0^2 + \eta_0\eta_1\phi_{0z}^2 + \tfrac{2}{3}\eta_0^3\phi_0\phi_{0z} \\
&\quad + \eta_1\phi_0\phi_{1z} + \eta_1\phi_{0z}\phi_{1zz} + \tfrac{1}{2}\eta_0^2\phi_{0z}\phi_{1z} + \eta_0^2\phi_0\phi_{1zz} + \tfrac{1}{2}\eta_0^2\phi_{0z}\phi_{1zzz} \\
&\quad \eta_0\phi_{1z}\phi_{1zz} + \eta_0\phi_0\phi_{2z} + \eta_0\phi_{0z}\phi_{2zz} + \phi_{0z}\phi_{3z} + \phi_{1z}\phi_{2z}, \\
F_3(x,z,t) &= \eta_1\phi_{0tz} + \tfrac{1}{2}\eta_0^2\phi_{0t} + \eta_0\phi_{1tz} + \phi_{2t} + \eta_0\phi_{0x}\phi_{0xz} \\
&\quad \phi_{0x}\phi_{1x} + \eta_0\phi_{0z}\phi_0 + \phi_{0z}\phi_{1z}.
\end{aligned}
$$

Using the Fredholm Alternative on (3.50)–(3.54) gives the solvability conditions

$$
\frac{2}{\pi^2}\int_0^{2\pi}\int_0^{\pi} F(x,t)\cos x \sin t\,dx dt - 0.62 h_1 C = \frac{4}{\pi}\tanh h_0, \tag{3.55}
$$

and $\sin\alpha_1 = 0$. Substituting the expressions for ϕ_i and η_i, $i = 0, 1, 2, 3$, into F and using (3.55) finally yields

$$
\lambda_0\varepsilon^{-4/5}\bar{A}\sinh h_0 + \bar{A}^3 h_1 H'(h_0) + 1.80\bar{A}^5 = \frac{4}{\pi}\tanh h_0 \cos\alpha_1. \tag{3.56}
$$

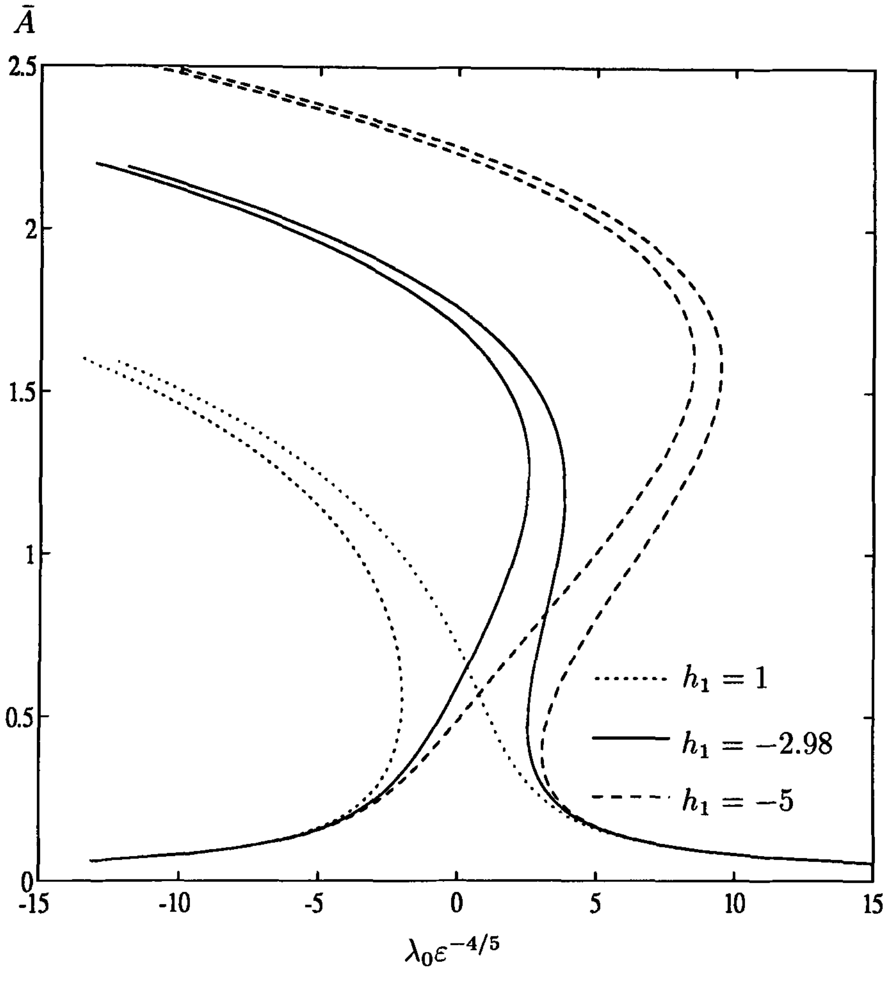

Figure 3.7: Response based on equation (3.14) showing the transition from soft to hard spring.

Figure 3.7 shows plots of the response $\bar{A}$ against $\lambda_0\varepsilon^{-4/5}$ for h_1 ranging from 1 to -5. It is clear that close to either side of this critical depth the large amplitude response is like that of a soft spring. As h_1 decreases through -2.98 the number of solutions changes from 3 to 5 and the hard spring response begins to emerge. When h_1 is very large and negative the large amplitude branches move off to infinity and the response will look like Figure 3.3 for $H < 0$. This can also be seen by taking the limit of (3.40) as $h \to h_0$. To do this we write $h = h_0 + \varepsilon^{2/5}h_1$ in (3.40) to get

$$\lambda_0\varepsilon^{-2/3}A\sinh h_0 + \varepsilon^{2/5}A^3h_1H'(h_0) + o(\varepsilon^{2/5}) = \frac{4}{\pi}\tanh h_0\cos\alpha_1,$$

which matches (3.56) as h_1 grows to $O(\varepsilon^{2/5})$ with $\bar{A} = \varepsilon^{2/15}A$.

3.4 Summary of results and surface tension effects

In this chapter we have concentrated on the resonant response due to the excitation of the fundamental eigenmode and, in particular, the change in this response when the fundamental frequency is degenerate. We considered three detuning ranges, namely $\lambda_0 \gg \varepsilon^{2/3}$ when we have a linear response, $\lambda_0 \sim \varepsilon^{2/3}$ when the nonlinear terms contain the resonant growth and $\lambda_0 \sim \varepsilon^{4/5}$ because the one-dimensional solution breaks down at a critical depth. These three cases represent the first five entries in Table 3.1 which summarises the different resonant regimes.

The other entries in the table pertain to the excitation of more than one longitudinal mode. This is the situation we will now discuss and it is of interest because it provides a stepping stone towards the infinite mode responses encountered in Part II and, in particular, will be useful in the general discussions of Chapter 6.

For the eigenfrequencies $\omega_{2,0}$ *or* $\omega_{3,0}$ to be commensurate with the forcing frequency we need to introduce surface tension into the problem. We discuss the effect of surface tension on the two-dimensional deep water model (where $\nu_{wd} = 0$) and derive the form of the response in Appendix B. We see that there is a breakdown in the solution procedure for values of σ (where σ measures the surface tension) given by (B.7) and (B.8) and, from (B.1), we see this corresponds to $\omega_{2,0} = 2\omega_{1,0}$ and $\omega_{3,0} = 3\omega_{1,0}$ respectively. We now discuss the form of the response when either

Type of Wave	Detuning Size	Breadth b	Amplitude
Longitudinal Wave[a]	$\lambda_0 \gg O(\varepsilon^{2/3})$	$\neq n$	$O(\varepsilon/\lambda_0)$
Longitudinal and Transverse Wave[b]	$\lambda_0 \gg O(\varepsilon^{2/3})$	1	$O(\varepsilon/\lambda_0)$
Longitudinal Wave[a]	$\lambda_0 \sim O(\varepsilon^{2/3})$	$\neq n$	$O(\varepsilon^{1/3})$
Longitudinal and Transverse Wave[b]	$\lambda_0 \sim O(\varepsilon^{2/3})$	1	$O(\varepsilon^{1/3})$
Longitudinal Wave[ac]	$\lambda_0 \sim O(\varepsilon^{4/5})$	$\neq n$	$O(\varepsilon^{1/5})$
Longitudinal Waves[d]	$\lambda_0 \sim O(\varepsilon^{1/2})$	$\neq n$[e]	$O(\varepsilon^{1/2})$
Longitudinal Wave[f]	$\lambda_0 \sim O(\varepsilon^{4/5})$	$\neq n$[e]	$O(\varepsilon^{2/5})$
Longitudinal Waves[g]	$\lambda_0 \sim O(\varepsilon^{2/3})$	$\neq n$[h]	$O(\varepsilon^{1/3})$

[a] $\phi_0 = A\cos x \cosh(z+h)\sin(t+\alpha_1)$.
[b] $\phi_0 = (A\cos x\sin(t+\alpha_1) + B\cos y\sin(t+\beta_1))\cosh(z+h)$.
[c] Critical depth at $h = 1.06$ such that $H(h) = 0$.
[d] $\phi_0 = A\cos x\cosh(z+h)\sin(t+\alpha_1) + C\cos 2x\cosh 2(z+h)\sin 2(t+\alpha_2)$.
[e] Critical balance between depth and surface tension, $3\sigma = \tanh^2 h$.
[f] $\phi_0 = C\cos 2x\cosh 2(z+h)\sin 2(t+\alpha_2)$.
[g] $\phi_0 = A\cos x\cosh(z+h)\sin(t+\alpha_1) + D\cos 3x\cosh 3(z+h)\sin 3(t+\alpha_3)$.
[h] Critical balance between surface tension and depth, $\sigma = (1+3\coth^2 h)^{-1}$.

Table 3.1: Different parameter regimes for resonant sloshing.

of these conditions hold (Peake [58] carried out a similar calculation in the acoustic case).

3.4.1 Second eigenfrequency commensurate with first

When (B.7) holds[3], we have $\omega_{2,0} = 2\omega_{1,0}$ and (3.1) is violated for $(n,m) = (2,0)$. This is the well known "ripple" depth first noted by Wilton [78] in his analysis of standing waves[4]. The leading-order response will be a combination of a $\sin t$ and a $\sin 2t$ term so that we only need to go to *second order* to generate $\sin t$ terms to balance with the forcing. Hence we consider the regime $\lambda_0 \sim O(\varepsilon^{1/2})$ and write

$$\lambda_0 = \lambda\varepsilon^{1/2} \quad , \quad \lambda \sim O(1),$$

[3] Note, in practice, this happens only for small h. For water, $\Gamma = 0.074$ N m^{-1}, $\rho = 1$ g cm^{-3} and the dimensional depth hL is then approximately 0.15 cm regardless of the length. Hence the length to depth aspect ratio is only $O(1)$ for tanks of short length.

[4] It is at this critical depth where dispersive and surface tension terms balance in the shallow water problem. This leads to the idea of a ripple-tank where the depth is chosen to be at this critical value and this can be exploited in experiments, where the ripple-tank is used to illustrate sound propagation (see, for example, Lighthill [40]). (Of course, as $h \to 0$, the leading-order solution comprises an infinite set if modes and not just the first two, as we shall see in the next chapter.)

in (2.17)–(2.25), and expand ϕ and η in powers of $\varepsilon^{1/2}$,

$$\begin{aligned}\phi &= \varepsilon^{1/2}\phi_0 + \varepsilon\phi_1 + \cdots,\\ \eta &= \varepsilon^{1/2}\eta_0 + \varepsilon\eta_1 + \cdots.\end{aligned}$$

The leading-order problem is the same as in previous sections, but this time the solution is

$$\begin{aligned}\phi_0 &= A\cos x\cosh(z+h)\sin(t+\alpha_1)\\ &\quad +C\cos 2x\cosh 2(z+h)\sin 2(t+\alpha_2) &(3.57)\\ \eta_0 &= -A\cos x\sinh h\cos(t+\alpha_1) - C\cos 2x\sinh 2h\cos 2(t+\alpha_2), &(3.58)\end{aligned}$$

where $A, C > 0$. Proceeding to the second order we retrieve (B.4) except that now $\phi_{1x} = \sin t$ on $x = 0, \pi$ and the penultimate equation becomes

$$(1-\sigma)\eta_1 + \tanh h(\phi_{1t} + \lambda\phi_{0t} + \eta_0\phi_{0tz} + \tfrac{1}{2}(\phi_{0x}^2 + \phi_{0z}^2)) = \sigma\eta_{0xx} \quad \text{on} \quad z = 0.$$

The Fredholm Alternative then implies that $\sin\alpha_1 = \sin 2\alpha_2 = 0$ and

$$\lambda A\cos\alpha_1 + \frac{AC}{2}\cos\alpha_1\cos 2\alpha_2(1 + 2\cosh^2 h) = \frac{4}{\pi\cosh h}, \qquad (3.59)$$

$$\lambda C\cos 2\alpha_2 = \frac{-A^2}{16\cosh 2h}(3 + 2\sinh^2 h). \qquad (3.60)$$

Figures 3.8 and 3.9 show plots of A against λ and C against λ respectively. There are some interesting features which arise due to the interaction of these two modes. Firstly, both responses exhibit the bending over reminiscent of the Duffing response and there are two branches as in the case of Section 3.2.2. More intriguing is what happens as $\lambda \to 0$ and we force the tank at exactly the fundamental frequency. As $\lambda \to 0$ the size of the first mode, A, approaches zero and the size of the second mode grows. Indeed as $\lambda \to 0$, $C \sim O(\lambda^{-1/3})$ and the solution will just contain the second mode. As C grows the term C^3 will grow and eventually come into (3.60). When this happens we will need to balance A^2, C^3 and λC and for this to be possible the leading-order response will be $O(\varepsilon^{2/5})$ in the detuning range $\lambda_0 \sim O(\varepsilon^{4/5})$. The result is expected to produce a Duffing-like effect on the solution C in this range so that the singular behaviour of C in Figure 3.9 is bent over by the nonlinearity.

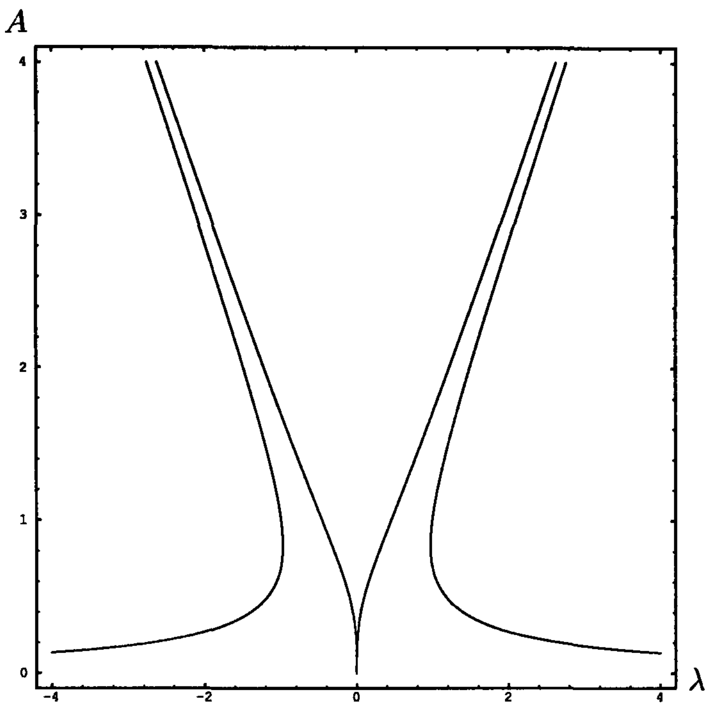

Figure 3.8: Plot of the size of the first mode in the special case when the first two modes interact.

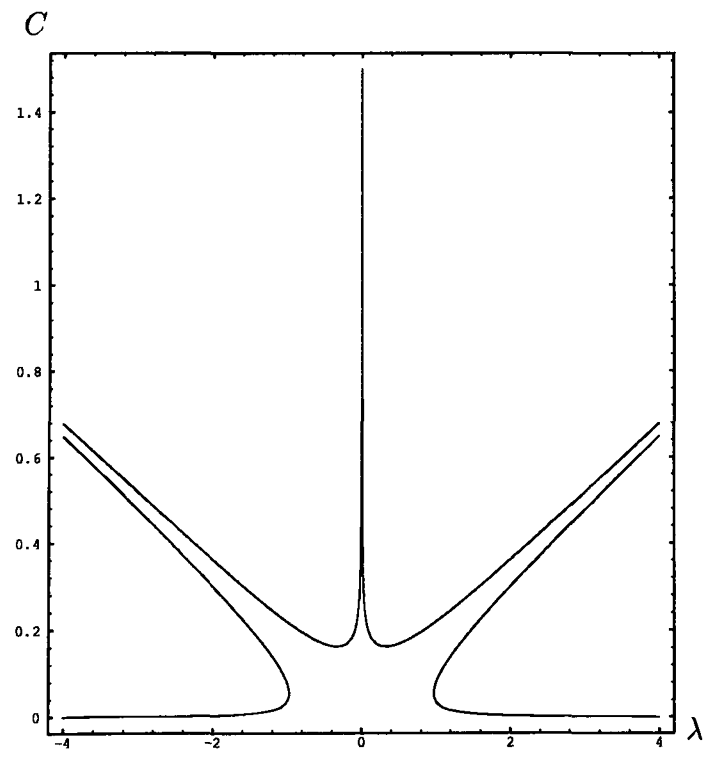

Figure 3.9: Plot of the size of the second mode in the special case when the first two modes interact.

3.4.2 Third eigenfrequency commensurate with first

When (B.8) holds the third mode is now commensurate with the first ($\omega_{3,0} = 3\omega_{1,0}$) and the leading-order response will be

$$\phi \sim \varepsilon^{1/3}(A\cos x\cosh(z+h)\sin(t+\alpha_1) + D\cos 3x\cosh 3(z+h)\sin 3(t+\alpha_3)),$$

in the detuning band $\lambda_0 = \varepsilon^{2/3}\lambda_d$. The solution will be of the form

$$\begin{aligned}(\lambda_d A + a_1A^3 + a_2AD^2)\cos\alpha_1 + a_3A^2D\cos 3\alpha_3 &= \frac{4}{\pi\cosh h},\\ (\lambda_d D + a_4D^3 + a5A^2D)\cos 3\alpha_3 + a6A^3\cos\alpha_1 &= 0,\end{aligned}$$

where $a_1, \ldots, a_6$ depend on h only and $\sin\alpha_1 = \sin 3\alpha_3 = 0$.

The two cases considered in Sections 3.4.1 and 3.4.2 show that, as more eigenfrequencies become commensurate with the fundamental, the leading-order solution may contain more than one mode. Indeed, if the first n eigenfrequencies are commensurate then the response contains the modes associated with these frequencies with their amplitudes satisfying n coupled cubic equations. Clearly the type of response becomes more complex and in Part II we will see how the response changes as $n \to \infty$.

Finally, we note that the effect of damping on all the responses listed in Table 3.1 will be to round of the resonant peaks in the same way as for Duffing's equation (see Figure 1.1).

Part II

Shallow water sloshing and analogies with acoustic oscillations

Chapter 4

One-dimensional solutions of the problems of shallow water sloshing and acoustics

We have seen in the last chapter that, when $h \geq O(1)$ for a tank with a rectangular cross-section, it is generally the case that only the fundamental eigenmode is excited and at most, in certain special cases, two modes are excited. The key to why only one or two modes are excited was seen to lie in the non-commensurability of the spectrum. In this chapter we will consider what happens when $h \ll 1$ and the fundamental observation in this case is that the number of commensurate eigenvalues changes from one or two to an infinite number. This can be seen simply by considering (2.12) which, for $h \ll 1$, gives

$$\omega_{n,m} \sim \left(n^2 + \frac{m^2}{b^2}\right)^{\frac{1}{2}} \omega_{1,0} + o(h),$$

so $\omega_{n,0}$ are all commensurate with $\omega_{1,0}$ and, when $b = l$, all $\omega_{n,m}$ such that

$$n^2 + \frac{m^2}{l^2} = \text{integer}^2, \tag{4.1}$$

are commensurate. Hence the shallow water problem is very different from the case $h \geq O(1)$.

Historically, water waves in shallow water have been of great interest. After Scott Russell's [62] observation of a solitary wave, Kortweg & de Vries [37] derived the scalings which led to the famous Korteweg-de Vries equation that determines the evolution of one-dimensional[1] wave packets and predicted the solitary wave observed by Russell [62]. Another interesting feature of shallow water theory is that, under the assumptions that the mean depth is comparable to the amplitude of the surface waves but small compared with the wavelength of the waves, Euler's equations can be written in the form

$$\left[\frac{\partial}{\partial t} + (u \pm s)\frac{\partial}{\partial x}\right](u \pm 2s) = 0,$$

(in dimensional form) where u is the velocity and $s = \sqrt{g\tilde{\eta}}$ (where $\tilde{\eta}$ is the depth of the fluid). This form of the equations is the same as for homentropic one-dimensional gas dynamics if we identify s with the speed of sound, a, and set the ratio of specific heats, γ, to be 2 (see, for instance, Stoker [66] or Whitham [79]). For small amplitude disturbances both problems thus satisfy the one-dimensional wave equation. We have to go to second order to see the difference that dispersive effects have on the shallow water problem and, even then, these effects can be removed by introducing weak surface tension into the problem and considering the "ripple depth" (see Lighthill [40]).

The resonance problem was tackled first by Chester [14] for one-dimensional acoustic oscillations in a resonator with a piston at one end (see Figure 1.2(a)). He showed that the leading-order velocity potential took the form $g(t+x) + g(t-x)$ where g satisfies what is commonly referred to as Chester's equation,

$$\lambda g'' + (\gamma + 1)g'g'' = -\frac{1}{\pi}\sin t, \tag{4.2}$$

has period 2π and g' has zero mean over one period. This equation provides the fundamental building block for any analysis of either acoustic oscillations or shallow water sloshing. The most interesting consequence of this equation is that, for sufficiently small λ, the solution contains a jump or shock. A unique solution is found in this detuning range by considering a one-dimensional stability analysis of the possible solutions (see Appendix A.1.2). This shows that perturbations to a constant-velocity shock only die away when the shock is compressive, i.e. when g'

[1]Throughout the work on shallow water we will refer to solutions depending only on x and t as one-dimensional and ones depending on x, y and t as two-dimensional. Thus we regard one-dimensional shallow water solutions as the limiting case of two-dimensional deep water solutions.

decreases across the shock, and we use this condition for the shock solutions that we will consider.

We can build additional physical mechanisms into this model. Dissipation can be included through a viscous boundary layer in the walls of the resonator (Chester [14]) or on the base of the tank (Chester [15]) in the form of a convolution term (see Section 4.7). For shallow water (setting $\gamma = 2$), Chester [15] included an integral term representing dispersion but Ockendon & Ockendon [54] derived a generalised form of (4.2) with a fourth-order derivative term representing dispersion and this is identical to the highest-order term found in the Korteweg-de Vries equation. The coefficient of this fourth-order term, when weak surface tension effects are included, was found by Johnson [33] to be $\sigma_s - \kappa^2/3$ (σ_s and κ denoting the scaled surface tension coefficient and depth respectively) and we regain Chester's equation at the ripple depth, $\sigma_s = \kappa^2/3$.

The introduction of small area variations in the resonator was shown by Keller [36] to introduce, on the right-hand side of (4.2), a convolution term between g and the function representing cross-sectional area. The effect of this term on solutions to (4.2) has been studied by Keller [36], Ockendon *et al* [57], Peake [58], Chester [18] and Ellermeier [25], who all found that increasing the size of the area variation decreases the ranges of λ for which shock solutions occur. However, parameter regimes emerged away from $\lambda = 0$ where shocks were to be found. Ockendon *et al* and Peake have shown how this ties in with the increasing destruction of the commensurability of the spectrum as the area variation increases.

The goals for the rest of this thesis are thus as follows. Firstly, we wish to carry out an analysis similar to that of Keller's in the acoustic case to see how the higher-order Chester equation derived by Ockendon & Ockendon for the shallow water problem is altered by perturbing the base of a sloshing tank. Hence, in Section 4.1, we formulate the shallow water limit of the problem given in Section 2.1. The leading-order solution is found to satisfy the two-dimensional wave equation and its form is determined by a solvability condition on the second-order problem. However, when there are no variations in the back wall[2] ($\nu_{w0} = 0$), we find that the leading-order velocity potential is independent of y and is just $f(t + x) + f(t - x)$

[2]We will consider the effect of wall variations in the next chapter.

where f satisfies an integro-differential equation that we show to be equivalent to Keller's equation in the absence of dispersion.

We then concentrate on the nonlinear and geometric terms in this integro-differential equation by ignoring dispersion. In Section 4.4 we recall the solutions of Chester's equation (found by setting $\nu_{b0} = 0$) and then in Section 4.4.2 we analyse the effect of geometric imperfections $\nu_{b0} \sim O(\varepsilon^{1/2})$ on these solutions. The work of Ockendon *et al* [57] suggests a finite mode response when $\nu_{b0} \sim O(1)$, but we find in Section 4.5 that for special classes of geometry, the response still contains an infinite number of modes.

In Section 4.6, we re-introduce dispersion and discuss its effects on the solutions already found. Finally, in Section 4.7, we summarise the results in this chapter and discuss the implications that dissipation may have on the solution.

4.1 Shallow water sloshing

4.1.1 Re-scalings

As we discussed in Section 2.1, the correct detuning regime when there are an infinite number of commensurate eigenfrequencies is $\lambda_0 \sim O(\varepsilon^{1/2})$ where $\phi \sim O(\varepsilon^{1/2})$ (and the detuning balances with the nonlinearity and forcing at second order). Hence we take

$$\lambda_0 = \lambda\varepsilon^{1/2} \quad , \quad \lambda \sim O(1). \tag{4.3}$$

The correct depth scale can be found by considering the expression (2.16) for the forcing frequency which, for $h = \varepsilon^{\beta}\kappa$ ($\beta > 0$), gives

$$\Omega^2 = \frac{g}{L}\varepsilon^{\beta}\kappa(1+\lambda\varepsilon^{1/2})(1+\varepsilon^{2\beta}\kappa^2).$$

We choose β so that the dispersive term balances with the detuning, i.e. $\beta = 1/4$, and we put

$$h = \kappa\varepsilon^{1/4} \quad , \quad \kappa \sim O(1); \tag{4.4}$$

we also rescale z by writing $z = \varepsilon^{1/4}\bar{z}$. The linearised free surface height is, from (2.23) and (2.27),

$$\begin{aligned}\eta &\sim (\varepsilon/\lambda_0)A\sinh h\cos x\sin t\\ &\sim \varepsilon^{3/4}A\kappa\cos x\sin t,\end{aligned}$$

in this regime and hence we scale ϕ and η by

$$\phi = \varepsilon^{1/2}\bar{\phi} \quad , \quad \eta = \varepsilon^{3/4}\bar{\eta},$$

so that, in dimensional quantities, the surface height is $O(\varepsilon^{3/4}L)$ which is much greater than the amplitude of the forcing which is $O(\varepsilon L)$, but is less than the depth of the water which is $O(\varepsilon^{1/4}L)$. Finally, we choose ν_{w0} and ν_{b0} so that the effect of the back wall and base geometry comes in at the same order as dispersion. Hence we write

$$\nu_{b0} = \nu_b \varepsilon^{1/2} \quad , \quad \nu_{w0} = \nu_w \varepsilon^{1/2} \quad , \quad \nu_b, \nu_w \sim O(1), \tag{4.5}$$

although we could deal with stronger geometric effects and this will be discussed in more detail in Sections 4.5 and 6.1.

4.1.2 Shallow water model

With these scalings, (2.17)–(2.25) become

$$\begin{aligned}
\bar{\phi}_{\bar{z}\bar{z}} &= -\varepsilon^{1/2}(\bar{\phi}_{xx} + \bar{\phi}_{yy}), && (4.6)\\
\bar{\phi}_x &= \varepsilon^{1/2}\sin t \quad \text{on} \quad x = -\varepsilon\cos t, \pi - \varepsilon\cos t, && (4.7)\\
\bar{\phi}_y &= 0 \quad \text{on} \quad y = 0, && (4.8)\\
\bar{\phi}_y &= \nu_w b\pi\varepsilon^{1/2}\bar{\phi}_x a_w'(x) \quad \text{on} \quad y = b\pi[1 + \nu_w\varepsilon^{1/2}a_w(x)], && (4.9)\\
\bar{\phi}_{\bar{z}} &= -\nu_b\kappa\varepsilon\bar{\phi}_x a_b'(x) \quad \text{on} \quad \bar{z} = -\kappa[1 + \nu_b\varepsilon^{1/2}a_b(x)], && (4.10)\\
\nabla\bar{\phi}(x, y, \varepsilon^{1/4}\bar{z}, t) &= \nabla\bar{\phi}\,(x, y, \varepsilon^{1/4}\bar{z}, t + 2\pi), && (4.11)
\end{aligned}$$

and, on $\bar{z} = \varepsilon^{1/2}\bar{\eta}$,

$$\begin{aligned}
\bar{\phi}_{\bar{z}} &= \varepsilon^{1/2}\bar{\eta}_t + \varepsilon\bar{\phi}_x\bar{\eta}_x + \varepsilon\bar{\phi}_y\bar{\eta}_y, && (4.12)\\
\bar{\eta} &+ \kappa\left(1 - \frac{\kappa^2}{3}\varepsilon^{1/2} + O(\varepsilon)\right)\left(1 + \lambda\varepsilon^{1/2}\right)\\
&\left(\bar{\phi}_t + \frac{1}{2}\left[\bar{\phi}_{\bar{z}}^2 + \varepsilon^{1/2}\left\{\bar{\phi}_x^2 + \bar{\phi}_y^2\right\}\right]\right) = 0. && (4.13)
\end{aligned}$$

We now proceed to expand $\bar{\phi}$ and $\bar{\eta}$ in powers of $\varepsilon^{1/2}$ as

$$\begin{aligned}
\bar{\phi} &= \phi_0 + \varepsilon^{1/2}\phi_1 + \varepsilon\phi_2 + \cdots, && (4.14)\\
\bar{\eta} &= \eta_0 + \varepsilon^{1/2}\eta_1 + \varepsilon\eta_2 + \cdots, && (4.15)
\end{aligned}$$

and look to find a solvability condition on the second-order problem, in much the same way as in Chapter 3. Hence we first consider the $O(1)$ terms arising from (4.6)–(4.13) when (4.14) and (4.15) are substituted in. These are

$$\begin{aligned}
\phi_{0\bar{z}\bar{z}} &= 0, \\
\phi_{0\bar{z}} &= 0 \quad \text{on} \quad \bar{z} = -\kappa, \\
\phi_{0x} &= 0 \quad \text{on} \quad x = 0, \pi, \\
\phi_{0y} &= 0 \quad \text{on} \quad y = 0, b\pi, \\
\eta_0 &= -\kappa\phi_{0t} \quad \text{on} \quad \bar{z} = 0, \\
\nabla\phi_0(x, y, 0, t) &= \nabla\phi_0(x, y, 0, t + 2\pi),
\end{aligned}$$

and have solution

$$\phi_0 = A(x, y, t), \tag{4.16}$$

$$\eta_0 = -\kappa A_t, \tag{4.17}$$

where $A(x, y, t)$ is an unknown function which satisfies

$$A_x = 0 \quad \text{on} \quad x = 0, \pi, \tag{4.18}$$

$$A_y = 0 \quad \text{on} \quad y = 0, b\pi, \tag{4.19}$$

$$\nabla A(x, y, t) = \nabla A(x, y, t + 2\pi). \tag{4.20}$$

At $O(\varepsilon^{1/2})$ equations (4.6), (4.10) and (4.11) yield

$$\begin{aligned}
\phi_{1\bar{z}\bar{z}} &= -\phi_{0xx} - \phi_{0yy}, \\
\phi_{1\bar{z}} &= 0 \quad \text{on} \quad \bar{z} = -\kappa, \\
\nabla\phi_1(x, y, 0, t) &= \nabla\phi_1(x, y, 0, t + 2\pi),
\end{aligned}$$

which can be solved to give

$$\phi_1 = -\frac{1}{2}\left(A_{xx} + A_{yy}\right)\left(\bar{z} + \kappa\right)^2 + B(x, y, t), \tag{4.21}$$

where $B(x, y, t)$ is an unknown function with

$$\nabla B(x, y, t) = \nabla B(x, y, t + 2\pi). \tag{4.22}$$

Also, on $\bar{z} = 0$, (4.12) gives at $O(\varepsilon^{1/2})$

$$\phi_{1\bar{z}} = \eta_{0t},$$

which, using (4.17) and (4.21), results in A satisfying the two-dimensional wave equation

$$A_{xx} + A_{yy} = A_{tt}. \tag{4.23}$$

Finally to $O(\varepsilon^{1/2})$ note that (4.7), (4.8) and (4.9) give

$$\begin{aligned}
\phi_{1x} &= \sin t \quad \text{on} \quad x = 0, \pi, &(4.24)\\
\phi_{1y} &= 0 \quad \text{on} \quad y = 0, &(4.25)\\
\phi_{1y} &= b\pi\nu_w\left[A_x a'_w(x) - A_{yy} a_w(x)\right] \quad \text{on} \quad y = b\pi, &(4.26)
\end{aligned}$$

and, on $\bar{z} = 0$, (4.13) gives

$$\eta_1 + \kappa\phi_{1t} + \left(\lambda - \frac{\kappa^2}{3}\right)\phi_{0t} + \frac{\kappa}{2}\left(\phi_{0x}^2 + \phi_{0y}^2\right) = 0. \tag{4.27}$$

The $O(\varepsilon)$ terms in (4.6) and (4.10) are

$$\begin{aligned}
\phi_{2\bar{z}\bar{z}} &= -\phi_{1xx} - \phi_{1yy},\\
\phi_{2\bar{z}} &= \nu_b\kappa[\phi_{0\bar{z}\bar{z}} a_b(x) - \phi_{0x} a'_b(x)] \quad \text{on} \quad \bar{z} = -\kappa,
\end{aligned}$$

which imply that

$$\begin{aligned}
\phi_{2\bar{z}} = {} & \frac{1}{6}\left(A_{xxxx} + 2A_{xxyy} + A_{yyyy}\right)(\bar{z} + \kappa)^3 - \left(B_{xx} + B_{yy}\right)(\bar{z} + \kappa)\\
& -\nu_b\kappa[A_x a'_b(x) + (A_{xx} + A_{yy}) a_b(x)]. &(4.28)
\end{aligned}$$

Also, from (4.12),

$$\phi_{2\bar{z}} = \eta_{1t} + \phi_{0x}\eta_{0x} + \phi_{0y}\eta_{0y} - \eta_0\phi_{1\bar{z}\bar{z}} \quad \text{on} \quad \bar{z} = 0, \tag{4.29}$$

so combining (4.27) and (4.29),

$$\begin{aligned}
\phi_{2\bar{z}} = {} & -\kappa\phi_{1tt} + \left(\frac{\kappa^2}{3} - \lambda\right)\phi_{0tt} - \kappa\phi_{0x}\phi_{0xt}\\
& -\kappa\phi_{0y}\phi_{0yt} + \phi_{0x}\eta_{0x} + \phi_{0y}\eta_{0y} - \eta_0\phi_{1\bar{z}\bar{z}} \quad \text{on} \quad \bar{z} = 0.
\end{aligned}$$

Using this with (4.16), (4.17), (4.21) and (4.28) we find that B satisfies the following non-homogeneous two-dimensional wave equation,

$$\begin{aligned} B_{xx} + B_{yy} - B_{tt} &= -\frac{\kappa^2}{3}\left(A_{xxxx} + 2A_{xxyy} + A_{yyyy}\right) + A_t A_{tt} \\ &\quad + \left(\lambda - \frac{\kappa^2}{3}\right) A_{tt} + 2A_x A_{xt} + 2A_y A_{yt} \\ &\quad - \nu_b[a_b'(x)A_x + a_b(x)A_{tt}], \end{aligned} \tag{4.30}$$

and conditions (4.24)–(4.26) and (4.22) become

$$B_x = \sin t \quad \text{on} \quad x = 0, \pi, \tag{4.31}$$

$$B_y = 0 \quad \text{on} \quad y = 0, \tag{4.32}$$

$$B_y = \nu_w b\pi\left[A_x a_w'(x) - A_{yy} a_w(x)\right] \quad \text{on} \quad y = b\pi, \tag{4.33}$$

$$\nabla B(x,y,t) = \nabla B(x,y,t+2\pi). \tag{4.34}$$

Hence, to determine the leading-order response, we need to find a solution of

$$A_{xx} + A_{yy} = A_{tt}, \tag{4.35}$$

$$A_x = 0 \quad \text{on} \quad x = 0, \pi, \tag{4.36}$$

$$A_y = 0 \quad \text{on} \quad y = 0, b\pi, \tag{4.37}$$

$$\nabla A(x,y,t) = \nabla A(x,y,t+2\pi), \tag{4.38}$$

such that a solution to (4.30)–(4.34) exists.

We will return to this fully two-dimensional problem in the next chapter but for the rest of this chapter we set $\nu_w = 0$, so that the problem is independent of y, and we have to solve the problem shown in Table 4.1 with

$$\begin{aligned} F(x,t) &= -\frac{\kappa^2}{3} A_{xxxx} + \left(\lambda - \frac{\kappa^2}{3}\right) A_{tt} + 2A_x A_{xt} \\ &\quad + A_t A_{tt} - \nu_b[a_b'(x)A_x + a_b(x)A_{tt}], \end{aligned} \tag{4.39}$$

and $f_1 = 1$.

4.2 Acoustic oscillations

For the purpose of comparing the acoustic problem outlined in Section 2.2 with one-dimensional solutions of the shallow water sloshing problem, we consider a

Homogeneous Problem	Inhomogeneous Problem
$A_{xx} - A_{tt} = 0$	$B_{xx} - B_{tt} = F(x,t)$
$A_x = 0 \quad \text{on} \quad x = 0, \pi$	$B_x = f_1 \sin t \quad \text{on} \quad x = 0$
	$B_x = \sin t \quad \text{on} \quad x = \pi$
∇A 2π-periodic in t	∇B 2π-periodic in t

Table 4.1: The one-dimensional problem for shallow water sloshing and acoustics where $F(x,t)$ is quadratic in A.

simplified problem by taking $\nu_{w0} = 0$ and $a_b(x,y) = a_b(x)$ in (2.56)–(2.61). Then, putting

$$\nu_{b0} = \nu_b \varepsilon^{1/2} \quad , \quad \nu_b \sim O(1), \tag{4.40}$$

as in the last section, and expanding φ as

$$\varphi = A(x,t) + \varepsilon^{1/2} B(x,t) + \cdots, \tag{4.41}$$

we arrive at the same problem as in Table 4.1, where $F(x,t)$ is this time given by

$$F(x,t) = \lambda A_{tt} + 2A_x A_{xt} + (\gamma - 1) A_t A_{tt} - \nu_b a_b'(x) A_x, \tag{4.42}$$

and $f_1 = 0$.

4.3 Integro-differential equations for one-dimensional problems

4.3.1 The Fredholm Alternative applied to an inhomogeneous wave equation

The paradigm problem for one-dimensional resonant sloshing and acoustics has been shown to be given by the problems in Table 4.1. The solution for $A(x,t)$ is determined by applying the Fredholm Alternative to the inhomogeneous problem for $B(x,t)$. This is done, following the technique presented in Ockendon *et al* [57], by multiplying the wave equation for $B(x,t)$ by all the solutions to the homogeneous problem for $A(x,t)$, integrating by parts and using the boundary conditions to get

$$\int_\theta^{2\pi+\theta} \int_0^\pi F(x,t) \cos nx \cos n(t-\theta) \mathrm{d}x \mathrm{d}t = -(1 + f_1)\pi \sin\theta \delta_{n1}, \tag{4.43}$$

for any θ. Summing (4.43) over all n and using the completeness relation (see Lighthill [39])

$$\begin{aligned}\sum_{n=1}^{\infty} \cos nx \cos n(t-\theta) &= -\frac{1}{2} + \frac{\pi}{2}\left(\sum_{-\infty}^{\infty} \delta(x+t-\theta-2n\pi)\right. \\ &\quad \left. + \sum_{-\infty}^{\infty} \delta(x-t+\theta-2n\pi)\right), \end{aligned} \tag{4.44}$$

for $0 < t-\theta < 2\pi$, we find

$$\int_t^{t+\pi} F(s-t,s)\mathrm{d}s + \int_{t+\pi}^{t+2\pi} F(t+2\pi-s,s)\mathrm{d}s = -2(1+f_1)\sin t. \tag{4.45}$$

Peake (private correspondence) has shown conversely that starting from (4.45) it is possible to satisfy all the orthogonality conditions inferred from the Fredholm Alternative.

4.3.2 Integro-differential equations

We are now in a position to solve the problems for $A(x,t)$ for both sloshing and acoustic problems.

Shallow water sloshing

The leading-order problem clearly has the solution

$$\phi_0 = A(x,t) = f_+ + f_-, \tag{4.46}$$

where $f_\pm = f(t \pm x)$ and f is 2π-periodic. Thus we find (4.39) can be written as

$$\begin{aligned} F(x,t) &= -\frac{\kappa^2}{3}(f_+^{(iv)} + f_-^{(iv)}) + \left(\lambda - \frac{\kappa^2}{3}\right)(f_+'' + f_-'') \\ &\quad +2(f_+' - f_-')(f_+'' - f_-'') + (f_+'' + f_-'')(f_+' + f_-') \\ &\quad -\nu_b[a_b'(x)(f_+' - f_-') + a_b(x)(f_+'' + f_-'')], \end{aligned} \tag{4.47}$$

and using (4.45) yields

$$\begin{aligned} \frac{\kappa^2}{3} f^{(iv)}(t) + \left(\frac{\kappa^2}{3} - \lambda + \frac{\nu_b}{\pi}\int_0^\pi a_b(s)\mathrm{d}s\right) f''(t) - 3f'(t)f''(t) = \frac{2}{\pi}\sin t \\ -\frac{\nu_b}{4\pi}\int_0^\pi f'(2s+t)[a_b'(s) - a_b'(\pi - s)]\mathrm{d}s, \end{aligned} \tag{4.48}$$

where f is 2π-periodic and, because ϕ is a velocity potential, f is continuous or, by virtue of the periodicity, f' has zero mean over one period. Also, in the anticipation of shock solutions, we require f' to decrease across any shocks for the reasons given at the start of this chapter (see also Appendix A.1.2). The detuning in (4.48) is shifted by an amount proportional to the average value of the base variation and this could have been predicted by the effect of small base variations on the linearised fundamental frequency. The effect of the average base variation can hence be removed by redefining λ and from now on we assume this average is zero, although we will renew our interest in this term when we consider the case $\nu_b \sim O(1)$ in Section 4.5. We also note that the introduction of weak surface tension (see Appendix B) just results in (4.48) with $\kappa^2/3$ being replaced everywhere by $\kappa^2/3-\sigma_s$ (where $\sigma = \varepsilon^{1/2}\sigma_s$ measures the strength of surface tension) and dispersive effects are removed at the ripple depth, $\sigma_s = \kappa^2/3$.

Acoustic oscillations

We write the leading-order solution as

$$\varphi_0 = g(t+x) + g(t-x), \tag{4.49}$$

where g is 2π-periodic and is used instead of f to discern between the two problems. A similar expression to (4.47) is found from (4.42) and (4.45) this time gives

$$\lambda g'' + (\gamma+1)g'g'' + \frac{1}{\pi}\sin t = \frac{\nu_b}{2\pi}\int_0^{\pi}[a_b'(\tau) - a_b'(\pi-\tau)]g'(t+2\tau)\mathrm{d}\tau, \tag{4.50}$$

where g has period 2π, g' has zero mean over one period and decreases across any shocks. We refer to this as Keller's equation.

In the absence of dispersion, (4.48) and (4.50) are of the same form and we can transform between the two using

$$g \longleftrightarrow \left(\frac{3}{2(\gamma+1)}\right)^{\frac{1}{2}} f \ , \ \lambda \longleftrightarrow \left(\frac{\gamma+1}{6}\right)^{\frac{1}{2}} \lambda \ , \ \nu_b \longleftrightarrow \frac{\nu_b}{4}\left(\frac{2(\gamma+1)}{3}\right)^{\frac{1}{2}}, \tag{4.51}$$

where the acoustic variables are on the left and the fluid variables are on the right. Hence all results for the sloshing problem in the absence of dispersion can be simply related to the acoustic problem.

4.4 Geometric effects in one dimension

We now focus our attention on the effect that the slowly varying geometry has on the type of solutions that arise. Hence we will defer consideration of dispersive effects until Section 4.6 by setting $\kappa = 0$ in (4.48) (and hence we could be studying (4.50)). To see the effect of non-zero ν_b we first summarise the solutions found by taking $\nu_b = 0$ and then see how these solutions change as ν_b increases.

4.4.1 Basic solution

For $\nu_b = \kappa = 0$, (4.48) becomes

$$\lambda f''(t) + 3f'(t)f''(t) = -\frac{2}{\pi}\sin t, \tag{4.52}$$

Chester's equation, where f is 2π-periodic, f' has zero mean over one period and decreases across any shocks. Solutions of this equation can readily be found by integrating (4.52) once and rearranging to give

$$\left(f'(t) + \frac{\lambda}{3}\right)^2 = \frac{8}{3\pi}\left(\cos^2\frac{t}{2} + c\right), \tag{4.53}$$

where c is a constant depending on the value of λ, chosen so that f' has zero mean. Thus, for continuous solutions, this is only possible for $|\lambda| \geq \lambda^* = \pm(96/\pi^3)^{1/2}$ (where $\lambda = \pm\lambda^*$ corresponds to $c = 0$) because c must remain positive to ensure that the right-hand side of (4.53) is positive throughout the period. Hence, for $|\lambda| \geq \lambda^*$, we have

$$f'(t) = -\frac{\lambda}{3} \pm \left(\frac{8}{3\pi}\left[\cos^2\frac{t}{2} + c\right]\right)^{\frac{1}{2}}, \tag{4.54}$$

where we take the positive root for λ positive and vice versa. The condition that f' has zero mean then yields

$$\frac{\pi\lambda}{3} = \pm\left(\frac{8}{3\pi}\right)^{\frac{1}{2}}\int_0^{\pi}\left(\cos^2\frac{t}{2} + c\right)^{\frac{1}{2}} dt \quad \text{or} \quad \lambda = \pm\left(\frac{96}{\pi^3}\right)^{\frac{1}{2}}(1+c)E([1+c]^{1/2}), \tag{4.55}$$

where E is the complete elliptic integral of the second kind. Hence, given c we can find λ from a table of elliptic integrals (e.g. Byrd & Friedman [12]).

For $|\lambda| < \lambda^*$, we fix $c = 0$ and construct a discontinuous solution, based on the work of Betchov [6], where

$$f'(t) + \frac{\lambda}{3} = \left(\frac{8}{3\pi}\right)^{\frac{1}{2}} \begin{cases} \cos\frac{t}{2}, & -\pi < t < t^*, \\ -\cos\frac{t}{2}, & t^* < t < \pi, \end{cases} \tag{4.56}$$

and t^* is determined from the zero mean condition to be

$$t^* = 2\arcsin\left[\frac{1}{4}\left(\frac{\pi^3}{6}\right)^{\frac{1}{2}}\lambda\right] \tag{4.57}$$

Note that this unique solution has been found by enforcing the condition that f' decreases across a shock (see Appendix A.1.2). Figure 4.1 shows plots of $(f' + \lambda/3)$ for various values of λ. Shock solutions similar to those shown have been observed experimentally by Chester & Bones [16], Bridges [8] (for sloshing) and Sturtevant [69] (for acoustics).

4.4.2 Geometrical effects

Let us now consider (4.48) when $\kappa = 0$ but $\nu_b \neq 0$, that is

$$\lambda f''(t) + 3f'(t)f''(t) = -\frac{2}{\pi}\sin t + \frac{\nu_b}{4\pi}\int_0^\pi f'(2s+t)[a_b'(s) - a_b'(\pi - s)]\mathrm{d}s, \tag{4.58}$$

which is just Keller's equation (4.50) after the use of (4.51). The convolution term on the right-hand side of (4.58) is, in general, difficult to deal with. However, there are several cases when this equation simplifies and progress can be made.

(a) For an anti-symmetric base, $a_b'(x) = a_b'(\pi - x)$, (4.58) clearly reduces to Chester's equation and the geometry has no effect to this order.

(b) For a parabolic base, $a_b'(x) = 2x$, (4.48) reduces to an ordinary differential equation,

$$\lambda f'' + 3f'f'' + \frac{2}{\pi}\sin t = \frac{\nu_b}{2}f.$$

This was solved numerically by Peake [58] to see where in the (λ, ν_b)-plane shock solutions occured. When $\nu_b = 0$, we recall that the shock band is given by $|\lambda| \leq \lambda^*$. As ν_b increases this shock region changes and new shock regions, away from $\lambda = 0$, emerge (as can be seen with forward reference to

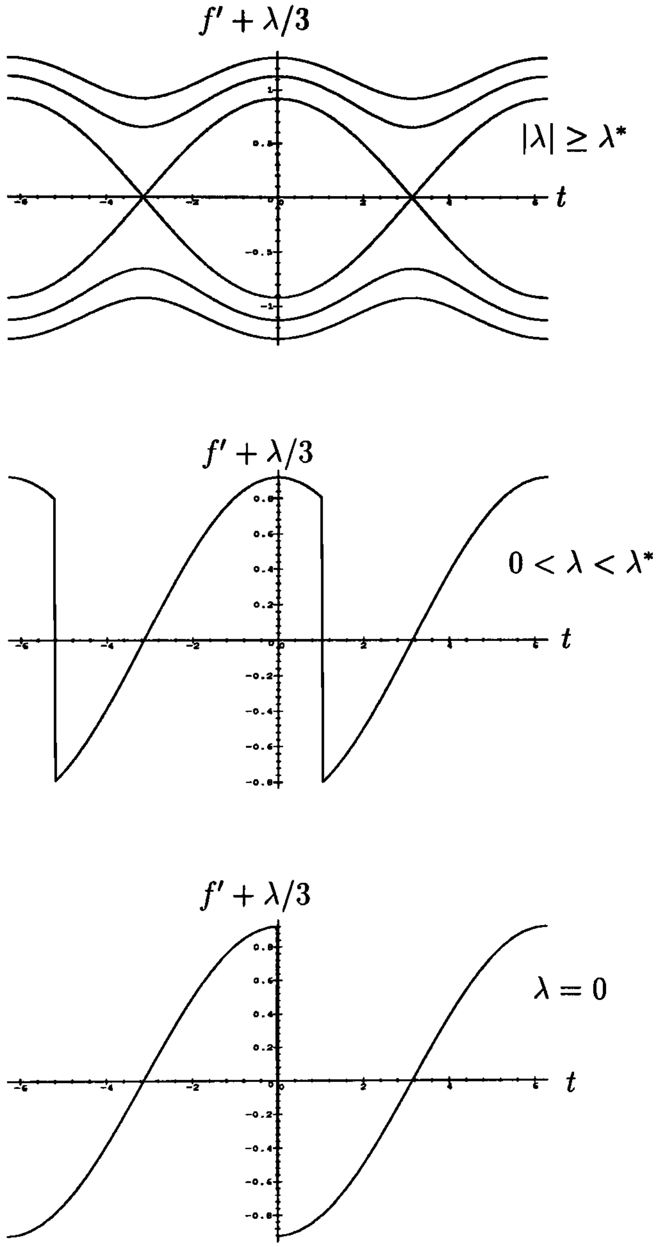

Figure 4.1: Continuous and discontinuous solutions of (4.52).

Figure 4.2). These shock regions take the form of "fingers" that get thinner as ν_b increases. The final picture, indicating the shock/no-shock interface, looks like a finger centred on $\lambda = 0$ with additional fingers attached to it, lying along the lines $\lambda = -\nu_b/(2n^2)$, for all $n = 1, 2, \ldots$. These lines correspond to the resonant growth of a single mode in the solution as $\nu_b \to \infty$ with $\lambda \sim \nu_b$ as can be seen by writing, in this limit, $f \sim \nu_b^{-1} f_0 + \nu_b^{-3} f_1 + \cdots$ to get

$$f \sim \frac{2}{\pi(2\lambda + \nu_b)} \sin t + \frac{48}{\pi^2(2\lambda + \nu_b)^2(8\lambda + \nu_b)} \sin 2t + \cdots .$$

(c) If we write $a_b(x)$ and $f'(t)$ as Fourier series,

$$a_b(x) = \sum_{n=1}^{\infty} \gamma_{bn} \cos nx, \tag{4.59}$$

$$f'(t) = \sum_{n=1}^{\infty} A_n \cos(nt + \alpha_n), \tag{4.60}$$

then (4.58) yields

$$\lambda f' + \frac{3}{2}(f')^2 = c + \frac{2}{\pi} \cos t - \frac{\nu_b}{2} \sum_{n=1}^{\infty} A_n \gamma_{b2n} \cos(nt + \alpha_n), \tag{4.61}$$

where c is a constant. Note that only the *even* harmonics of $a_b(x)$ are important. This is because the boundary condition (4.33) has as its right-hand side terms of the form $A_x a_b'(x)$ and the only resonant contribution from these terms is due to the even terms in the Fourier series for $a_b(x)$. Progress can now be made by taking a finite number of even harmonics in the Fourier series for $a_b(x)$. Keller [36] considered the case $\gamma_{b2n} = 0$ $(n \neq 1)$ and Chester [18] considered the case $\gamma_{b2n} = 0$ $(n \neq 1, 2)$. Both analyses showed the emergence of fingers in the (λ, ν)-plane and a generalisation of the limiting argument given in (b) shows that these fingers lie close to the lines

$$\lambda = -\frac{\gamma_{b2n}}{2} \nu_b. \tag{4.62}$$

To illustrate this effect we extend the method of Chester [18] to the case $\gamma_{b2n} = 0$ $(n \neq 1, 2, 3)$.

Shock structure when $\gamma_{b2n} = 0$ for $n \neq 1, 2, 3$

We use the case where only the first three even harmonics of $a_b(x)$ do not vanish to illustrate how progress can be made analytically on (4.61) and to confirm the numerical predictions of Peake [58] and the asymptotic predictions of (4.62). Hence we aim to find where in the (λ, ν_b)-plane the solution contains a shock. To do this we consider (4.61) which, in this instance, can be written as

$$\begin{aligned}\left(f' + \frac{\lambda}{3}\right)^2 &= \frac{4}{3\pi}[c + \cos t] - \frac{\nu_b}{3}[\gamma_{b2} A_1 \cos(t + \alpha_1) \\ &\quad + \gamma_{b4} A_2 \sin(2t + \alpha_2) + \gamma_{b6} A_3 \cos(3t + \alpha_3)]. \qquad (4.63)\end{aligned}$$

Clearly, as in the last section, continuous solutions can be found for a fixed value of ν_b in detuning ranges determined by the condition that f' has zero mean and by varying c. However, there will again be situations where no continuous solution can be found and shock solutions occur. We have calculated these regions analytically using a method similar to Chester [18] but the details are very involved so we do not give them here. Instead, we illustrate the resulting shock pictures in two cases.

- We first confirm the numerical results of Peake [58] using a truncated Fourier series of $a_b'(x) = 2x$. Hence we write

$$a_b(x) = \sum_{n=1}^{7} 4\frac{(-1)^n}{n^2} \cos nx$$

  (where we could include further *odd* harmonics). The resulting (λ, ν_b) picture is shown in Figure 4.2 along with the approximation for $a_b(x)$. The region between the solid lines (in the same sense as Figure 4.3) shows where shocks occur. We also plot the result when $\gamma_{b6} = 0$ (the dotted line) to illustrate how the introduction of the third even harmonic alters the structure of the solution. The introduction of a third (thinner) finger can clearly be seen.

- Next we emphasise the *decreasing* importance of an increasing number of harmonics in $a_b(x)$ by considering the case $\gamma_{b2} = \gamma_{b4} = 0$ and we take $\gamma_{b6} = 1$ without loss of generality and this leads to the shock picture given in Figure 4.3 (where shocks are found in the shaded region). This should be contrasted with Chester's [18] Figure 2(a) (only γ_{b2} non-zero) and Figure 2(b)

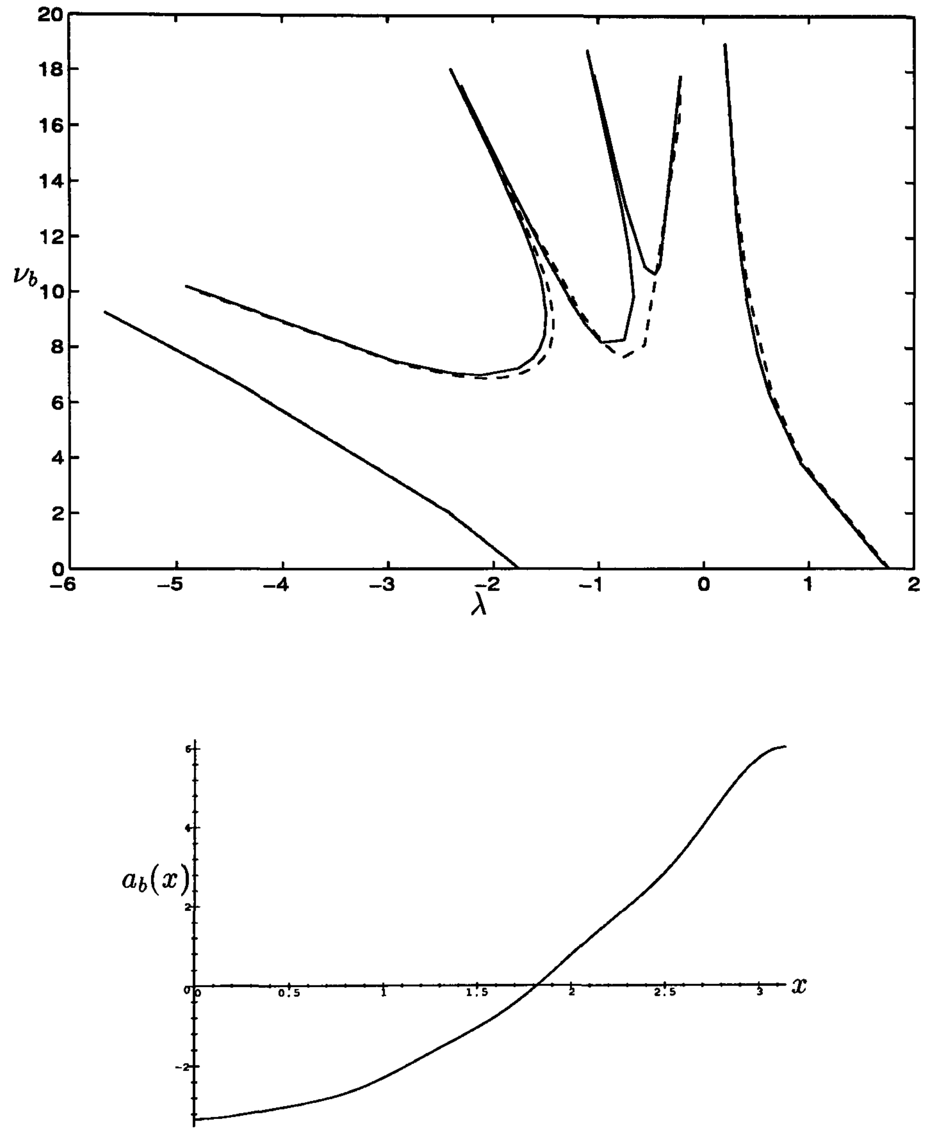

Figure 4.2: Shock region and geometry when we approximate $a_b' = 2x$ with its first three even harmonics. The dotted line shows the corresponding shock region when we include just the first two even harmonics.

(only γ_{b4} non-zero). The shock-finger gets increasingly thinner and the effect on the central shock region diminishes as we consider the cases γ_{b2}, γ_{b4} and γ_{b6} being separately non-zero. The inclusion of higher harmonics in $a_b(x)$ clearly has weaker and weaker effects on the form of the shock region and the response. This will be seen again in the asymptotic analysis of Section 5.1.2.

In both cases, the location of the fingers can be seen to lie close to the lines (4.62).

4.4.3 Proof that shocks must exist near $\lambda = 0$

Finally in this section, we note that it is very simple to see that, whatever γ_{bn} we choose, shocks always exist in a thin detuning band near $\lambda = 0$ for $\nu_{b0} \sim O(\varepsilon^{1/2})$. The proof is straightforward if, considering (4.61), we note that any continuous solution must necessarily be of the form

$$f' = -\frac{\lambda}{3} \pm \left(c + \frac{2}{\pi}\cos t - \frac{\nu_b}{2}\sum_{n=1}^{\infty} A_n \gamma_{b2n} \cos(nt + \alpha_n)\right)^{\frac{1}{2}}. \tag{4.64}$$

Now, when $\lambda = 0$, the zero mean condition implies that

$$\int_{-\pi}^{\pi} \left(c + \frac{2}{\pi}\cos t - \frac{\nu_b}{2}\sum_{n=1}^{\infty} A_n \gamma_{b2n} \cos(nt + \alpha_n)\right)^{\frac{1}{2}} dt = 0.$$

This is the integral of something which *must* be positive and hence only holds if the integrand vanishes almost everywhere. Hence we need the summation term and the forcing term to balance and in this case (4.64) gives $f' = 0$ which, from (4.60), implies that $A_n = 0$ and this is in contradiction with the summation/forcing balance. Hence, no continuous solutions exist near $\lambda = 0$ regardless of the γ_{bn}. However, it is also clear from (4.64) that, as ν_b increases, the response will be $O(1/\nu_b)$ for the geometric and forcing terms to balance. Hence, although shocks persist near $\lambda = 0$ for any ν_b, their strength diminishes as ν_b grows.

It is also apparent from the last subsection that other shock-branches exist. In the special case $a_b'(x) = 2x$ we saw that more and more branches emerge as the number of harmonics in the geometry increases. It seems likely that this will also be the case in more general situations and that the inclusion of further harmonics in $a_b(x)$ will not remove these branches but increase the number of fingers in the (λ, ν_w)-plane.

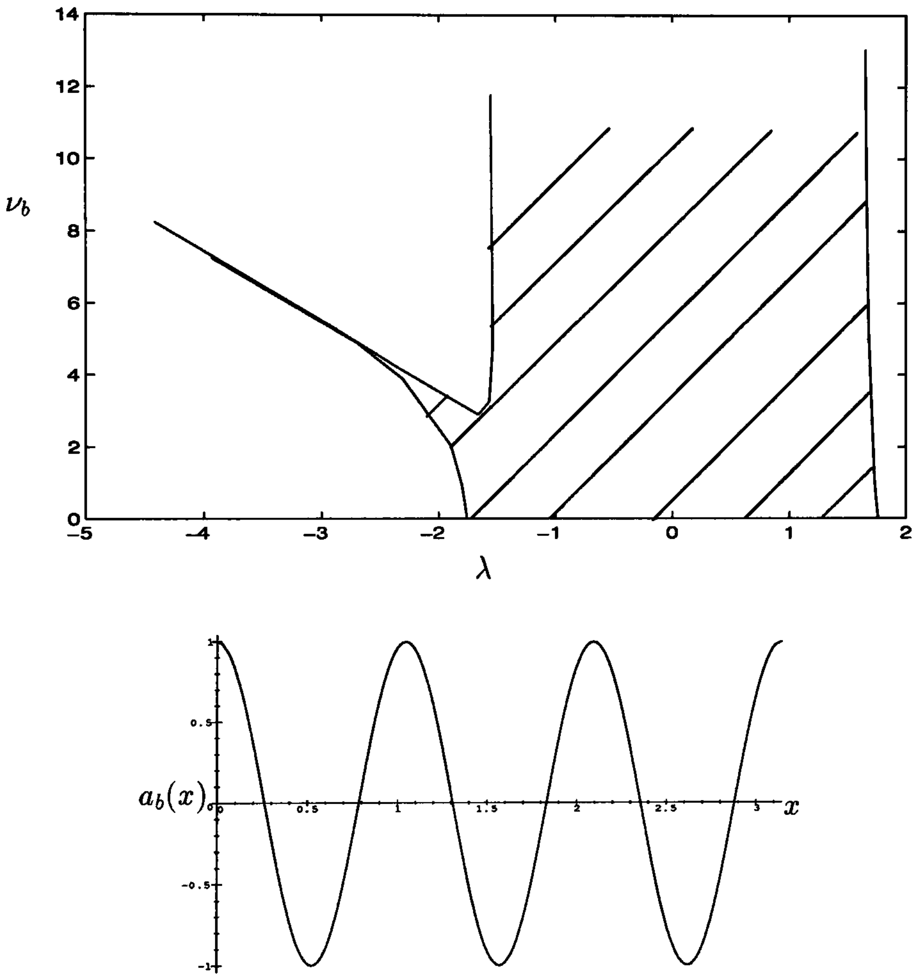

Figure 4.3: Shock region and geometry when only $\gamma_{b6} \neq 0$.

4.5 Stronger geometric variations

As we remarked in Section 4.4.2, geometric variations of $O(\varepsilon^{1/2})$ have no effect when we restrict ourselves to forms of geometry, $a_b(x)$, such that $a_b'(x) = a_b'(\pi - x)$ and, for the sloshing problem we also require $a_b(x)$ to have zero mean (see (4.48)). Ockendon *et al* [57] have considered larger geometric variations by taking $\nu_{b0} \sim O(\varepsilon^{1/4})$ and again retrieve Chester's equation if $a_b(x)$ satisfies a further set of restrictions. Hence, a special geometry, $a_b(x)$, begins to emerge as $\nu_{b0} \to O(1)$ where the spectrum remains commensurate and the leading-order solution satisfies a Chester-like equation and may contain a shock in certain detuning ranges.

In general, of course, for $\nu_{b0} \sim O(1)$, the spectrum is likely to be non-commensurate and we expect a single Duffing-like mode. The possibility of these special geometries is, however, a more interesting situation and it is the search for these geometries that we are concerned with in this section. Hence, we consider the one-dimensional sloshing and acoustic problems for $\nu_{b0} \sim O(1)$ and we see how the two problems now satisfy different wave equations to leading order.

4.5.1 Acoustic oscillations in a resonator with varying sides

Taking $\nu_{b0} \sim O(1)$ in (2.56)-(2.58) with $a_b(x, y) = a_b(x)$ yields, to $O(1)$,

$$\varphi_{xx} + \frac{A_b'(x)}{A_b(x)}\varphi_x = \varphi_{tt}, \tag{4.65}$$

$$\varphi_x = 0 \quad \text{on} \quad x = 0, \pi, \tag{4.66}$$

where $A_b(x) = 1 + \nu_{b0} a_b(x)$. It will be useful to consider this as a Stürm-Liouville problem and we write

$$\varphi_x = \frac{v(x)}{\sqrt{A_b(x)}} e^{i\omega_n t},$$

to give

$$\frac{\mathrm{d}^2 v}{\mathrm{d}x^2} + [\omega_n^2 - U(x)]v = 0, \tag{4.67}$$

$$v = 0 \quad \text{on} \quad x = 0, \pi, \tag{4.68}$$

where the potential $U(x)$ is given by

$$U(x) = \frac{3}{4}\frac{(A_b')^2}{A_b^2} - \frac{A_b''}{2A_b}. \tag{4.69}$$

We are now interested in the question of which $U(x)$ yield $\omega_n = n$. Vasiliev (private communication) has brought to our attention the following argument proposed by Prof. Kotlyarov. Consider the problems

$$\begin{aligned} &\text{(i)} \quad v'' + (\lambda_n - U(x))v = 0, \quad &&\text{(ii)} \quad v'' + (\nu_n - U(x))v = 0, \\ &\qquad v(0) = v(\pi) = 0, &&\qquad v(0) = v'(\pi) = 0. \end{aligned}$$

We now appeal to Theorem 3.4.3 from Marchenko's [41] monograph: the pair $\{\lambda_n\}, \{\nu_n\}$ uniquely define the potential $U(x)$ if and only if

$$-\infty < \nu_1 < \lambda_1 < \nu_2 < \lambda_2 < \ldots < \infty,$$

and satisfy the asymptotic formulae

$$\lambda_n = n^2 - 2A + a_n \quad , \quad \nu_n = \left(n - \frac{1}{2}\right)^2 - 2A + b_n,$$

where A is an arbitrary number and

$$\sum_{n=1}^{\infty} a_n^2 < \infty \quad , \quad \sum_{n=1}^{\infty} b_n^2 < \infty.$$

Now we can put $\omega_n^2 = \lambda_n = n^2$, $n = 1, 2, 3, \ldots$ and $\nu_n = (n - 1/2)^2 + b_n$ (where $A = \int_0^\pi U(x)\mathrm{d}x = 0$). The numbers ν_n can be chosen arbitrarily subject to the condition

$$\sum_{n=1}^{\infty} b_n^2 < \infty,$$

and each different set of ν_n yields a different $U(x)$ by the theorem. An infinite subset of these $U(x)$ has been found by Pöschel & Trubowitz [60] (whose work was brought to our attention by Dr A. Holst) and are given by

$$U_{p,q}(x) = -\frac{2}{\pi^2}\frac{\mathrm{d}^2}{\mathrm{d}x^2}\log\left(1 + \frac{(e^p - 1)}{\pi}\int_x^\pi 2\sin^2 qs\mathrm{d}s\right), \tag{4.70}$$

where q is an arbitrary positive integer and p is an arbitrary real number.

The simplest case is when $b_n = 0$ ($n = 1, 2, 3, \ldots$) or $p = 0$ and $U(x) \equiv 0$. For other b_n or p, $U(x)$ will be non-zero and solving (4.69) for the area variation $A_b(x)$ will present a formidable challenge. Hence we only consider the case $U(x) \equiv 0$ which yields

$$A_b(x) = \frac{1}{(ax + d)^2}, \tag{4.71}$$

the special geometry considered by Keller [36], who also showed that in this case,

$$\varphi_0 = (ax+d)[g'(t+x)+g'(t-x)] + a[g(t-x)-g(t+x)],$$

where g satisfies a Chester-like equation.

Note that if we take $d = 1$ and a to be small then

$$\nu_{b0}a_b(x) \sim -2ax + \cdots,$$

and we can see that for $a \sim O(\varepsilon^{1/2})$, $\nu_{b0} \sim O(\varepsilon^{1/2})$, putting $a_b(x) = -2x$ means $a_b'(x)$ is even about $x = \frac{\pi}{2}$. It is clear that the restrictions discussed above are satisfied in this case and it seems reasonable to assume that (4.71) evolves from an infinite set of restrictions found as ν_{b0} increases from $O(\varepsilon^{1/2})$ to $O(1)$.

Finally, we note that Pöschel & Trubowitz [60] have also shown that the restriction $U(\pi - x) = U(x)$ leads to $U(x) \equiv 0$ being the *unique* potential that yields $\omega_n = n$. This result ties in with the restriction that $a_b'(\pi - x) = a_b'(x)$ because taking $a_b'(x)$ to be even about $\pi/2$ yields $U(\pi - x) = U(x)$.

4.5.2 Fluid in a tank with a varying cross-section

In this case, with $\nu_{b0} \sim O(1)$, we use the method of Section 4.1.2 to find that, to first order,

$$A_f(x)\phi_{xx} + A_f'(x)\phi_x = \phi_{tt}, \tag{4.72}$$

$$\phi_x = 0 \quad \text{on} \quad x = 0, \pi, \tag{4.73}$$

where $A_f(x) = 1 + \nu_{b0}a_b(x)$. We first write this in terms of $\psi(x) = A_f(x)\phi_x e^{i\omega_n t}$ as

$$\psi'' + V(x)\omega_n^2\psi = 0, \tag{4.74}$$

$$\psi = 0 \quad \text{on} \quad x = 0, \pi, \tag{4.75}$$

$(V(x) = 1/A_f(x))$ which is the same problem that arises for oscillations in a gas with an initially stratified density[3]. This can then be turned into a Stürm-Liouville problem by using the Liouville transformation

$$u(\xi) = V^{1/4}(x)\psi(x),$$

[3]This can be readily seen if we consider the one-dimensional equations (in dimensional form) governing the gas flow,

$$\begin{aligned} \rho_T + (\rho u)_X &= 0, \\ \rho(u_T + uu_X) &= -p_X, \end{aligned}$$

where

$$\xi = \int_0^x V^{1/2}(t)\mathrm{d}t,$$

to give

$$u''(\xi) + [\omega_n^2 - q(\xi)]u(\xi) = 0, \tag{4.76}$$

$$u(0) = u\left(\int_0^\pi V^{1/2}(t)\mathrm{d}t\right) = 0, \tag{4.77}$$

with

$$q(\xi) = \frac{V_{xx}}{4V^2} - \frac{5(V_x)^2}{16V^3}.$$

We again look for when $\omega_n = n$ and consider the case $q \equiv 0$ where

$$V(x) = \frac{1}{(Ax+B)^4}, \tag{4.78}$$

but we also need the boundary conditions to be at $\xi = 0, \pi$ so that A and B, from (4.77), are related by

$$B(A\pi + B) = 1. \tag{4.79}$$

Hence,

$$\nu_{b0}a_b(x) = (Ax+B)^4 - 1,$$

$$\rho_\tau + u\rho_X = a^2(\rho_\tau + u\rho_X),$$

where $a^2 = \gamma p/\rho$. If we perturb this from an initial state including density stratification (Ellermeier [25]) by writing

$$\begin{aligned} u &= \bar{a}_0(\epsilon u_1(x,t) + \cdots), \\ \rho &= \bar{\rho}_0(\rho_0(x) + \epsilon\rho_1(x,t) + \cdots), \\ p &= p_0(1 + \epsilon p_1(x,t) + \cdots), \\ a &= \bar{a}_0(a_0(x) + \epsilon a_1(x,t) + \cdots), \end{aligned}$$

where $\bar{\rho}_0$ is the average initial density, $\bar{a}_0^2 = \gamma p_0/\bar{\rho}_0$ and u_1, ρ_0, etc. are all dimensionless quantities, and $x = X/L$ and $t = \bar{a}_0\tau/L$ are non-dimensional variables. The $O(\epsilon)$ terms in the equations of motion can then be shown to yield

$$\frac{\partial^2 u_1}{\partial t^2} = \frac{1}{\rho_0(x)}\frac{\partial^2 u_1}{\partial x^2},$$

so we can associate $A_f(x)$ with $1/\rho_0(x)$.

together with (4.79), and the leading-order solution will satisfy

$$\phi_{0x} = \frac{1}{(Ax+B)^3}\left[f\left(t+\frac{x}{B(Ax+B)}\right) - f\left(t-\frac{x}{B(Ax+B)}\right)\right],$$

where f is unknown and has period 2π. Note also that writing

$$B = 1 + \varepsilon^{1/2}B_1 + O(\varepsilon)$$

gives, from (4.79),

$$A = -\frac{2\varepsilon^{1/2}B_1}{\pi} + O(\varepsilon),$$

so that for weak variations

$$\nu_{b0}a_b(x) \sim 4\varepsilon^{1/2}B_1\left(1-\frac{2x}{\pi}\right).$$

This gives $\nu_{b0} \sim O(\varepsilon^{1/2})$, $a_b(x) \sim (1-2x/\pi)$ which satisfies the condition $a_b'(x)$ is even about $x = \frac{\pi}{2}$ and also the criterion that $a_b(x)$ has zero mean. Again, we see this special geometry evolving out of a set of restrictions.

4.5.3 Other geometries

For completeness we have included a list of geometries where the spectrum can be found explicitly (Table 4.2), although this is probably by no means a comprehensive list. This gives the geometry $A_b(x)$ for the acoustic case (Section 4.5.1) and the corresponding eigenvalues, which are the roots of the equations given. The last entry in the table is a result that can be found in Titchmarsh [72]. Note that we can interpret these results in terms of the fluid case by calculating $U(x)$ for each $A_b(x)$, work out the corresponding $q(\xi)$ (noting (4.67) and (4.76) are of the same form), and relate this back to $A_f(x)$ (bearing in mind that the boundary conditions must be at $\xi = 0, \pi$).

4.6 Dispersive effects

So far we have neglected the fourth-order dispersive term in (4.48). This term will, in reality, be important in the sloshing problem although, as we have already noted, it is negligible at the ripple depth (when surface tension is included).

$A_b(x)$	Eigenvalues
1	$\omega_n = n$
$\dfrac{1}{(ax+d)^2}$	$\omega_n = n$
x^2	$\tan \omega_n \pi = \omega_n \pi$
x	$J_1(\omega_n \pi) = 0$
e^{ax}	$\omega_n^2 = \dfrac{a^2}{4} + n^2$
$\sin x$	$\omega_n^2 = (n+1)(n+2)$

Table 4.2: Geometries with known eigenvalues.

For large values of κ, the solution will be dominated by a single mode as can be seen by writing $f \sim \kappa^{2/3} A^* \sin t + O(\kappa^{-2/3})$ with $\lambda \kappa^{2/3} \sim O(1)$ in (4.48); this solution matches the shallow water limit of the deep water solution (3.39). A more detailed analysis of this matching is given in Section 5.2 for the two-dimensional case.

The transition to this single mode response was discussed in detail in Ockendon *et al* [56] and Johnson [33] and we now give a brief outline of some of their results. We put

$$f' = -\frac{\lambda}{3} + \frac{\kappa^2}{9} + D(t),$$

to get

$$\kappa^2 D'' = \frac{9}{2}(D^2 - u^2) \quad , \quad u = \left[\frac{4}{3\pi}(\cos t + c_2)\right]^{\frac{1}{2}},$$

where c_2 is a constant. The solution $D^2 = u^2$ corresponds to those discussed in Section 4.4.1. For κ small, we can seek solutions close to $D^2 = u^2$ except when D'' is large, and write $t = t_0 + \kappa\tau$ so that,

$$\frac{d^2 D}{d\tau^2} = \frac{9}{2}(D^2 - u^2(t; c_2)).$$

Then as $|\tau| \to \infty$ it is possible for D to approach the solution $D = u$ that corresponds to a saddle-point in the (D, D_τ)-phase plane. It is possible to construct a solution which for the most part is near u but takes a finite number of excursions away from this solution in the form of 'spikes' as seen on the slow timescale t. These inner spikes can be matched to the outer solution $D = u$ as long as $u' = 0$ giving that the spikes can only occur at $t = n\pi$. Ockendon *et al* [56] also showed that any number of spikes can occur at $t = 0$ but only 1 at $t = \pi$.

These spike solutions lead to the possibility of multiple solutions in which the shocks found in Section 4.4.1 are no longer present. The response diagram consists of a collection of Duffing-like peaks centred around $\lambda = 0$ and these peaks may be rounded off by including dissipation. This response is then in good agreement with Chester & Bones [16] (and, in particular, with their Figure 14). Further analytical work on these dispersive effects has been carried out by Byatt-Smith [11] and Reynolds & Cox [61].

It is worth noting at this juncture that the above analysis explains well the experimental results found by Bridges [8] who considered one-dimensional oscillations of a tank containing water of a shallow depth. The dramatic variation in the type of solution he observed, by only a small change in his parameter values, could be due to the multiple solutions found for small dispersion.

4.7 Summary

We have formulated the model for two-dimensional shallow water sloshing that will be considered in detail in the next chapter. In this chapter, however, we have concentrated on one-dimensional solutions of this model and analogies with acoustic oscillations. We have been mainly interested in the effects of base variations in the tank on solutions of Chester's equation. In the regime $\nu_{b0} = \nu_b \varepsilon^{1/2}$, our analytical results for a truncated Fourier series representation for $a_b(x)$ confirm the previous work of Peake [58] and show how the even harmonics of $a_b(x)$ relate to fingers in the (λ, ν_b) shock picture (which become progressively less significant for higher harmonics). We also see the emergence of a single-mode response as ν_b grows large and this fits in with our intuition that, for $\nu_{b0} \sim O(1)$, the solution will just comprise a single mode because the spectrum is no longer nearly commensurate. However, an interesting class of tanks and resonators exist where, for $\nu_{b0} \sim O(1)$, the spectra remain commensurate and shock solutions are expected. These special geometries rely on solving an inverse eigenvalue problem and we have found, in Section 4.5, cases where this is possible.

For all the solutions considered, we must, of course, bear in mind the effect of viscosity on the solutions. This will probably come in the form of a viscous boundary layer in the base of the tank or walls of the resonator, and was first considered by Chester [15] and later by Ockendon & Ockendon [54] who showed that, using the assumption that the equations in the boundary layer are linear, the boundary layer has thickness $\varepsilon^{3/4}$ (assuming that $Re \sim \varepsilon^{-3/2}$) and the resulting change in the governing equation introduces the term

$$-\frac{\bar{\mu}}{\kappa\pi^{1/2}}\int_0^\infty \frac{f''(t-u)}{u^{1/2}}\mathrm{d}u \tag{4.80}$$

to the right-hand side of (4.48), where $\bar{\mu} = \varepsilon^{-3/4}(\pi Re)^{-1/2}$. The boundary layer equations will not be linear in general and a correct analysis would require solving Prandtl's boundary layer equations but no attempt will be made to do this here. Using the expression (4.80) for dissipation does, however, give good quantitative results. In the absence of dispersion Chester [15] showed that the effect of this damping term was to introduce an oscillation behind the shock and this was validated experimentally by Chester & Bones [16]. Ockendon *et al* [56] also showed this but did so by replacing the integral term by the more tractable term $\bar{\mu}f'''$ on the left-hand side of (4.48). When dispersion is included the effect of dissipation is to round off the Duffing-like peaks as noted in the previous section. Keller [35] has also given an account of the effect of viscosity on Chester's equation, using (4.80) to model viscous effects. Hence, in relating our results to any experiments, we must take into account these effects and, as we are mostly concerned with dispersive free problems, we expect our shocks solutions to be altered accordingly.

Finally, we note that two extensions to the models considered here are given in Appendix C where we consider acoustic oscillations close to a higher natural frequency and the evolution of the problem to a periodic response.

Chapter 5

Two-dimensional solutions of shallow water sloshing and acoustics

In the last chapter we developed a model, (4.35)–(4.38) and (4.30)–(4.34), for two-dimensional oscillations in shallow water but considered only one-dimensional solutions. In this chapter we will highlight some aspects of fully two-dimensional solutions in shallow water. To do this we let $\nu_w \neq 0$ and ignore base variations by putting $\nu_b = 0$ as this adds no interesting differences. It is fairly clear from the analysis of Section 4.2 that a similar model arises for the acoustic oscillations described in Section 2.2 when $\nu_{b0} = 0$ and $\nu_{w0} \sim O(\varepsilon^{1/2})$. The only differences between the two models are the higher-order dispersive terms found in the sloshing problem. However, as in the last chapter, we will be mainly concerned with dispersion-free solutions ($\kappa = 0$) so that the solutions we consider are relevant to the acoustic problem. Indeed, as in the last chapter, a simple transformation relates the two problems.

The solution of (4.35)–(4.38) is, as with deep water, critically dependent upon the breadth b. Whereas for deep water the solution changed form for b close to a natural number, we now see that the general solution of (4.35)–(4.38) will consist of an infinite number of two-dimensional modes whenever b is close to a rational number, p/q. Note that, correct to $O(\varepsilon)$, we can always write b as a rational number but the extent to which two-dimensional solutions are excited will depend on the size of q. This is because, for $b = p/q$, the first transverse mode will be $\cos qy \sin qt$ and, as we shall see later in this chapter, the amplitude of the mode diminishes as q increases. The largest amplitude case is when $q = 1$ and, as the form of the solution will then be the same for all p, we consider the case $b = 1$, for simplicity, from now on.

Hence, in Section 5.1, we consider the case $b = 1$ and obtain the form of the solution by first applying the Fredholm Alternative to the problem for B, solving the resulting set of equations in the limits $\nu_w \to 0$, $\lambda, \nu_w \to \infty$, and finally proposing an iteration scheme for $\nu_w \sim O(1)$. In the latter case we solve the first step of this iteration scheme for the example $a_w(x) = \cos x$. All the resulting solutions neglect dispersive effects but we re-introduce dispersion in Section 5.2 to bridge the gap between the solutions found here and those of the deep water case.

Finally in this chapter, we present two other situations where two-dimensional solutions may arise, namely those of forcing the tank at an angle and forcing the tank near a higher frequency.

Before we proceed, however, we need to make one general remark about the solutions we will encounter in the rest of this chapter. This concerns the intersection of two two-dimensional planar shocks of different families. The general theory for intersecting shocks (Liepmann & Roshko [38]; Illingworth [32]; Becker [5]) results in a picture similar to Figure 5.1 where we have taken a moving frame of reference so that the point P is at rest. For two shocks (S_1 and S_2) of different strengths

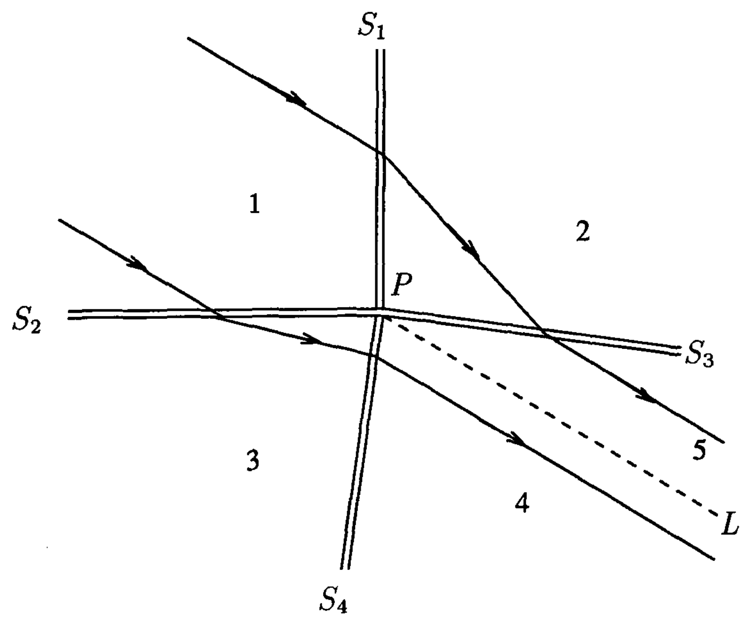

Figure 5.1: Intersecting shock waves

meeting at point P, the shocks are deflected as they pass through each other so that S_1 becomes S_4 and S_2 becomes S_3. The angle through which they turn is dictated by the requirement that the flow in region 5 (due to flow from region 1 passing through S_1 into region 2 and then through S_3) and region 4 (flow in region 1 passing through region 3 via S_2 and S_4) has the same pressure either side of PL and the same flow direction. However, the velocity and density either side of PL may not be the same and this line is thus referred to as a slipstream or vortex sheet.

For weak shocks of strength $O(\varepsilon^{1/2})$, two important points emerge. Firstly, as the physical quantities are only perturbed an $O(\varepsilon^{1/2})$ from their equilibrium state, the deflection of the shocks when they intersect each other will only need to be through an angle of $O(\varepsilon^{1/2})$ for the pressures in regions 4 and 5 to match at PL. Hence the shock location is unaltered to leading order. Secondly, because the entropy changes across these shocks are of $O(\varepsilon^{3/2})$ (see Appendix A.1.1), the continuity of pressure across PL ensures that density is also continuous to $O(\varepsilon^{1/2})$ and, hence, velocity does not change across PL (see (A.7)) to this order. Therefore, to leading order, the shock intersections that arise do so in such a way that the shocks pass through each other without change of form and without creating any new discontinuity.

5.1 Two-dimensional solutions when $b = 1$, $\nu_w \neq 0$

Following the above discussion we concentrate on the case $b = 1$ when the solution to (4.35)–(4.38) can be written as a Fourier series in the form

$$A(x, y, t) = \sum_{p,q} \cos px \cos qy (a_{p,q} \cos \lambda_{p,q} t + b_{p,q} \sin \lambda_{p,q} t), \tag{5.1}$$

where $\lambda_{p,q}^2 = p^2 + q^2$ and p, q are integers such that the $\lambda_{p,q}$ are integers. It is convenient to re-write A as

$$A(x, y, t) = \sum_{i,j} A_{i,j}(x, y, t), \tag{5.2}$$

where

$$A_{i,j} = f_{i,j}(t \pm l_{i,j} x \pm k_{i,j} y) \tag{5.3}$$

are 2π periodic (in time) plane waves in the $(\pm i, \pm j)$ directions, (i, j) denotes all the i, j such that $i^2 + j^2$ is the square of an integer and each pair (i, j) is coprime and

$$l_{i,j} = \frac{i}{(i^2+j^2)^{1/2}} \quad , \quad k_{i,j} = \frac{j}{(i^2+j^2)^{1/2}};$$

we have used the shorthand

$$\begin{aligned} f_{i,j}(t \pm l_{i,j}x \pm k_{i,j}y) &= f_{i,j}(t + l_{i,j}x + k_{i,j}y) + f_{i,j}(t + l_{i,j}x - k_{i,j}y) \\ &+ f_{i,j}(t - l_{i,j}x + k_{i,j}y) + f_{i,j}(t - l_{i,j}x - k_{i,j}y), \end{aligned}$$

where we refer to the $f_{i,j}$ as the "(i,j)-wavetrain". Thus

$$A_{i,j}(x,y,t) = \sum_{s=1}^{\infty} \cos six \cos sjy (a_{si,sj} \cos s\lambda_{i,j}t + b_{si,sj} \sin s\lambda_{i,j}t), \tag{5.4}$$

$$f_{i,j}(\tau) = \frac{1}{d} \sum_{s=1}^{\infty} (a_{si,sj} \cos s\lambda_{i,j}\tau + b_{si,sj} \sin s\lambda_{i,j}\tau), \tag{5.5}$$

and $d = 2$ for $(i, j) = (1, 0)$ or $(0, 1)$ or $d = 4$ otherwise.

The problem for B, (4.30)–(4.34), can now be considered, using (5.2) for A. We consider all the orthogonality conditions inferred from the Fredholm Alternative applied to (4.30)–(4.34). In particular, we multiply (4.30) by the eigensolutions $\cos npx \cos mpy G(t')$, where

$$G(t') = c_{np,mp} \cos(\lambda_{n,m} pt') + d_{np,mp} \sin(\lambda_{n,m} pt'),$$

and $c_{l,k}$, $d_{l,k}$ are arbitrary constants. Then, integrating over the whole domain, using the boundary conditions and summing over p, we find

$$\begin{aligned} &\sum_{p=1}^{\infty} \int_0^{2\pi} \int_0^{\pi} \int_0^{\pi} F(x,y,t') \cos npx \cos mpy G(t') \mathrm{d}x\mathrm{d}y\mathrm{d}t' \\ &= -\pi^2 \delta_{n1}\delta_{m0} d_{1,0} + \sum_{p=1}^{\infty} \int_0^{2\pi} \int_0^{\pi} B_y|_{y=\pi, t=t'} (-1)^{pm} \cos pnx G(t') \mathrm{d}x\mathrm{d}t', \end{aligned} \tag{5.6}$$

for each (n, m), where $F(x, y, t)$ is the right-hand side of (4.30). The crucial observation is that the only part of the $F(x, y, t')$ that produces terms which are not orthogonal to $\cos npx \cos mpy \sin(\lambda_{n,m}pt' + \alpha_{n,m})$ is the part containing only $A_{n,m}$, as we can show using the following proposition.

Proposition 5.1 *The conditions*

$$\int_0^{2\pi}\int_0^{\pi}\int_0^{\pi} A_{n_1,m_1}A_{n_2,m_2}\cos qn_3x\cos qm_3y\left\{\begin{array}{c}\cos q\lambda_{n_3,m_3}t'\\ \sin q\lambda_{n_3,m_3}t'\end{array}\right\}dx\,dy\,dt',$$

where $q = 1,2,\ldots$ *and the pairs* (n_i, m_i) *are coprime are non-zero if and only if* $n_1 = n_2 = n_3$ *and* $m_1 = m_2 = m_3$.

Proof. We see from (5.4) that the product $A_{n_1,m_1}A_{n_2,m_2}$ comprises four terms within a double summation. It is clear, however, that a similar proof follows for each of these four terms, so we just consider one of the four terms and so it is our aim to show that

$$\int_0^{2\pi}\int_0^{\pi}\int_0^{\pi}(\cos rn_1x\cos sn_2x\cos qn_3x)(\cos rm_1x\cos sm_2y\cos qm_3y)$$
$$(\cos r\lambda_1t'\cos s\lambda_2t'\cos q\lambda_3t')dxdydt',$$

($\lambda_i^2 = n_i^2 + m_i^2$, and r, s, q are any positive integers) is non-zero if and only if $n_1 = n_2 = n_3$ and $m_1 = m_2 = m_3$. This is only possible if

$$rn_1 \pm sn_2 = \pm qn_3 \quad , \quad rm_1 \pm sm_2 = \pm qm_3 \quad , \quad r\lambda_1 \pm s\lambda_2 = \pm q\lambda_3.$$

Hence there are 64 different ways in which this can happen and we will demonstrate one possibility, the others following similar lines. Consider the case

$$rn_1 + sn_2 = qn_3, \tag{5.7}$$
$$rm_1 + sm_2 = qm_3, \tag{5.8}$$
$$r\lambda_1 + s\lambda_2 = q\lambda_3. \tag{5.9}$$

Then, squaring (5.9) and using (5.7) and (5.8) gives

$$\lambda_1\lambda_2 = n_1n_2 + m_1m_2,$$

and squaring again finally yields

$$\begin{aligned}\frac{n_1}{m_1} &= \frac{n_2}{m_2},\\ &= \frac{n_3}{m_3}\ \text{using (5.7) and (5.8)},\end{aligned}$$

and, as (n_i, m_i) are coprime, this means that $n_1 = n_2 = n_3$ and $m_1 = m_2 = m_3$ which completes the proof. □

Thus, noting that most of the terms on the right-hand side of (4.30) have the same structure as A^2, we can appeal to Proposition 5.1 to prove the observation made above, and so we can replace F in (5.6) by $F_{n,m}$ where

$$
\begin{aligned}
F_{n,m}(x,y,t) &= -\frac{\kappa^2}{3}(A_{n,m})_{tttt} + \left(\lambda - \frac{\kappa^2}{3}\right)(A_{n,m})_{tt} + 2(A_{n,m})_x(A_{n,m})_{xt} \\
&\quad +2(A_{n,m})_y(A_{n,m})_{yt} + (A_{n,m})_t(A_{n,m})_{tt}.
\end{aligned}
$$

Hence, for $\nu_w = 0$, only (5.6) with $(n,m) = (1,0)$ is needed and the other orthogonality conditions are trivially satisfied, i.e. only $A_{1,0}$ is non-zero. For $\nu_w \neq 0$ the left-hand side of (5.6) can be integrated explicitly, and putting $c_{np,mp} = \cos\lambda_{n,m}pt$, $d_{np,mp} = \sin\lambda_{n,m}pt$ and, using the method of Section 4.3.1 to evaluate the sum in the left-hand side of (5.6). We finally find that the $f_{n,m}$, which are periodic with period 2π and zero mean satisfy

$$
\begin{aligned}
\mathcal{C}f_{n,m} &+ \frac{2}{\pi}\sin t\delta_{n1}\delta_{m0} = -\frac{2m^2\gamma_{w0}\nu_w}{\lambda^2_{n,m}}f''_{n,m} \\
&+\frac{\nu_w}{\pi^2}\sum_{p=1}^{\infty}\int_0^{2\pi}\int_0^{\pi} R(x,t')(-1)^{pm}\cos pnx\cos p\lambda_{n,m}(t'-t)\mathrm{d}x\mathrm{d}t', \quad (5.10)
\end{aligned}
$$

for all (n,m)[1], where $\mathcal{C}f_{n,m}$ is shorthand for

$$
\mathcal{C}f_{n,m} = -\frac{\kappa^2}{3}\frac{\mathrm{d}^4 f_{n,m}}{\mathrm{d}t^4} + \left(\lambda - \frac{\kappa^2}{3}\right)\frac{\mathrm{d}^2 f_{n,m}}{\mathrm{d}t^2} + 3\frac{\mathrm{d}f_{n,m}}{\mathrm{d}t}\frac{\mathrm{d}^2 f_{n,m}}{\mathrm{d}t^2}, \quad (5.11)
$$

the right-hand side is linear in $f_{n,m}$ with

$$
R(x,t) = a'_w(x)A_x(x,\pi,t) - (a_w(x) - \gamma_{w0})A_{yy}(x,\pi,t), \quad (5.12)
$$

$A(x,y,t)$ is given by (5.3) and we recall (3.21)

$$
a_w(x) = \sum_{n=0}^{\infty}\gamma_{wn}\cos nx.
$$

The right-hand sides of (5.10), representing the coupling between the $f_{n,m}$'s, are not so easy to deal with, even though, as with the one-dimensional problem, the introduction of the functions $f_{n,m}$ reduces the dimensionality of the problem; we have changed from having to solve for the doubly-infinite set of coefficients $a_{n,m}$ and $b_{n,m}$ (see (5.1)) to the singly-infinite set of equations (5.10). Evaluation of these

[1]We will use the expression "for all (n,m)" to mean the (n,m) that satisfy the conditions that n, m and $\sqrt{n^2+m^2}$ are integers, and n and m are coprime.

right-hand sides is theoretically possible and, for example, for $(n,m) = (1,0)$, the method of Section 4.3.1 yields

$$\mathcal{C}f_{1,0} + \frac{2}{\pi}\sin t = -\frac{\nu_w}{2\pi}\int_0^\pi [a_w'(\pi - t') - a_w'(t')][f_{1,0}'(t + 2t') + \cdots]\mathrm{d}t'$$
$$-\frac{\nu_w}{\pi}\int_0^\pi a_w'(\pi - t')[f_{0,1}'(t + t') - f_{0,1}'(t - t') + \cdots]\mathrm{d}t', \qquad (5.13)$$

where only the first two wavetrains have been included in the integrals. These expressions simplify in several special cases:

(i) when $a_w'(x) = 2x$, i.e. the back wall is parabolic, the equations reduce to a set of ordinary differential equations where, for example, (5.13) reduces to

$$\mathcal{C}f_{1,0} = -\frac{2}{\pi}\sin t + \nu_w\left(f_{1,0} + 4f_{0,1} + \cdots\right);$$

(ii) when $a_w(x)$ has a finite number of Fourier components, a reduced, but still infinite number of $f_{i,j}$ occur on the right-hand side of (5.10);

(iii) when $a_w'(x) = a_w'(\pi - x)$, i.e. the back wall is anti-symmetric, we see, for, example, that (5.13) simplifies and, in general, the right-hand side of (5.10) will again contain a reduced number of $f_{i,j}$.

For the rest of this section we ignore dispersive effects and set $\kappa = 0$ in (5.10). There are several limiting cases of (5.10) that we first study before making some more general statements about these equations. We can immediately see from (5.10) that, as γ_{w0} gets large, $f_{n,m} \sim O(1/\gamma_{w0})$ for $(n,m) \neq (1,0)$ and $f_{1,0}$ satisfies Chester's equation to leading order.

5.1.1 The limit $\nu_w \to 0$

When $\nu_w = 0$, the right-hand sides of (5.10) are zero and the equations decouple leaving Chester's equation for $f_{1,0}$ and all the other $f_{n,m}$ are zero. In this section we consider what happens for small ν_w. When $\lambda \sim O(1)$ we can see from (5.10) that $f_{1,0} \sim O(1)$ and $f_{n,m} \sim O(\nu_w)$ for all other (n,m). Hence, we write

$$f_{n,m} = \delta_{n1}\delta_{m0}f_{n,m}^{(0)} + \nu_w f_{n,m}^{(1)} + \cdots,$$

and, to $O(1)$, $f_{1,0}^{(0)}$ satisfies (4.52) which has solutions given in Section 4.4.1 and, in particular, has discontinuous solutions for $|\lambda| < (96/\pi^3)^{1/2}$ where

$$f_{1,0}^{(0)\prime} + \frac{\lambda}{3} = \left(\frac{8}{3\pi}\right)^{\frac{1}{2}} \begin{cases} \cos\frac{t}{2}, & -\pi < t < t_0^*, \\ -\cos\frac{t}{2}, & t_0^* < t < \pi, \end{cases} \tag{5.14}$$

and

$$\lambda = \left(\frac{96}{\pi^3}\right)^{\frac{1}{2}} \sin\frac{t_0^*}{2}. \tag{5.15}$$

Here we recall that we have used the fact that $f_{1,0}$ is periodic and continuous. To $O(\nu_w)$ we get

$$\begin{aligned} &\lambda f_{n,m}^{(1)\prime\prime} + 3\left(f_{n,m}^{(0)\prime} f_{n,m}^{(1)\prime\prime} + f_{n,m}^{(1)\prime} f_{n,m}^{(0)\prime\prime}\right)\delta_{n1}\delta_{m0} \\ &= \frac{1}{\pi^2}\sum_{p=1}^{\infty}\int_0^{2\pi}\int_0^{\pi} R^{(0)}(x,t')(-1)^{pm}\cos pnx \cos p\lambda_{n,m}(t'-t)\mathrm{d}x\mathrm{d}t'. \end{aligned} \tag{5.16}$$

where $R^{(0)}(x,t) = [f_{1,0}^{(0)\prime}(t+x) - f_{1,0}^{(0)\prime}(t-x)]a_w'(x)$. Note that the first term on the right-hand side of (5.10) has no effect at this order, so the solutions considered throughout this subsection are independent of the choice of γ_{w0}. The effects of the geometry can now be considered in terms of

(i) the modulation of the one-dimensional solution described by the nonlinear equation (5.16) with $(n,m) = (1,0)$ and

(ii) the excitation of "cross wavetrains" which are described by the linear equations (5.16) with $(n,m) \neq (1,0)$.

To analyse the change in the one-dimensional solution, we write the shock location as

$$t^* = t_0^* + \nu_w t_1^* + \cdots,$$

and solve a perturbed free boundary problem for $f_{1,0}'$. The continuity condition $[f_{1,0}] = 0$ implies

$$[f_{1,0}^{(1)}] = -t_1^*[f_{1,0}^{(0)\prime}], \tag{5.17}$$

where square brackets denote jumps from $t_0^* - 0$ to $t_0^* + 0$. To simplify matters, we consider the case $a_w'(x) = 2x$ (although, other $a(x)$ could be considered, resulting in more complicated, but qualitatively similar, results), and we can integrate (5.16) for $(n,m) = (1,0)$ to give

$$\left(\frac{24}{\pi}\right)^{\frac{1}{2}} \cos\frac{t}{2} f_{1,0}^{(1)\prime} = \frac{\lambda}{6}(\pi^2 - t^2)$$
$$+2\left(\frac{8}{3\pi}\right)^{\frac{1}{2}} \left(d_1(t+\pi) - 2\cos\frac{t}{2}\right), \qquad -\pi < t < t_0^*,$$

and

$$-\left(\frac{24}{\pi}\right)^{\frac{1}{2}} \cos\frac{t}{2} f_{1,0}^{(1)\prime} = \frac{\lambda}{6}(\pi^2 - t^2)$$
$$+2\left(\frac{8}{3\pi}\right)^{\frac{1}{2}} \left(d_1\pi + d_2 t - 4\cos\frac{t_0^*}{2} - 2t_0^*\sin\frac{t_0^*}{2} + 2\cos\frac{t}{2}\right), \qquad t_0^* < t < \pi.$$

Hence $f_{1,0}$ is periodic if

$$\begin{aligned} d_1 &= \frac{1}{\pi}\left[2\cos\frac{t_0^*}{2} + (t_0^* - \pi)\sin\frac{t_0^*}{2}\right], \\ d_2 &= \frac{1}{\pi}\left[2\cos\frac{t_0^*}{2} + (t_0^* + \pi)\sin\frac{t_0^*}{2}\right], \end{aligned}$$

and we can use (5.17) to find t_1^*. The result is plotted in Figure 5.2, in which the singularity as $|\lambda| \to \lambda^*$ reflects the fact that the shock regime in the (λ, ν_w)-plane shifts slightly as ν_w increase from zero (see Figure 4.2). We can also see that the strength of the perturbed discontinuity in $f_{1,0}^{(0)\prime} + \nu_w f_{1,0}^{(1)\prime}$ decreases for $\lambda > 0$ and increases for $\lambda < 0$ in accordance with this shift in the shock regime.

Now we consider the other $f_{n,m}$ for $(n,m) \neq (1,0)$ and the simplest case is $a_w(x) = \cos x$ (where $f_{1,0}$ is unaffected to $O(\nu)$). Once again, more general $a_w(x)$ can be considered and the results are qualitatively the same. We use the representation (5.5) and write

$$f_{1,0}^{(0)} = \frac{1}{2}\sum_{n=1}^{\infty}(a_{n,0}^{(0)}\cos n\tau + b_{n,0}^{(0)}\sin n\tau),$$

and, for $\lambda \sim O(1)$, (5.16) gives

$$f_{0,1}^{(1)} = \frac{1}{2\lambda}(a_{1,0}^{(0)}\cos t + b_{1,0}^{(0)}\sin t) \quad , \quad f_{4,3}^{(1)} = \frac{1}{20\lambda}(a_{5,0}^{(0)}\cos 5t + b_{5,0}^{(0)}\sin 5t), \qquad (5.18)$$

and so on where $f_{n,m}^{(1)} = 0$ unless $\lambda_{n,m} - n = 1$. For continuous solutions for $f_{1,0}^{(0)}$, we have, as $n^2 + m^2 \to \infty$, $f_{n,m}^{(1)} \sim O(\lambda_{n,m}^{-5})$ and the lowest-order cross wavetrains are single mode responses with decreasing amplitudes for higher order wavetrains.

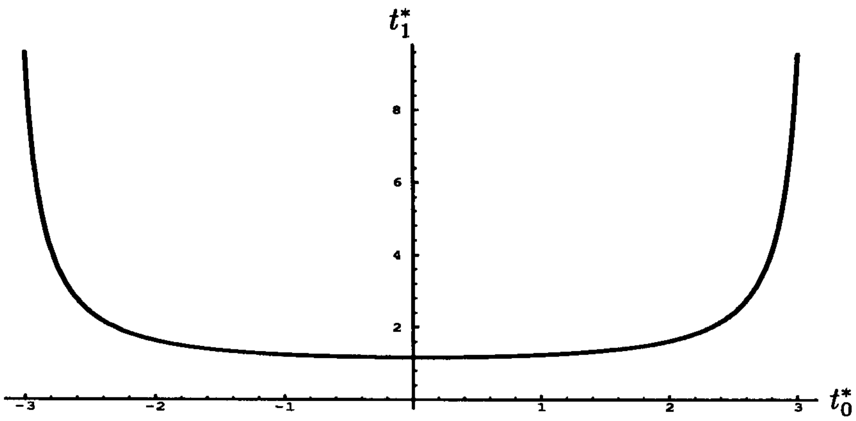

Figure 5.2: Plot of t_1^* against t_0^* where the shock is located at $t^* = t_0^* + \nu_w t_1^*$.

There is a more interesting regime in which the degeneracy has a dramatic effect, as can be discerned from (5.18). This is when λ is so small that a rescaling of (5.10) is necessary in order to keep the nonlinearity in balance with the detuning. In fact we can see the existence of a fine detuning band near $\lambda = 0$ on physical grounds by noting that the primary forcing of $O(\varepsilon)$ produces a primary response of $O(\sqrt{\varepsilon})$, and hence a cross wavetrain forcing (due to the interaction of the $O(\nu_w\sqrt{\varepsilon})$ geometry variation with this response) of $O(\nu_w\varepsilon)$; then, because of the degeneracy of the fundamental, the cross wavetrain response is of $O(\sqrt{\nu_w\varepsilon})$. Indeed, inspection of (5.10) shows that we need to write

$$\lambda = \sqrt{\nu_w}\tilde{\lambda} \quad , \quad f_{n,m} = \sqrt{\nu_w} g_{n,m}^{(1)} + \cdots ,$$

in order to retain the nonlinear terms in the limit $\nu_w \to 0$. This leads to

$$\begin{aligned} &\tilde{\lambda} g_{n,m}^{(1)\prime\prime} + 3 g_{n,m}^{(1)\prime} g_{n,m}^{(1)\prime\prime} \\ &= \frac{1}{\pi^2} \sum_{p=1}^{\infty} \int_0^{2\pi} \int_0^{\pi} R^{(0)}(x,t')(-1)^{pm} \cos pnx \cos p\lambda_{n,m}(t'-t) \mathrm{d}x\mathrm{d}t', \end{aligned} \tag{5.19}$$

for all $(n,m) \neq (1,0)$, with $f_{1,0}$ given by (5.14) and, from (5.15),

$$t^* = \left(\frac{\pi^3}{24}\right)^{\frac{1}{2}} \sqrt{\nu_w}\tilde{\lambda}.$$

We now have the possibility of a much more interesting cross wavetrain response, which we again illustrate in the case $a_w(x) = \cos x$. Then (5.14) and (5.19) give

$$\left.\begin{aligned} \left(g_{0,1}^{(1)'} + \frac{\tilde{\lambda}}{3}\right)^2 &= \frac{16}{9}\left(\frac{8}{3\pi^3}\right)^{\frac{1}{2}}[c_1 - \sin t], \\ \left(g_{4,3}^{(1)'} + \frac{\tilde{\lambda}}{3}\right)^2 &= \frac{8}{297}\left(\frac{8}{3\pi^3}\right)^{\frac{1}{2}}[c_2 - \sin 5t], \end{aligned}\right\} \qquad (5.20)$$

and so one for the higher-order wavetrains, where c_1, c_2 are constants. Consideration of these expressions shows that discontinuous solutions for $g_{0,1}^{(1)}$ occur for $|\tilde{\lambda}| < 1.95$ and for $g_{4,3}^{(1)}$ when $|\tilde{\lambda}| < 0.24$. To highlight this case with minimum algebraic complexity we consider the case $\tilde{\lambda} = 0$, so

$$\begin{aligned} g_{0,1}^{(1)'} &= \frac{4}{3}\left(\frac{8}{3\pi^3}\right)^{\frac{1}{4}}\begin{cases} (1-\sin t)^{1/2}, & -\frac{3}{2}\pi < t < -\frac{1}{2}\pi, \\ -(1-\sin t)^{1/2}, & -\frac{1}{2}\pi < t < \frac{1}{2}\pi, \end{cases} \\ g_{4,3}^{(1)'} &= \left(\frac{8}{297}\right)^{\frac{1}{2}}\left(\frac{8}{3\pi^3}\right)^{\frac{1}{4}}\begin{cases} (1-\sin 5t)^{1/2}, & -\frac{11}{10}\pi < t < -\frac{1}{10}\pi, \\ -(1-\sin 5t)^{1/2}, & -\frac{1}{10}\pi < t < \frac{9}{10}\pi, \end{cases} \end{aligned}$$

and so on, where the interaction of these shocks with that of the primary wavetrain is negligible as we discussed at the start of this chapter. We illustrate this case, plotting A_t (which is proportional to the free surface height) at $t = -\pi/4$ in Figure 5.3(a) for $\nu_w = 0$ and Figure 5.3(b) for $\nu_w = 0.2$ (with just the first three wavetrains). The $f_{4,3}$-wavetrain can just be seen and the introduction of further wavetrains has a negligible effect.

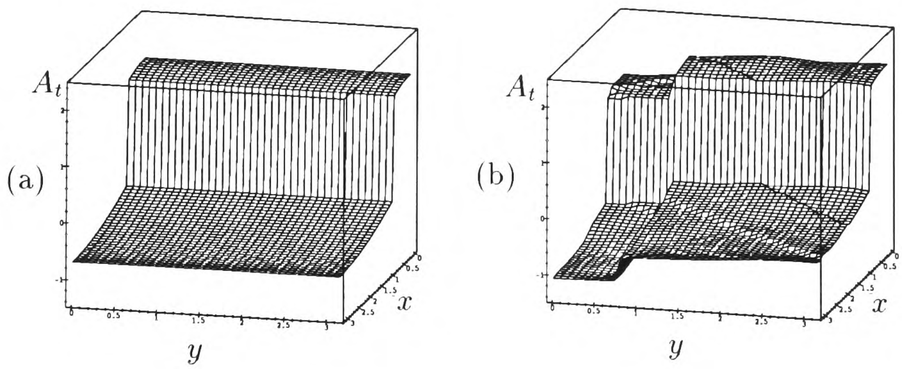

Figure 5.3: Plot of A_t for (a) $\nu_w = 0$ and (b) $\nu_w = 0.2$.

Consideration of other forms of $a_w(x)$ confirm that in all cases the primary wavetrains ($f_{1,0}$ and $f_{0,1}$) are much larger than the higher-order wavetrains. This evidence will be useful in our discussions on the problem when $\nu_w \sim O(1)$, in Section 5.1.3.

5.1.2 The limits $\lambda, \nu_w \to \infty$

As ν_w tends to infinity in equations (5.10), the solution is $O(1/\nu_w)$ or smaller for each $f_{n,m}$ to leading order and it is only when $\lambda \sim \nu_w$ that a resonant response is possible. Away from resonance, with $\lambda \sim \nu_w$, we expand the $f_{n,m}$ as

$$f_{n,m} = \frac{1}{\nu_w} f^{(0)}_{n,m} + \frac{1}{\nu_w^3} f^{(1)}_{n,m} + \frac{1}{\nu_w^5} f^{(2)}_{n,m} + \cdots.$$

Elementary, but rather longwinded, calculations then give

$$\begin{aligned} f_{1,0} &= \frac{2(\lambda + 2\gamma_{w0}\nu_w)}{\pi(\lambda - s^+_{1,0}\nu_w)(\lambda - s^-_{1,0}\nu_w)} \sin t && (5.21)\\ &+ \frac{3(\gamma_{w2}\gamma^2_{w1}\nu^3_w - (\lambda + 2\gamma_{w0}\nu_w)^3)}{2\pi^2(\lambda - s^+_{1,0}\nu_w)^2(\lambda - s^-_{1,0}\nu_w)^2(\lambda - s^+_{2,0}\nu_w)(\lambda - s^-_{2,0}\nu_w)} \sin 2t + \cdots, \\ f_{0,1} &= \frac{2\gamma_{w1}\nu_w}{\pi(\lambda - s^+_{0,1}\nu_w)(\lambda - s^-_{0,1}\nu_w)} \sin t && (5.22)\\ &+ \frac{3\nu_w(\gamma_{w2}(\lambda + 2\gamma_{w0}\nu_w)^2 - \nu_w\gamma^2_{w1}[\lambda + \gamma_{w4}\nu^2_w])}{2\pi^2(\lambda - s^+_{0,1}\nu_w)^2(\lambda - s^-_{0,1}\nu_w)^2(\lambda - s^+_{0,2}\nu_w)(\lambda - s^-_{0,2}\nu_w)} \sin 2t + \cdots, \\ f_{n,m} &= O\left(\nu_w^{1-2(n^2+m^2)^{1/2}}\right), && (5.23) \end{aligned}$$

where

$$s^\pm_{n,0} = s^\pm_{0,n} = \frac{-(2\gamma_0 + \gamma_{2n}) \pm \left[(2\gamma_0 - \gamma_{2n})^2 + 4\gamma^2_n\right]^{1/2}}{2}, \tag{5.24}$$

and it becomes apparent that the modes $\left\{ \begin{array}{c} \cos nx \\ \cos ny \end{array} \right\} \sin nt$ grow close to the spectral lines

$$\lambda = s^\pm_{n,0}\nu_w. \tag{5.25}$$

More complicated expressions can be found for the other $s^\pm_{n,m}$ but we do not pursue this. Instead, we can make the following remarks. In the one-dimensional case, where the lines of blow-up are along $\lambda + \gamma_{b2n}\nu_b/2 = 0$ (see Section 4.4.2), Peake [58] showed that these lines lie roughly along the fingers. Hence, by analogy, we expect similar shock fingers close to the lines (5.25) and a rather *ad hoc* way of determining the shock picture is then to plot these lines and draw the interface between shock and no-shock regimes around them. Chester's shock pictures can be fitted into this scheme as can the one-dimensional shock pictures found in Section 4.4.2. Clearly this method would give some indication of the shock structure but would not hint at where within these fingers shocks travelling in different directions occur.

Finding more terms in the expansion for, say, $f_{1,0}$ introduces more $\sin t$ terms and, as we approach the lines $\lambda = s_{1,0}^{\pm}\nu_w$, these higher-order terms grow to balance with the leading-order $\sin t$ term and our expansion breaks down. Higher-order terms balance with the growth witnessed at the other spectral lines but the outcome is different from case to case. This process emphasises the importance of the first few modes, and hence the primary wavetrains, and we summarise the details below, where we look close to $\lambda = s_{n,0}^{+}\nu_w$, although a similar analysis could be carried through when $\lambda \sim s_{n,0}^{-}\nu_w$.

1. $\lambda \sim s_{1,0}^{+}\nu_w$. Here we find a detuning range of $O(\nu_w^{-1/3})$ where $f_{1,0}$ and $f_{0,1}$ grow to $O(\nu_w^{1/3})$. Hence we write

$$\lambda - s_{1,0}^{+}\nu_w = \hat{\lambda}\nu_w^{-1/3},$$

and

$$\begin{aligned} f_{1,0} &= A\nu_w^{1/3}\sin t + O(\nu_w^{-1/3}), \\ f_{0,1} &= B\nu_w^{1/3}\sin t + O(\nu_w^{-1/3}). \end{aligned}$$

To simplify the algebra, we consider the case $\gamma_{w0} = 0$, although similar results can be found for $\gamma_{w0} \neq 0$. In this case, it can be shown that

$$B = \frac{\gamma_{w1}}{s_{1,0}^{+}}A, \tag{5.26}$$

and

$$\hat{\lambda}A\left(1 + \frac{\gamma_{w1}^2}{s_{1,0}^{+^2}}\right) + \frac{9A^3}{8}\frac{[\gamma_{w1}^2\gamma_{w2}s_{1,0}^{+} - s_{1,0}^{+^3} - \gamma_{w1}^3(s_{1,0}^{+} + \gamma_{w4}) + s_{1,0}^{+^2}]}{s_{1,0}^{+^2} + \gamma_{w4}s_{1,0}^{+} - \gamma_{w2}^2} = \frac{2}{\pi}, \tag{5.27}$$

a Duffing-like response. (Notice that there is the possibility of the denominator of the coefficient of A^3 vanishing — this corresponds to the second mode also growing and an analysis is possible in this case. This is reminiscent of the work done in Section 3.4.1.) On the upper branches of the Duffing curve, $f_{1,0}$ and $f_{0,1}$ grow to $O(\nu_w)$. Peake [58] has given a detailed analysis of the form of the solution along these upper branches in the one-dimensional case.

2. $\lambda \sim s^+_{2,0}\nu_w$. In this case the detuning band is $O(\nu_w^{-5/3})$ and $f_{0,1}$ and $f_{1,0}$ are $O(\nu_w^{-1/3})$.

3. $\lambda \sim s^+_{3,0}\nu_w$. Here, in the detuning range $O(\nu_w^{1/3})$, the leading-order response for both $f_{0,1}$ and $f_{1,0}$ is a combination of $\sin t$ and $\sin 3t$ terms, both of amplitude $O(\nu_w^{-1})$.

4. For any other spectral line, the term in the expansion will not grow to be the same size as the leading-order terms in the $f_{1,0}$ and $f_{0,1}$ expansions — the nonlinear effects take over before the mode in question reaches a size of $O(\nu_w^{-1})$. Hence, even though there is resonant growth of these higher-order modes, they never dominate the solution.

We conclude that the first three fingers are the most important. The other fingers are "subdominant" in that, because they are so thin, the strength of the shock is very weak and there is very little difference between the continuous regions and the shock regions in this case. So, for $\lambda, \nu_w \to \infty$, we see that the leading-order response is either

$$\phi \sim \frac{4[(\lambda + 2\gamma_{w0}\nu_w)\cos x + \nu_w\gamma_{w1}\cos y]\sin t}{\pi(\lambda - s^+_{1,0}\nu_w)(\lambda - s^-_{1,0}\nu_w)},$$

or comprises one or more of the "sub-resonant" modes $\left\{\begin{array}{c}\cos x\\ \cos y\end{array}\right\}\sin t$, $\left\{\begin{array}{c}\cos 2x\\ \cos 2y\end{array}\right\}$ $\sin 2t$ or $\left\{\begin{array}{c}\cos 3x\\ \cos 3y\end{array}\right\}\sin 3t$. Hence, as in the limit $\nu_w \to 0$, we see that the primary wavetrains are of the most importance as the possible fingers related to the higher-order wavetrains can be seen from (5.23) to have a small amplitude asymptotically.

In conclusion, both the limits ν_w small and ν_w large suggest that the two primary wavetrains are of the most importance and this suggests that in the regime $\nu_w \sim O(1)$ the same may also be true.

5.1.3 Iteration scheme for $\nu_w \sim O(1)$

The limiting solutions found in Sections 5.1.1 and 5.1.2 have a recurring theme. In all cases modes associated with the two primary wavetrains, $f_{1,0}$ and $f_{0,1}$, have dominated the solution. Thus we propose the following iteration scheme to solve the set of equations (5.10) in the absence of dispersion; we write (5.10) as

$$\begin{aligned}\mathcal{C}f_{n,m}^{(i+1)} &+ \frac{2}{\pi}\sin t\delta_{n1}\delta_{m0} = -\frac{2m^2\gamma_{w0}\nu_w}{\lambda_{n,m}^2}f_{n,m}^{(i)''} \\ &+\frac{\nu_w}{\pi^2}\sum_{p=1}^{\infty}\int_0^{2\pi}\int_0^{\pi}R^{(i)}(x,t')(-1)^{pm}\cos pnx\cos p\lambda_{n,m}(t'-t)\mathrm{d}x\mathrm{d}t',\end{aligned} \tag{5.28}$$

where $f_{n,m}^{(i+1)}$ is the $(i+1)^{\text{th}}$ approximation to $f_{n,m}$ and $R^{(i)}$ is the expression found for R by using the approximations $f_{n,m}^{(i)}$ for the $f_{n,m}$. We take as our initial approximation to the solution $A(x,y,t)$,

$$A(x,y,t) = f_{1,0}^{(0)}(t\pm x) + f_{0,1}^{(0)}(t\pm y),$$

so our starting values for the $f_{n,m}$ are

$$f_{n,m}^{(0)} = 0 \quad (n,m)\neq(1,0) \quad \text{or} \quad (0,1), \tag{5.29}$$

where $f_{1,0}^{(0)}$ and $f_{0,1}^{(0)}$ satisfy (5.10) with $f_{n,m}=0$ ($(n,m)\neq(1,0)$ or $(0,1)$) formally set to zero

$$\begin{aligned}\lambda f_{1,0}^{(0)''} + 3f_{1,0}^{(0)'}f_{1,0}^{(0)''} &= -\frac{2}{\pi}\sin t + \frac{\nu_w}{2\pi}\int_0^{\pi}[a_w'(t') - a_w'(\pi-t')]f_{1,0}^{(0)'}(t+2t')\mathrm{d}t' \\ &\quad +\frac{\nu_w}{\pi}\int_0^{\pi}a_w'(\pi-t')[f_{0,1}^{(0)'}(t-t') - f_{0,1}^{(0)'}(t+t')]\mathrm{d}t', \end{aligned}\tag{5.30}$$

$$\begin{aligned}\lambda f_{0,1}^{(0)''} + 3f_{0,1}^{(0)'}f_{0,1}^{(0)''} &= \frac{\nu_w}{\pi}\int_0^{\pi}a_w'(\pi-t')[f_{1,0}^{(0)'}(t-t') - f_{1,0}^{(0)'}(t+t')]\mathrm{d}t' \\ &\quad -2\gamma_{w0}\nu_w f_{0,1}^{(0)''}.\end{aligned}\tag{5.31}$$

We may estimate the rate of convergence by noting that $a_{k,0}$ and $a_{0,k}$ are $O(1/k^3)$ for continuous solutions and $O(1/k^2)$ for shock solutions. Now consider the contribution from $f_{1,0}^{(0)}$ or $f_{0,1}^{(0)}$ to the right-hand side of (5.28) for $i=0$. This feedback term into the equation for $f_{n,m}^{(1)}$ contains a term involving $a_{(n^2+m^2)^{1/2},0}$ from the $f_{1,0}^{(0)}$-wavetrain. Hence, bearing in mind the definitions (5.5) for $f_{n,m}$ and the size of the $a_{k,0}$, it is consistent that $f_{n,m}^{(1)} \sim O(\lambda_{n,m}^{-5})$ for continuous solutions and $f_{n,m}^{(1)} \sim O(\lambda_{n,m}^{-4})$ for shock solutions. This argument indicates that the higher-order wavetrains have an amplitude that is smaller numerically than the primary wavetrains by a factor of at least $(n^2 + m^2)^{-2}$.

In the next section we consider the case $a_w(x) = \cos x$ (so that $\gamma_{w0} = 0$) to demonstrate the effectiveness of this iterative procedure, leaving a discussion of the effect of non-zero γ_{w0} until Section 5.1.5. Finally note that, in the special case $a'_w = 2x$ with $\gamma_{w0} = 0$, we would need to solve, for the first approximation, the system

$$\begin{aligned}
\lambda f''_{1,0} + 3f'_{1,0}f''_{1,0} &= -\frac{2}{\pi}\sin t + \nu_w(f_{1,0} + 4f_{0,1}), \\
\lambda f''_{0,1} + 3f'_{0,1}f''_{0,1} &= 4\nu_w f_{1,0},
\end{aligned}$$

which can be written as one fourth-order equation for either $f_{1,0}$ or $f_{0,1}$. No work has been done on this, but it is expected that a similar shock region picture to the one-dimensional case will emerge, with fingers along the lines $\lambda/\nu_w = (-1 \pm \sqrt{65})/(2n^2)$ (see (5.25)).

5.1.4 Example, $a_w(x) = \cos x$

We now try to quantify some of the arguments given above by taking the simplest analytical case, $a_w(x) = \cos x$. We will present the mathematical detail in obtaining the solution in this case. This illustrates the way in which we solved for the shock regions in Section 4.4.2 and is based on the method of Chester [18]. The details are quite involved and the reader may wish to proceed to Figure 5.5 which summarises the results.

We consider the solution for $f^{(0)}_{n,m}$ given by (5.30) and (5.31). Dropping the superscript (0) for the rest of this subsection and writing

$$f'_{1,0} = \sum_m A_m \cos(mt + \alpha_m), \tag{5.32}$$

$$f'_{0,1} = \sum_m B_m \cos(mt + \beta_m), \tag{5.33}$$

for simplicity (where, from (5.5), $A_m \cos\alpha_m = \frac{1}{2}mb_{m,0}$, $A_m \sin\alpha_m = \frac{1}{2}ma_{m,0}$, $B_m \cos\beta_m = \frac{1}{2}mb_{0,m}$ and $B_m \sin\beta_m = \frac{1}{2}ma_{0,m}$), we get, after integrating,

$$\left(f'_{1,0} + \frac{\lambda}{3}\right)^2 = \frac{4}{3\pi}\left[\cos t\left(1 + \frac{\nu_w\pi}{2}B_1\cos\beta_1\right) - \frac{\nu_w\pi}{2}B_1\sin\beta_1\sin t + c_1\right], \tag{5.34}$$

$$\left(f'_{0,1} + \frac{\lambda}{3}\right)^2 = \frac{4}{3\pi}\left[\frac{\nu_w\pi}{2}A_1\cos\alpha_1\cos t - \frac{\nu_w\pi}{2}A_1\sin\alpha_1\sin t + c_2\right], \tag{5.35}$$

where c_1 and c_2 are constants. We can now proceed by first looking for continuous solutions of (5.34) and (5.35). Hence we first transform these equations by writing

$$\left.\begin{aligned} 1+\frac{\nu_w\pi}{2}B_1\cos\beta_1 &= F_1^2\sin\theta_1, \\ \frac{\nu_w\pi}{2}B_1\sin\beta_1 &= -F_1^2\cos\theta_1, \\ \frac{\nu_w\pi}{2}A_1\cos\alpha_1 &= F_2^2\sin\theta_2, \\ \frac{\nu_w\pi}{2}A_1\sin\alpha_1 &= -F_2^2\cos\theta_2, \end{aligned}\right\} \tag{5.36}$$

and

$$\left.\begin{aligned} 2\tau_1 = t+\theta_1-\frac{\pi}{2} \quad &, \quad \lambda=\pm F_1\lambda_{01}, \\ 2\tau_2 = t+\theta_2-\frac{\pi}{2} \quad &, \quad \lambda=\pm F_2\lambda_{02}, \end{aligned}\right\} \tag{5.37}$$

to give, for continuous solutions,

$$f_{1,0}'(\tau_1) = \frac{\lambda}{\lambda_{01}}\left(-\frac{\lambda_{01}}{3}+\left(\frac{8}{3\pi}\right)^{\frac{1}{2}}(\cos^2\tau_1+c_1)^{1/2}\right), \quad c_1\geq 0, \tag{5.38}$$

$$f_{0,1}'(\tau_2) = \frac{\lambda}{\lambda_{02}}\left(-\frac{\lambda_{02}}{3}+\left(\frac{8}{3\pi}\right)^{\frac{1}{2}}(\cos^2\tau_2+c_2)^{1/2}\right), \quad c_2\geq 0. \tag{5.39}$$

If we use the new time variable, τ_1, in (5.32) and compare the resulting expression with (5.38) by multiplying each expression for $f_{1,0}'$ by $\sin 2\tau_1$ or $\cos 2\tau_1$ and integrating over one period, we find (with similar results coming from the two expressions for $f_{0,1}'$)

$$\cos(\alpha_1-\theta_1)=0 \quad , \quad \cos(\beta_1-\theta_2)=0, \tag{5.40}$$

and

$$\sin(\alpha_1-\theta_1)=-\frac{\lambda\lambda_{11}}{\lambda_{01}A_1} \quad , \quad \sin(\beta_1-\theta_2)=-\frac{\lambda\lambda_{12}}{\lambda_{02}B_1}, \tag{5.41}$$

where

$$\lambda_{i1}=\left(\frac{32}{3\pi^3}\right)^{1/2}\int_{-\frac{\pi}{2}}^{\frac{\pi}{2}}(\cos^2 s+c_i)^{1/2}\cos 2s\,ds. \tag{5.42}$$

Also, the zero mean condition gives

$$\lambda_{i0}=\left(\frac{24}{\pi^3}\right)^{1/2}\int_{-\frac{\pi}{2}}^{\frac{\pi}{2}}(\cos^2 s+c_i)^{1/2}ds. \tag{5.43}$$

For (5.40) and (5.41) to be consistent with (5.36) requires that $\alpha_1 = \beta_1 = 0$ and

$$\theta_1 = \begin{cases} \frac{\pi}{2} & 1+\frac{\nu_w\pi}{2}B_1 > 0, \\ -\frac{\pi}{2} & 1+\frac{\nu_w\pi}{2}B_1 < 0, \end{cases} \quad , \quad F_1^2 = \left|1+\frac{\nu_w\pi}{2}B_1\right|,$$

$$\theta_2 = \begin{cases} \frac{\pi}{2} & \frac{\nu_w\pi}{2}A_1 > 0, \\ -\frac{\pi}{2} & \frac{\nu_w\pi}{2}A_1 < 0, \end{cases} \quad , \quad F_2^2 = \left|\frac{\nu_w\pi}{2}A_1\right|,$$

and, recalling the expressions for F_1 and F_2 in (5.37), gives, after some algebra,

$$\frac{\lambda^2}{\lambda_{01}^2} = s_1\left(1+s_2\nu_w\frac{\pi\lambda\lambda_{12}}{2\lambda_{02}}\right) \quad , \quad \frac{\lambda^2}{\lambda_{02}^2} = s_1 s_2\nu_w\frac{\pi\lambda\lambda_{11}}{2\lambda_{01}}, \tag{5.44}$$

where

$$s_1 = \operatorname{sgn}\left(1+\frac{\nu_w\pi}{2}B_1\right) \quad , \quad s_2 = \operatorname{sgn}\left(\frac{\nu_w\pi}{2}A_1\right).$$

Noting that $\eta_0(0,0,t)$ is proportional to $f'_{1,0}(t) + f'_{0,1}(t)$, we will take as a guide to the amplitude the following definition

$$A_s = (\max f'_{1,0} - \min f'_{1,0}) + (\max f'_{0,1} - \min f'_{0,1}), \tag{5.45}$$

which is the same definition as the one used in Chapter 3. Hence, for continuous solutions, we have

$$A_s = \left(\frac{8}{3\pi}\right)^{1/2}\left[\left|\frac{\lambda}{\lambda_{01}}\right|\left\{(1+c_1)^{1/2} - c_1^{1/2}\right\} + \left|\frac{\lambda}{\lambda_{02}}\right|\left\{(1+c_2)^{1/2} - c_2^{1/2}\right\}\right]. \tag{5.46}$$

Therefore we can vary c_1 and c_2 to determine λ_{i0} and λ_{i1} and hence determine λ and ν_w from (5.44) and finally determine A_s from (5.46).

To determine the shock regimes we seek zeros of c_1 or c_2. It becomes apparent that shocks emerge in the x- and y-directions at different places in the (λ, ν_w)-plane. Therefore, we can fix $c_1 = 0$ and vary $c_2 \geq 0$ to give a line showing the interface between shock and no-shock regimes in the x-direction. Similarly, we can fix $c_2 = 0$ and vary $c_1 \geq 0$. This provides the picture given in Figure 5.4 where we have indicated which line represents the x-direction interface and which the y-direction interface between shock and no-shock regimes. Clearly we do not know, for example, where to the left of the x-direction interface shocks in the y-direction start. To determine this, and also the response in the shock regions, we have to consider three scenarios, just shocks in the x-direction, just shocks in the y-direction and shocks in both directions.

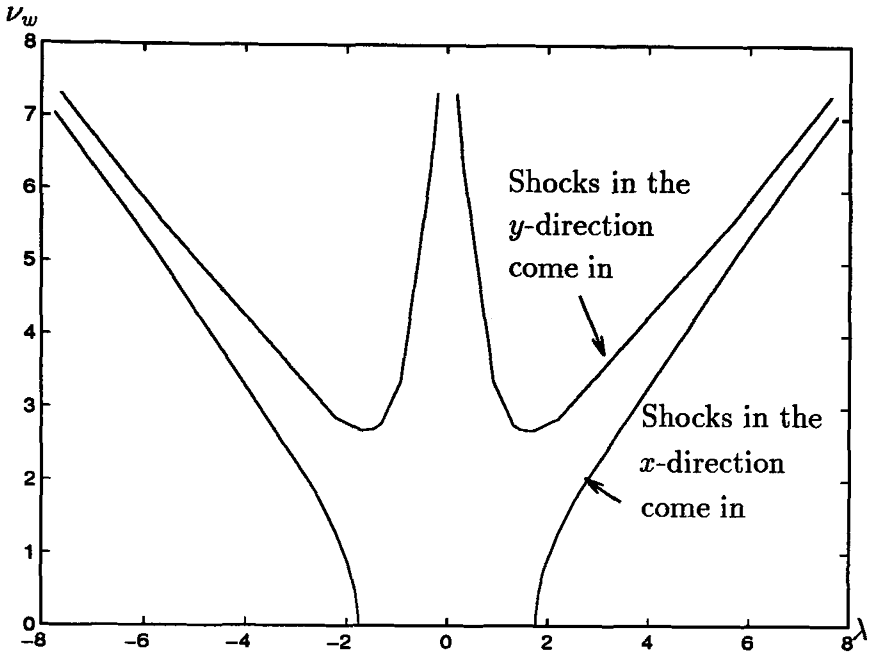

Figure 5.4: Picture showing the emergence of the shock regions.

Shock in one direction only

We will first consider the case when there is a shock in the x-direction and none in the y-direction. Hence we fix $c_1 = 0$ and starting with (5.34) and (5.35) we use the same transformations (5.36) and (5.37) except we redefine λ_{01} to be

$$\lambda = \pm \left(\frac{96}{\pi^3}\right)^{\frac{1}{2}} \lambda_{01} F_1, \tag{5.47}$$

to give

$$f'_{1,0}(\tau_1) = -\frac{\pi\lambda}{6}\left[\frac{2}{\pi} + \frac{1}{\lambda_{01}}\cos\tau_1\right], \quad \arcsin\lambda_{01} < \tau_1 < \pi + \arcsin\lambda_{01}, \tag{5.48}$$

where $0 \leq \lambda_{01} \leq 1$, and this has been chosen to satisfy the zero mean condition and have a compressive shock. Equation (5.39) for $f'_{0,1}$ remains the same.

We again have

$$\cos(\beta_1 - \theta_2) = 0 \quad , \quad \sin(\beta_1 - \theta_2) = -\frac{\lambda\lambda_{12}}{\lambda_{02}B_1}, \tag{5.49}$$

where λ_{02} and λ_{12} are the same as before. Comparison of the expressions (5.32) and (5.48) this time yields

$$A_1\cos(\alpha_1 - \theta_1) \quad = \quad \frac{4}{9}\frac{\lambda}{\lambda_{01}}(1 - \lambda_{01}^2)^{3/2}, \tag{5.50}$$

$$A_1 \sin(\alpha_1 - \theta_1) = -\frac{2}{3}\lambda\left(1 - \frac{2}{3}\lambda_{01}^2\right). \tag{5.51}$$

After some manipulation, (5.49)–(5.51) and (5.36) give

$$\left[\left(F_1^2F_2^2 - \frac{\nu_w^2\pi^2}{4}g_{21}a_2\right)\psi + \frac{\nu_w\pi}{2}g_{21}\right]^2 = \frac{\nu_w^4\pi^4}{16}g_{11}^2a_2^2(1-\psi^2), \tag{5.52}$$

$$\frac{\nu_w^2\pi^2}{4}g_{11}^2\left[1 - \frac{\nu_w\pi}{2}a_2\psi\right]^2 = \left[\frac{\nu_w^2\pi^2}{4}g_{21}a_2 - F_1^2F_2^2\right]^2(1-\psi^2), \tag{5.53}$$

where

$$g_{1i} = \frac{4}{9}\frac{\lambda}{\lambda_{0i}}(1-\lambda_{0i}^2)^{3/2} \quad , \quad g_{2i} = -\frac{2}{3}\lambda\left(1 - \frac{2}{3}\lambda_{0i}^2\right),$$

$$\psi = \sin\theta_2 = \frac{4 + \nu_w^2\pi^2a_2^2 - 4F_1^4}{4\nu_w\pi a_2} \quad , \quad a_i = -\frac{\lambda\lambda_{1i}}{\lambda_{0i}}.$$

Finally, we can use the expressions

$$F_1^2 = \frac{\pi^3}{96}\frac{\lambda^2}{\lambda_{01}^2} \quad , \quad F_2^2 = \frac{\lambda^2}{\lambda_{02}^2},$$

so that (5.52) and (5.53) represent two equations for λ and ν_w linked through the parameters c_2 and λ_{01}. By now fixing $c_2 = 0$ we can vary λ_{01} to produce the y-direction interface between shock and no-shock regimes which lies inside the x-direction shock region. We now have enough information to determine the response in the region where there are shocks in the x-direction but continuous solutions in the y-direction. Using (5.45) we get

$$A_s = \left(\frac{8}{3\pi}\right)^{\frac{1}{2}}\left|\frac{\lambda}{\lambda_{02}}\right|\left\{(1+c_2)^{1/2} - c_2^{1/2}\right\} + \frac{\pi}{6}\left|\frac{\lambda}{\lambda_{01}}\right|\left\{1 + (1-\lambda_{01}^2)^{1/2}\right\}. \tag{5.54}$$

We can complete a similar calculation for the region where there is just a shock in the y-direction. We will just give the results. Fixing $c_2 = 0$ we again have (5.36) and (5.37) except now

$$\lambda = \pm\left(\frac{96}{\pi^3}\right)^{\frac{1}{2}}\lambda_{02}F_2,$$

and

$$f_{0,1}'(\tau_2) = -\frac{\pi\lambda}{6}\left[\frac{2}{\pi} + \frac{1}{\lambda_{02}}\cos\tau_2\right], \quad \arcsin\lambda_{02} < \tau_2 < \pi + \arcsin\lambda_{02}, \tag{5.55}$$

for $0 \leq \lambda_{02} \leq 1$ and $f'_{1,0}$ satisfies (5.38). Then this time we find,

$$\left(\frac{\nu_w \pi}{2} g_{22} - \frac{2F_1^2 F_2^2}{\nu_w \pi a_1}\right)^2 = 1 - \frac{\nu_w^2 \pi^2}{4} g_{12}^2, \tag{5.56}$$

$$\lambda^2 = \frac{\nu_w^2 \pi^2 \lambda_{11}^2 \lambda_{02}^4}{4\lambda_{01}^2} \left(\frac{96}{\pi^3}\right)^4, \tag{5.57}$$

where λ_{11} and λ_{01} are as in (5.42) and (5.43). Again, using expressions for F_1 and F_2, this represents two equations for λ and ν_w linked through the parameters c_1 and λ_{02}. As before, we can fix $c_1 = 0$ and compute the interface between shock and no-shock regimes in the x-direction. The final picture is shown in Figure 5.5(a), the region between the solid lines (in the same sense as Figure 4.3) representing shocks in the x-direction and the region between the dotted lines shocks in the y-direction. Also, in this case, the amplitude is given by

$$A_s = \left(\frac{8}{3\pi}\right)^{\frac{1}{2}} \left|\frac{\lambda}{\lambda_{01}}\right| \left\{(1+c_1)^{1/2} - c_1^{1/2}\right\} + \frac{\pi}{6}\left|\frac{\lambda}{\lambda_{02}}\right| \left\{1 + (1-\lambda_{02}^2)^{1/2}\right\}. \tag{5.58}$$

The shock picture, Figure 5.5(a), is different to its one-dimensional equivalent in that there are two fingers associated with the introduction of one harmonic into $a_w(x)$ rather than one. This is due to the coupling between the two wavetrains and we note that the symmetry about the line $\lambda = 0$ in this case is just a consequence of taking $a_w(x) = \cos x$. For more general $a_w(x)$ we see from (5.25) that the fingers lie along lines that are not symmetric about $\lambda = 0$.

Shocks in both directions

To complete the analysis we now consider the case when shocks occur in both directions. In the same way as in the last section we construct shock solutions from (5.34) and (5.35) by using (5.36) and (5.37) except now λ_{01} and λ_{02} are defined by

$$\left(\frac{\pi^3}{96}\right)^{\frac{1}{2}} \lambda = \pm\lambda_{01} F_1 = \pm\lambda_{02} F_2, \tag{5.59}$$

to give

$$f'_{1,0}(\tau_1) = -\frac{\pi\lambda}{6}\left[\frac{2}{\pi} + \frac{1}{\lambda_{01}}\cos\tau_1\right], \quad \arcsin\lambda_{01} < \tau_1 < \pi + \arcsin\lambda_{01}, \tag{5.60}$$

$$f'_{0,1}(\tau_2) = -\frac{\pi\lambda}{6}\left[\frac{2}{\pi} + \frac{1}{\lambda_{02}}\cos\tau_2\right], \quad \arcsin\lambda_{02} < \tau_2 < \pi + \arcsin\lambda_{02}, \tag{5.61}$$

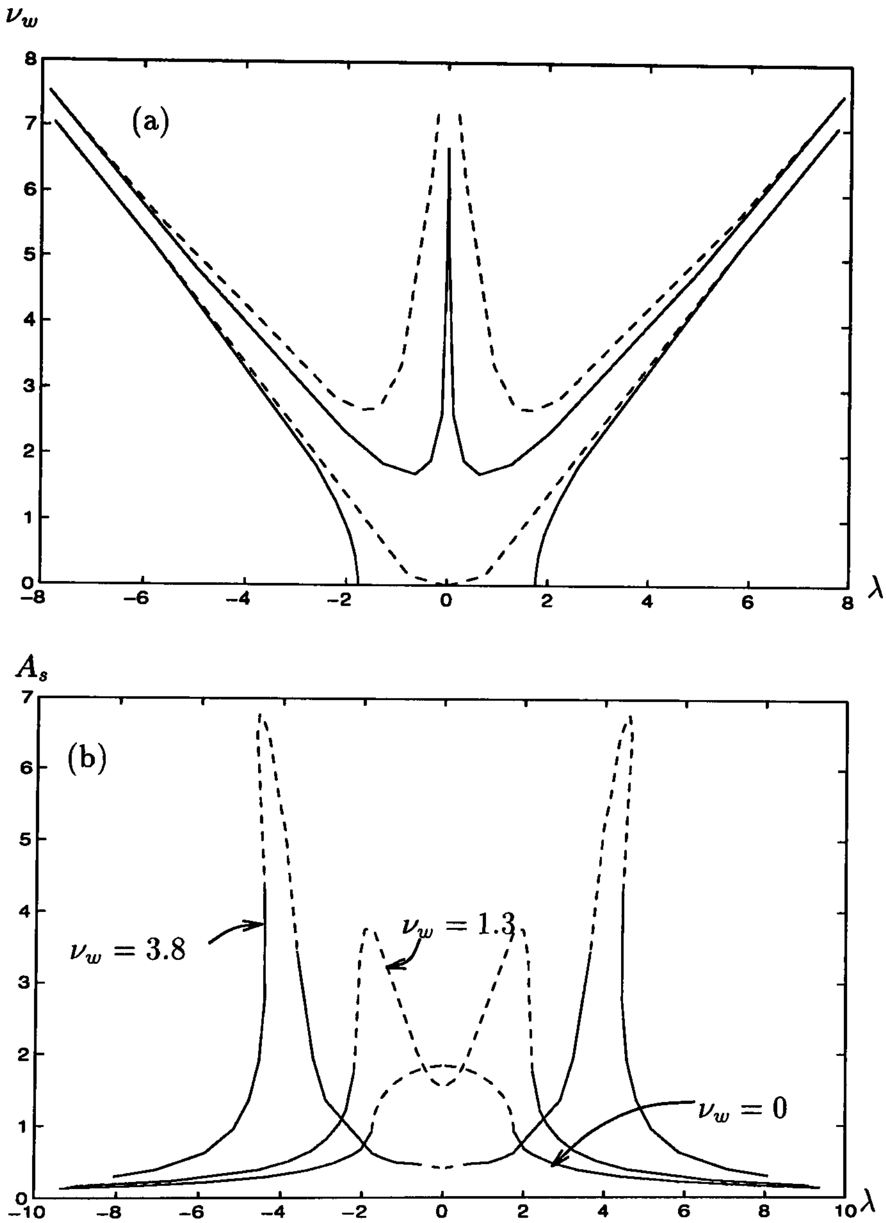

Figure 5.5: Plot showing, for $a_w(x) = \cos x$, (a) the interface between shock and continuous solutions where there are shocks in the longitudinal direction between the solid lines and shocks in the transverse direction between the dashed lines, and (b) the response where the dashed part of the curve indicates a shock in any direction.

where $0 \leq \lambda_{01}, \lambda_{02} \leq 1$. Comparison of these equations with (5.32) and (5.33) yields

$$A_1 \cos(\alpha_1 - \theta_1) = g_{11} \quad , \quad A_1 \sin(\alpha_1 - \theta_1) = g_{21},$$
$$B_1 \cos(\beta_1 - \theta_2) = g_{12} \quad , \quad B_1 \sin(\beta_1 - \theta_2) = g_{22}.$$

Using (5.36) gives, after some consideration,

$$F_2^4 = \frac{\nu_w^2 \pi^2}{4}(g_{11}^2 + g_{21}^2), \tag{5.62}$$

$$F_2^4 - \frac{\nu_w^4 \pi^4}{16}(g_{12}g_{21} + g_{11}g_{22})^2 = \left[F_1^2 F_2^2 + \frac{\nu_w^2 \pi^2}{4}(g_{12}g_{11} - g_{21}g_{22})\right]^2. \tag{5.63}$$

Finally, using expressions for F_1 and F_2 from (5.59) we have two expressions for ν_w and λ with parameters λ_{01} and λ_{02}. In this case the amplitude is

$$A_s = \frac{\pi}{6}\left(\left|\frac{\lambda}{\lambda_{01}}\right|\left\{1 + (1 - \lambda_{01}^2)^{1/2}\right\} + \left|\frac{\lambda}{\lambda_{02}}\right|\left\{1 + (1 - \lambda_{02}^2)^{1/2}\right\}\right). \tag{5.64}$$

We now know the form of the response everywhere in the (λ, ν_w)-plane and use this information to produce Figure 5.5(b) where we have plotted the amplitude (using (5.46), (5.54), (5.58) and (5.64)) against λ for various ν_w. The two Duffing-type branches seen here correspond to the growth of the $\sin t$ term in the expansions for $f_{1,0}$ and $f_{0,1}$ and the right-hand branch matches very well with the formula (5.27) despite ν_w being only 3.8.

We also plot, in Figure 5.6, $A_t(x, y, t)$ for $t = -\pi/4$ and $\lambda = 0$, $\nu_w = 1.3$ which can be compared to Figure 5.3 and we see the growth of the $f_{0,1}$ wavetrain and a change in its phase.

Iteration procedure

Proceeding to the next stage we have, from (5.28), $f_{1,0}^{(0)} = f_{1,0}^{(1)}$, $f_{0,1}^{(0)} = f_{0,1}^{(1)}$, $f_{3,4}^{(1)} = 0$ and

$$\mathcal{C} f_{4,3}^{(1)} = -\frac{5\nu_w}{4}\left[a_{5,0}^{(0)} \cos 5t + b_{5,0}^{(0)} \sin 5t\right], \tag{5.65}$$

and so on for the other $f_{n,m}^{(1)}$. For $i = 1$, (5.28) gives

$$\mathcal{C} f_{1,0}^{(2)} = -\frac{\nu_w}{2}\left(a_{0,1}^{(1)} \cos t + b_{0,1}^{(1)} \sin t + \frac{5}{2}[a_{4,3}^{(1)} \cos 5t + b_{4,3}^{(1)} \sin 5t] + \cdots\right)$$
$$-\frac{2}{\pi} \sin t, \tag{5.66}$$

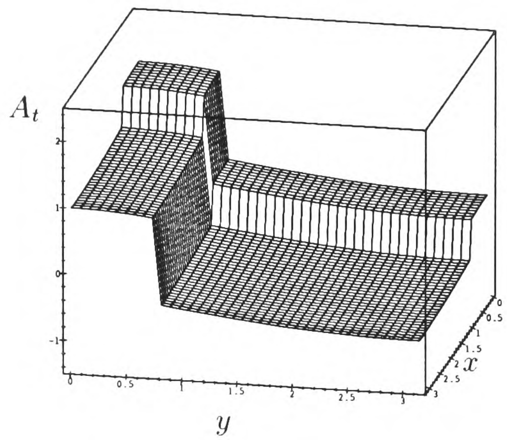

Figure 5.6: Plot of A_t for $\lambda = 0$, $\nu_w = 1.3$ and $t = -\pi/4$.

$$\mathcal{C}f^{(2)}_{0,1} = -\frac{\nu_w}{2}(a^{(1)}_{1,0}\cos t + b^{(1)}_{1,0}\sin t + \cdots), \tag{5.67}$$

$$\mathcal{C}f^{(2)}_{3,4} = -\frac{13\nu_w}{4}(a^{(1)}_{4,3}\cos 5t + b^{(1)}_{4,3}\sin 5t + \cdots), \tag{5.68}$$

$$\mathcal{C}f^{(2)}_{4,3} = -\frac{\nu_w}{4}(5[a^{(1)}_{5,0}\cos 5t + b^{(1)}_{5,0}\sin 5t] + 13[a^{(1)}_{3,4}\cos 5t + b^{(1)}_{3,4}\sin 5t] + \cdots), \tag{5.69}$$

and so on, where we have just included terms from the first four wavetrains as an illustration.

In theory we can solve these equations and carry on the iterative process; in practice, we solve (5.65) and (5.66)–(5.69) (although the details are very arduous so we do not present them here) and show that these solutions to the third step in the iteration differ only marginally from the original approximation. The most extreme case of the higher-order wavetrains growing was found close to $\lambda = 0$ for $\nu_w > 0$ but even in this case the contribution from the higher order wavetrains is small and there is no noticeable change in the shock locations in the primary wavetrains.

5.1.5 Transition between two- and one- dimensional solutions

We can now relate the results of the last subsection to the one-dimensional Chester solution by varying the average of the back wall variation, γ_{w0}. Hence we consider the case $a(x) = \gamma_{w0} + \cos x$ and, in Figure 5.7, we draw the different shock pictures that are found by increasing the value of γ_{w0}. The dashed lines correspond to the

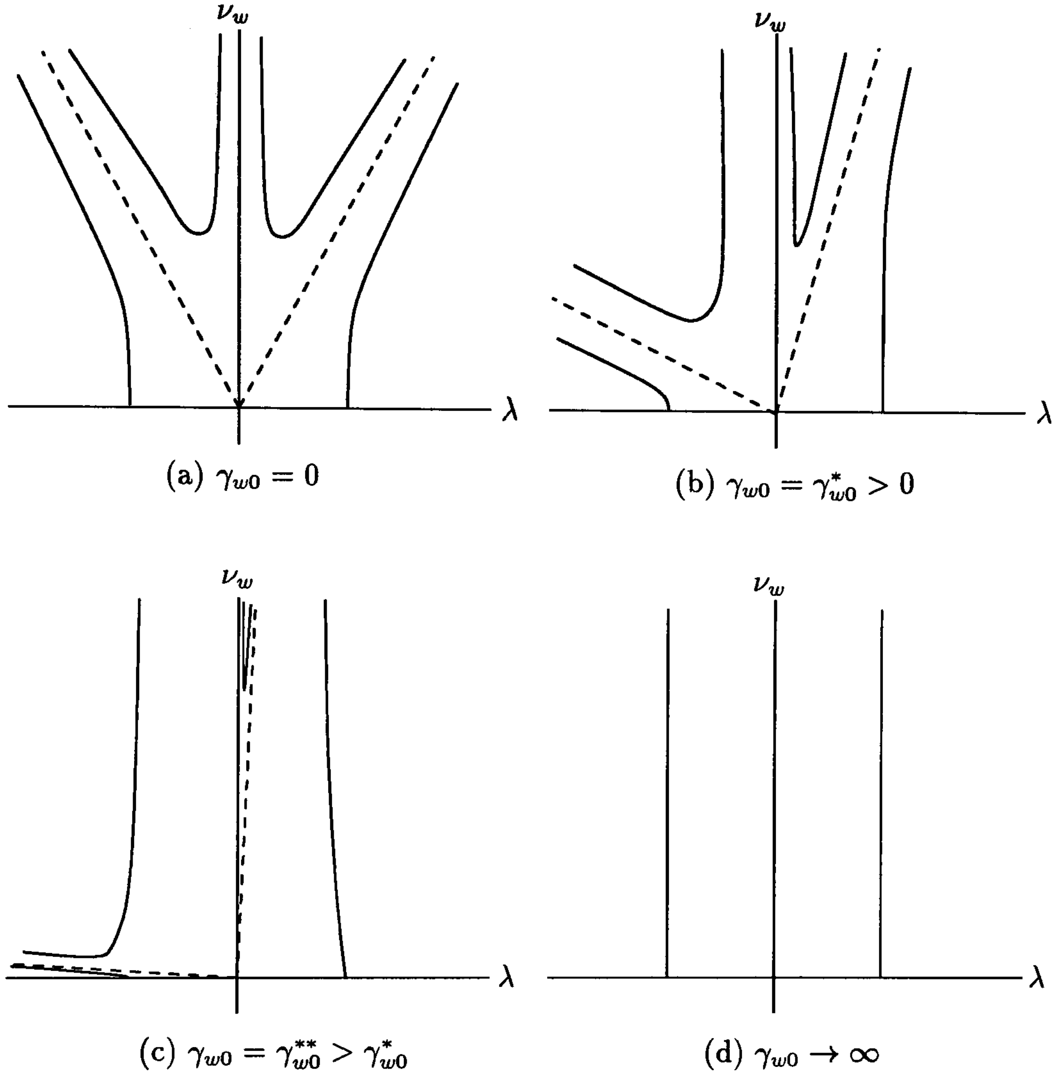

Figure 5.7: Transition between two- and one-dimensional solutions for $a(x) = \gamma_{w0}\cos x$ as γ_{w0} increases.

spectral lines (5.25) and we have not indicated where within the solid lines shocks in either direction occur, so that Figure 5.7(a) is the same as Figure 5.4. However, we recall that, as $\gamma_{w0} \to \infty$, (5.10) implies that $f_{1,0} \sim O(1/\gamma_{w0})$ so that the longitudinal wavetrain dominates by the time we arrive at Figure 5.7(d). Indeed, because we have chosen $a(x) = \gamma_{w0} + \cos x$, we can see from the one-dimensional analysis (in particular (4.61)) that the one-dimensional solution is unaffected by this geometry and this is borne out by Figure 5.7(d).

5.2 Dispersive effects

To tie in the shallow and deep water work we consider the limit of (5.10) as $\kappa \to \infty$ and show that it matches to the limit of the deep water response as $h \to 0$. To that extent, we consider (3.27), (3.37) and (3.38) with $b_d = 0$ as $h \to 0$, which gives

$$\phi \sim \varepsilon^{1/3}[A \cos x \sin(t + \alpha_1) + B \cos y \sin(t + \beta_1)], \tag{5.70}$$

with $\sin\alpha_1 = \sin\beta_1 = 0$ and

$$\frac{4}{\pi} = \left(\lambda_d A - \frac{9}{32h^2}A^3 - \frac{1}{4}AB^2 + \nu_{wd}\gamma_{w2}A\right)\cos\alpha_1 - \nu_{wd}\gamma_{w1}B\cos\beta_1, \tag{5.71}$$

$$0 = \left(\lambda_d B - \frac{9}{32h^2}B^3 - \frac{1}{4}A^2 B\right)\cos\beta_1 - \nu_{wd}\gamma_{w1}A\cos\alpha_1. \tag{5.72}$$

Using the shallow water scalings, (4.4)–(4.5) and scaling A and B as

$$A = \kappa^{2/3}\varepsilon^{1/6}A^* \quad , \quad B = \kappa^{2/3}\varepsilon^{1/6}B^*,$$

yields

$$\frac{4}{\pi} = \left(\lambda\kappa^{2/3}A^* - \frac{9}{32}A^{*^3} + \nu_w\kappa^{2/3}\gamma_{w2}A^*\right)\cos\alpha_1 - \nu_w\kappa^{2/3}\gamma_{w1}B^*\cos\beta_1, \tag{5.73}$$

$$0 = \left(\lambda\kappa^{2/3}B^* - \frac{9}{32}B^{*^3}\right)\cos\beta_1 - \nu_w\kappa^{2/3}\gamma_{w1}A^*\cos\alpha_1, \tag{5.74}$$

plus $O(\varepsilon^{1/2}\kappa^2)$ terms, where we have written $\lambda_d = \lambda\varepsilon^{-1/6}$, $\nu_{wd} = \nu_w\varepsilon^{-1/6}$, relating (2.29) and (2.30) to (4.3) and (4.5). To consider the deep water limit of (5.10) as $\kappa \to \infty$ we recall that the shallow water depth is $O(\varepsilon^{1/4})$ and the detuning range is $\lambda_0 \sim O(\varepsilon^{1/2})$. To match to the deep water scalings we require $\kappa \sim O(\varepsilon^{-1/4})$ and $\lambda \sim O(\varepsilon^{1/6})$ (so that we are in the detuning range $\lambda_0 \sim O(\varepsilon^{2/3})$) and hence we take the limit as $\kappa \to \infty$ with $\lambda\kappa^{2/3} \sim O(1)$. Similarly we require $\nu_w\kappa^{2/3} \sim O(1)$ for the correct scaling of ν_{w0} and we expand the $f_{n,m}$ as

$$f_{n,m} = \kappa^{2/3}f^{(0)}_{n,m} + \kappa^{-2/3}f^{(1)}_{n,m} + \kappa^{-2}f^{(2)}_{n,m} + \cdots \quad \forall(n,m).$$

Then, to $O(\kappa^{8/3})$, we get

$$\frac{\mathrm{d}^4 f^{(0)}_{n,m}}{\mathrm{d}t^4} + \frac{\mathrm{d}^2 f^{(0)}_{n,m}}{\mathrm{d}t^2} = 0 \quad \forall(n,m),$$

which has the solution

$$f^{(0)}_{n,m} = A_{n,m}\sin(t + \alpha_{n,m}) \quad \forall(n,m). \tag{5.75}$$

The $O(\kappa^{4/3})$ terms give

$$\frac{1}{3}\left(\frac{\mathrm{d}^4 f^{(1)}_{n,m}}{\mathrm{d}t^4}+\frac{\mathrm{d}^2 f^{(1)}_{n,m}}{\mathrm{d}t^2}\right)=3\frac{\mathrm{d}^2 f^{(0)}_{n,m}}{\mathrm{d}t^2}\frac{\mathrm{d}f^{(0)}_{n,m}}{\mathrm{d}t} \quad \forall(n,m),$$

which, using (5.75), have solution

$$f^{(1)}_{n,m}=C_{n,m}\sin\left(t+\beta_{n,m}\right)+\frac{3}{8}A^2_{n,m}\sin 2(t+\alpha_{n,m}) \quad \forall(n,m). \tag{5.76}$$

Finally, to $O(1)$,

$$\begin{aligned}\frac{1}{3}\left(\frac{\mathrm{d}^4 f^{(2)}_{n,m}}{\mathrm{d}t^4}+\frac{\mathrm{d}^2 f^{(2)}_{n,m}}{\mathrm{d}t^2}\right) &= 3\left(\frac{\mathrm{d}^2 f^{(0)}_{n,m}}{\mathrm{d}t^2}\frac{\mathrm{d}f^{(1)}_{n,m}}{\mathrm{d}t}+\frac{\mathrm{d}^2 f^{(1)}_{n,m}}{\mathrm{d}t^2}\frac{\mathrm{d}f^{(0)}_{n,m}}{\mathrm{d}t}\right)\\ &\quad -\frac{\nu_w\kappa^{2/3}}{2\pi}\int_0^{\pi}\left(\frac{\mathrm{d}f^{(0)}_{n,m}}{\mathrm{d}t}(2x+t)-\frac{\mathrm{d}f^{(0)}_{n,m}}{\mathrm{d}t}(t-2x)\right)a'_w(x)\mathrm{d}x\\ &\quad +\frac{2}{\pi}\delta_{n1}\delta_{m0}\sin t+\lambda\kappa^{2/3}\frac{\mathrm{d}^2 f^{(0)}_{n,m}}{\mathrm{d}t^2}.\end{aligned}$$

Now the Fredholm Alternative states that for there to exist periodic solutions of period 2π for $f^{(2)}_{n,m}$ then the right-hand side of these equations must be orthogonal to $\cos t$ and $\sin t$. So, using the expressions for $f^{(0)}_{n,m}$ and $f^{(1)}_{n,m}$, these orthogonality conditions imply that $\sin\alpha_{n,m}=0$ and

$$\left.\begin{aligned}\frac{2}{\pi} &= \left(\lambda\kappa^{2/3}-\frac{9}{8}A^2_{1,0}+\gamma_{w2}\nu_w\kappa^{2/3}\right)A_{1,0}\cos\alpha_{1,0}-\gamma_{w1}\nu_w\kappa^{2/3}A_{0,1}\cos\alpha_{0,1},\\ 0 &= \left(\lambda\kappa^{2/3}A_{0,1}-\frac{9}{8}A^3_{0,1}\right)\cos\alpha_{0,1}-\gamma_{w1}\nu_w\kappa^{2/3}A_{1,0}\cos\alpha_{1,0}\\ A_{n,m} &= 0 \quad (n,m)\neq(1,0)\text{ or }(0,1).\end{aligned}\right\} \tag{5.77}$$

Finally, noting that the leading-order velocity potential is now

$$\phi\sim 2\varepsilon^{1/2}[A_{1,0}\cos x\sin\left(t+\alpha_{1,0}\right)+A_{0,1}\cos y\sin\left(t+\alpha_{0,1}\right)],$$

we see that (5.77) matches (5.73) and (5.74) if we write $2A_{1,0}=A^*$, $2A_{0,1}=B^*$, $\alpha_{1,0}=\alpha_1$ and $\alpha_{0,1}=\beta_1$.

5.3 Other two-dimensional responses

We can exploit the fact that different wavetrains do not interact through the nonlinearity (Proposition 5.1) in two cases where we choose different forcing mechanisms to generate two-dimensional responses.

5.3.1 Forcing at an angle

A simple two-dimensional response can be obtained if we force the tank at an angle to its sides as in Figure 5.8. The boundary conditions (2.18), (2.20) and (2.21) are

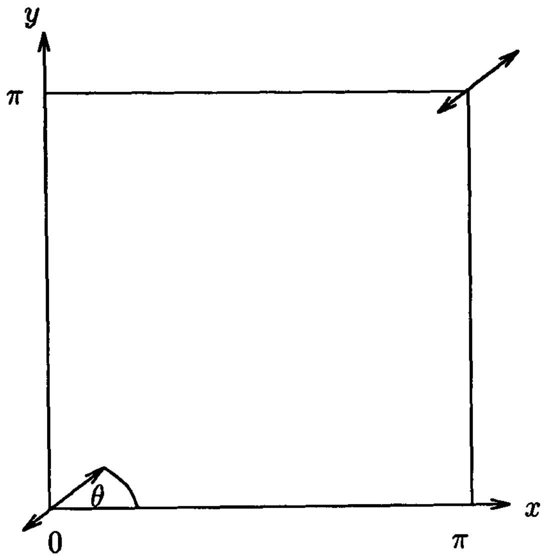

Figure 5.8: Top view of a tank being oscillated an an angle.

replaced with

$$\phi_x = \varepsilon \cos\theta \sin t \quad \text{on} \quad x = 0, \pi \quad , \quad \phi_y = \varepsilon \sin\theta \sin t \quad \text{on} \quad y = 0, \pi,$$

correct to $O(\varepsilon)$, so that the solution considered in Section 4.4.1 corresponds to $\theta = 0$. Now we can proceed as in Chapter 4 and we will be left with the same problem for A and B as on page 55 except that (4.31), (4.32) and (4.33) become

$$B_x = \cos\theta \sin t \quad \text{on} \quad x = 0, \pi, \tag{5.78}$$

$$B_y = \sin\theta \sin t \quad \text{on} \quad y = 0, \pi. \tag{5.79}$$

The orthogonality conditions (5.6) then give $A_{n,m} = 0$ except for $A_{1,0}$ and $A_{0,1}$ so that

$$A(x, y, t) = f_{1,0}(t \pm x) + f_{0,1}(t \pm y). \tag{5.80}$$

Now, using the knowledge that the wavetrains $A_{1,0}$ and $A_{0,1}$ are not coupled through the nonlinearity, we simply find that each of $f_{1,0}$ and $f_{0,1}$ satisfy modified versions of the higher-order Chester equation, that is

$$-\frac{\kappa^2}{3} f_{1,0}^{(iv)} + \left(\lambda - \frac{\kappa^2}{3}\right) f_{1,0}'' + 3 f_{1,0}' f_{1,0}'' = -\frac{2}{\pi} \cos\theta \sin t, \tag{5.81}$$

$$-\frac{\kappa^2}{3} f_{0,1}^{(iv)} + \left(\lambda - \frac{\kappa^2}{3}\right) f_{0,1}'' + 3 f_{0,1}' f_{0,1}'' = -\frac{2}{\pi} \sin\theta \sin t, \tag{5.82}$$

and hence, in the dispersion-free case, we find shocks are possible in the x-direction for $|\lambda| \leq \lambda_x^*$ and in the y-direction for $|\lambda| \leq \lambda_y^*$ where

$$\lambda_x^* = \left(\frac{96\cos\theta}{\pi^3}\right)^{\frac{1}{2}} \quad , \quad \lambda_y^* = \left(\frac{96\sin\theta}{\pi^3}\right)^{\frac{1}{2}}$$

Hence, depending on the values of θ and λ, it is possible to have one shock in either the x- or y-direction or two shocks crossing orthogonally to each other, where we have assumed that these shocks do not interact to first order, as was discussed at the start of this chapter.

5.3.2 Resonance of higher modes

We now consider a two-dimensional response caused by forcing a square tank ($\nu_w = 0$) not near the fundamental mode but near the (N, M)-mode. To do this, we write

$$\Omega^2 = \frac{g}{L}\lambda_{N,M}(1 + \lambda\varepsilon^{1/2})\tanh(\lambda_{N,M}h),$$

($\lambda_{N,M}^2 = N^2 + M^2$, (N, M) are coprime integers[2] and $\lambda_{N,M}$ is not too large so that we stay in the small rate limit discussed in Section C.1.1) instead of (2.16), where we non-dimensionalise with this new Ω as in Section 2.1.4. We are thus trying to excite the $\cos Nx \cos My \sin t$ mode and this will only happen if the boundary condition on the walls $x = 0, \pi$ is proportional to $\cos My \sin t$. Hence, instead of oscillating the tank from side to side, we take wavemakers at $x = 0, \pi$ and, for simplicity, we choose the ends to be at $x = -\varepsilon \cos My \cos t, \pi - \varepsilon \cos My \cos t$. The only modifications to the shallow water model (4.6)–(4.13) are then that (4.13) becomes

$$\bar{\eta} \;+\; \lambda_{N,M}^2\kappa\left(1 - \frac{\lambda_{N,M}^2\kappa^2}{3}\varepsilon^{1/2} + O(\varepsilon)\right)\left(1 + \lambda\varepsilon^{1/2}\right)$$
$$\left(\bar{\phi}_t + \frac{1}{2}\left[\bar{\phi}_{\bar{z}}^2 + \varepsilon^{1/2}\left\{\bar{\phi}_x^2 + \bar{\phi}_y^2\right\}\right]\right) = 0,$$

[2]We take this condition so that there is no possibility of more than one shock per period. For (N, M) not coprime, we may be able to construct solutions with more that one shock per period in the same way as at the start of Section C.1.1.

on $\bar{z} = \varepsilon^{1/2}\bar{\eta}$ and the boundary conditions (4.7) become

$$\bar{\phi}_x = \varepsilon^{1/2} \cos My \sin t - \varepsilon M \bar{\phi}_y \sin My \cos t \quad \text{on}$$
$$x = -\varepsilon \cos My \cos t, \pi - \varepsilon \cos My \cos t.$$

We now proceed as before, expanding $\bar{\phi}$ and $\bar{\eta}$ using (4.14) and (4.15) and the calculation follows the same steps as in Section 4.1.2. We will omit the details and just provide the final problems for $A(x,y,t)$ and $B(x,y,t)$, where $\phi_0 = A$ and $\phi_1 = -(1/2)(A_{xx} + A_{yy})(\bar{z} + \kappa)^2 + B$, which are

$$\begin{aligned} A_{xx} + A_{yy} &= \lambda_{N,M}^2 A_{tt}, & (5.83)\\ A_x &= 0 \quad \text{on} \quad x = 0, \pi, & (5.84)\\ A_y &= 0 \quad \text{on} \quad y = 0, \pi, & (5.85)\\ \nabla A(x,y,t+2\pi) &= \nabla A(x,y,t), & (5.86) \end{aligned}$$

and

$$\begin{aligned} B_{xx} + B_{yy} - \lambda_{N,M}^2 B_{tt} &= -\frac{\kappa^2}{3}(A_{xxxx} + 2A_{xxyy} + A_{yyyy}) \\ &\quad + \lambda_{N,M}^2 \left(\lambda - \frac{\kappa^2}{3}\lambda_{N,M}^2\right) A_{tt} \\ &\quad + 2\lambda_{N,M}^2 (A_x A_{xt} + A_y A_{yt}) + \lambda_{N,M}^4 A_t A_{tt}, & (5.87)\\ B_x &= \cos My \sin t \quad \text{on} \quad x = 0, \pi, & (5.88)\\ B_y &= 0 \quad \text{on} \quad y = 0, \pi, & (5.89)\\ \nabla B(x,y,t) &= \nabla B(x,y,t+2\pi). & (5.90) \end{aligned}$$

The general solution to (5.83)–(5.86) is

$$A = \sum_{p,q} \cos px \cos qy (a_{p,q} \sin \omega_{p,q} t + b_{p,q} \cos \omega_{p,q} t),$$

where we sum over all p, q such that $p^2 + q^2 = \omega_{p,q}^2 (N^2 + M^2)$ and $\omega_{p,q}$ are integers. However, as the forcing only excites the mode $\cos Nx \cos My \sin t$ and the nonlinearity only couples this to the modes $\cos sNx \cos sMy \sin st$ as a consequence of Proposition 5.1, we see that only the (N, M)-wavetrain is excited. Hence we can write

$$A = f_{N,M}(t \pm Nx \pm My), \tag{5.91}$$

where

$$f_{N,M}(\tau) = \frac{1}{4}\sum_s (a_{sN,sM}\cos s\tau + b_{sN,sM}\sin s\tau).$$

We can now apply the Fredholm Alternative to the problem for B and, using a similar method to that of Section 4.3.1, we eventually find

$$\begin{aligned} -\frac{\kappa^2}{3}\lambda_{N,M}^4 f_{N,M}^{(iv)}(t) + \lambda_{N,M}^2\left(\lambda - \frac{\kappa^2}{3}\lambda_{N,M}^2\right) f_{N,M}''(t) \\ +3\lambda_{N,M}^4 f_{N,M}'(t) f_{N,M}''(t) = -\frac{[1-(-1)^N]\sin t}{2\pi}, \end{aligned} \tag{5.92}$$

where $f_{N,M}$ is 2π-periodic and has zero mean over one period. This is just a modified form of (4.48) (with $\nu_b = 0$) where the coefficients have been altered depending on which modes we are exciting. Note that we require N to be odd for a non-trivial solution.

The dispersion free case, $\kappa = 0$, yields

$$\left(f_{N,M}' + \frac{\lambda}{3\lambda_{N,M}^2}\right)^2 = \frac{2}{3\pi\lambda_{N,M}^4}\left(\cos^2\frac{t}{2} + c\right),$$

so that shocks occur in the range

$$|\lambda| < \left(\frac{48}{\pi^3}\right)^{\frac{1}{2}},$$

a smaller detuning range than for the $(1,0)$ case.

As an example, we consider the case $(N,M) = (1,2)$ when the governing equation becomes

$$\lambda f_{1,2}''(t) + 10 f_{1,2}'(t) f_{1,2}''(t) = -\frac{1}{5\pi}\sin t. \tag{5.93}$$

The shock structure can be seen most easily by considering the case $\lambda = 0$, when

$$f_{1,2}'(t) = \frac{1}{5}\left(\frac{2}{3\pi}\right)^{1/2}\begin{cases} \cos\frac{t}{2}, & -\pi < t < 0, \\ -\cos\frac{t}{2}, & 0 < t < \pi. \end{cases} \tag{5.94}$$

and, using the fact that η_0 is proportional to $A_t = f_{1,2}'(t \pm x \pm 2y)$, we can plot Figures 5.9 and 5.10 to show how the free surface evolves over one complete period, using increments of $\pi/4$ in time ($t = -\pi, 0$ and π correspond to a flat free surface). The solution contains two shocks travelling in the $(\pm 1, \pm 2)$ directions.

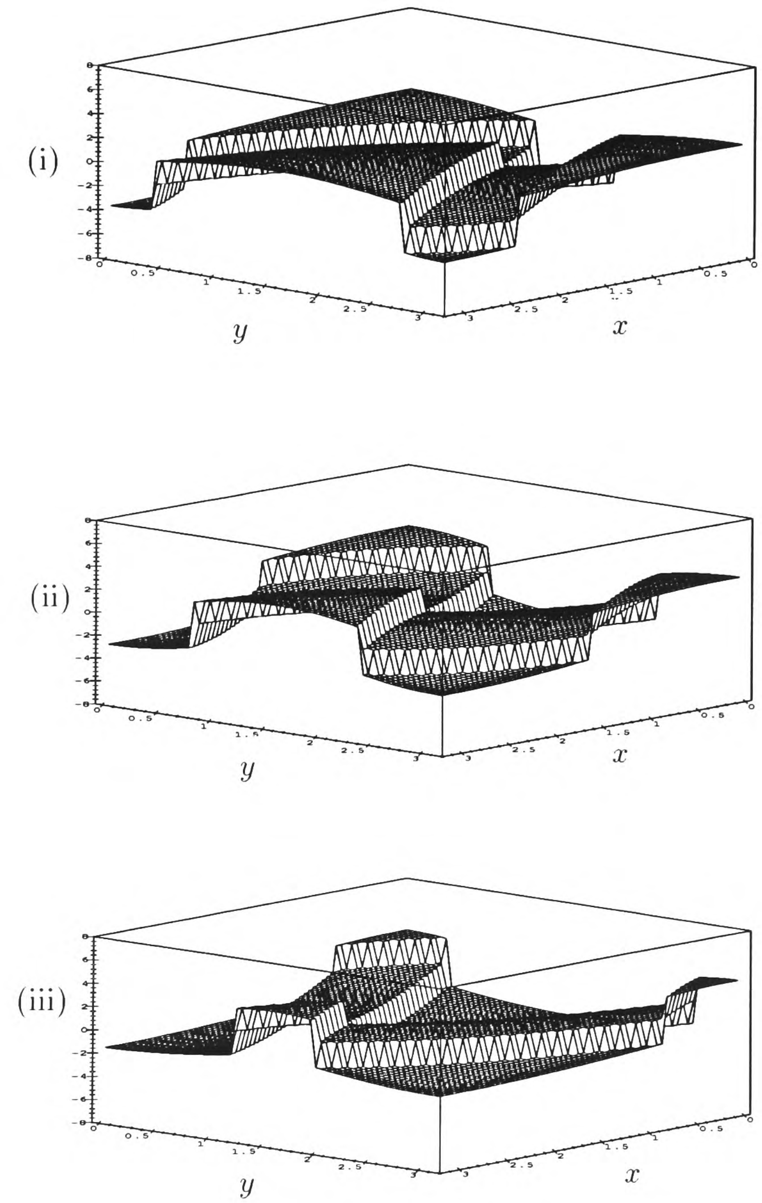

Figure 5.9: Evolution of shocks when the (1, 2)-mode is resonated: plot where the vertical axis is proportional to η_0 for (i) $t = -3\pi/4$, (ii) $t = -\pi/2$ and (iii) $t = -\pi/4$.

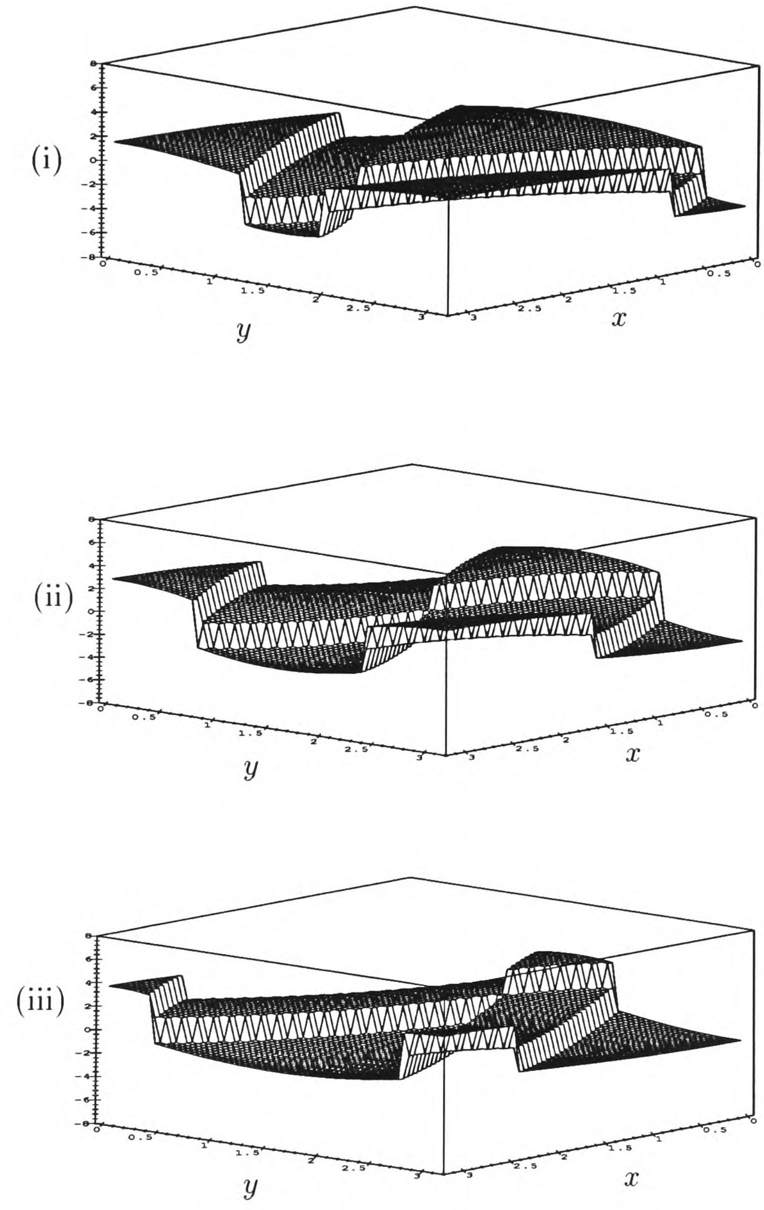

Figure 5.10: Evolution of shocks when the $(1,2)$-mode is resonated: plot where the vertical axis is proportional to η_0 for (i) $t = \pi/4$, (ii) $t = \pi/2$ and (iii) $t = 3\pi/4$.

Chapter 6

Generalisations

So far in this thesis we have been concerned, very broadly speaking, with two classes of problems concerning nearly square resonators; firstly, in deep water, we have found that the leading-order response consisted of one or, exceptionally, two modes (those having a frequency equal to that of the forcing). In contrast to this the shallow water or acoustic problem has solutions containing an infinite number of modes (one-dimensional) or, loosely speaking (see (5.1)), a doubly-infinite set (two-dimensional).

We are now in a position to review the types of responses we expect to find in tanks or resonators of any shape. The determination of this response will be dictated by the spectrum of the tank or resonator. For most shapes we expect a non-commensurate, non-degenerate spectrum and hence a single-mode response. Several authors have considered problems that fall into this class. Chester [17] considered acoustic oscillations in a sphere, resulting in a single mode response that is very similar to the problem of acoustic oscillations in a two-dimensional wedge, as considered by Ellermeier [26]. Also, a single mode response emerges in any paraboloid tank as found by Bauer & Eidel [4]. This is also true for semicircular horizontal cylinders and half-full spheres (Evans & Linton [27]) and other cylindrical and spherical tanks (McIver [42]).

There may also be spectra with a finite number of commensurate eigenfrequencies but no degenerate eigenfrequencies and the response will comprise the associated modes (or, perhaps, just a subset of these modes depending on which eigenfrequencies are commensurate), with their amplitudes satisfying coupled cubic equations. This was seen in Sections 3.4.1 and 3.4.2 and by Peake [58] and Can

& Askar [13] who considered oscillator models that are not necessarily realisable in a fluid resonance problem. When there are a finite number of commensurate and degenerate eigenfrequencies, we expect a generalisation of Section 3.2.2 where the amplitudes are again coupled, but this time we find two Duffing-type branches associated with each pair of degenerate eigenfrequencies.

For infinite sets of commensurate eigenfrequencies, we have the two possibilities considered in Chapters 4 and 5, corresponding to non-degenerate spectra and an infinite number of degenerate eigenfrequencies respectively, where there may be shocks in the longitudinal direction and/or in the transverse direction. However, by letting the amplitude of the wall variation get bigger, we can gradually move away from a tank or resonator of nearly square cross-section and see the emergence of a finite mode response as the eigenvalues become both non-commensurate and non-degenerate. This will be considered in Section 6.1.

There is also the possibility that there is simultaneously an infinite set of commensurate eigenfrequencies and a finite number of degenerate eigenfrequencies and this will be considered in Section 6.2.

6.1 Geometric imperfections $\gg O(\varepsilon^{1/2})$

As the size of the geometric variations gets bigger, the eigenvalues are increasingly perturbed from their original values. Ockendon *et al* [57] studied the effect of this on the response in the nearly one-dimensional case. The same ideas can be carried through to the two-dimensional case.

Let us consider what happens when $\nu_{w0} \gg \varepsilon^{1/2}$. The regime that is simplest to analyse that satisfies this condition is when $\nu_{w0} \sim O(\varepsilon^{1/4})$ so that we have to expand $\bar{\phi}$ and $\bar{\eta}$ in powers of $\varepsilon^{1/4}$ and then the geometry has a second-order effect whereas the forcing and nonlinearity balance at third order. Hence, when we come to repeat the analysis of Section 4.1.2 in this regime, the leading-order problem remains the same, but the orthogonality conditions at second order now correspond to the right-hand sides of (5.10) being zero, that is

$$\frac{1}{\pi^2}\sum_{p=1}^{\infty}\int_0^{2\pi}\int_0^{\pi} R(x,t')(-1)^{pm}\cos pnx\cos p\lambda_{n,m}(t'-t)\mathrm{d}x\mathrm{d}t' = \frac{2\gamma_{w0}m^2}{\lambda_{n,m}^2}f''_{n,m}, \quad (6.1)$$

for all (n,m). These integrals give

$$\left.\begin{array}{lll}(-1)^p\gamma_{wp}a_{p,0} & = & -2\gamma_{w0}a_{0,p}\\ \gamma_{w2p}a_{p,0} & = & -(-1)^p\gamma_{wp}a_{0,p}\end{array}\right\} \quad p\neq i\lambda_{n,m} \quad i=1,2,\ldots, \qquad (6.2)$$

where $\lambda_{n,m}$ is any integer given by $\lambda_{n,m}^2 = n^2+m^2$ (n, m coprime integers) except $\lambda_{n,m} = 1$, together with more complex expressions coupling the other $a_{p,q}$, and similar expressions for all the $b_{p,q}$.

We can see from (6.2) that, in general, the non-vanishing of the Fourier coefficients of $a_w(x)$ will mean that the leading-order solution is zero as we are far from all of the resonant frequencies. However, if some of the γ_{wn} do vanish we may find a finite mode response to leading-order. We note that the type of response is critically dependent on γ_{w0}. For $\gamma_{w0}\neq 0$, we find that (6.1) are only satisfied when $f_{n,m}=0$, $(n,m)\neq(1,0)$, and $f_{1,0}$ may contain a number of modes depending on the other γ_{wi} as in Ockendon *et al* [57]. For $\gamma_{w0}=0$, however, it is possible to find a response containing a number of modes in wavetrains other than the longitudinal wavetrain when the other γ_{wi} are suitably chosen. This difference can be seen by recalling that $\nu_{w0}\gamma_{w0}$ is the average of the back variation and, whenever this quantity is greater than $O(\varepsilon^{1/2})$, we are away from the square tank when the eigenfrequencies are nearly degenerate and hence, to leading order, we have a one-dimensional response. We now classify the type of response possible when $\gamma_{w0}=0$.

(a) $\gamma_{w1}\neq 0$. In this case the leading-order response is zero and $\bar{\phi}$ is $O(\varepsilon^{1/4})$. As Ockendon *et al* pointed out, this is because the fundamental frequency has shifted by $O(\varepsilon^{1/4})$ and to obtain a resonant response we need to shift λ by $O(\varepsilon^{1/4})$. If we do this, it is equivalent to taking $\gamma_{w1}=0$ and so we proceed with $\gamma_{w1}=0$ from now on.

(b) $\gamma_{w1}=0$, $\gamma_{w2}\neq 0$. This case highlights how considering (6.2) alone can be rather misleading. It first seems, from (6.2), that we may choose $a_{1,0}=0$, $a_{0,1}\neq 0$, $a_{2,0}=0$ and $a_{0,2}=0$ with the same for the corresponding $b_{n,m}$, and it is possible to construct a solution

$$f_{n,m}=\begin{cases} A\sin t, & (n,m)=(0,1),\\ 0, & \text{otherwise.}\end{cases}$$

As we proceed to second and third order, the analysis becomes very complicated and hence we will not provide the details but just the important features of the solution. We find, at second order, that the solvability conditions (6.1) are indeed satisfied but, at third order, we find that the second-order longitudinal mode that would couple the forcing with the geometry to determine A does not do so because we have chosen $\gamma_{w1} = 0$, and this means that $A = 0$. Hence the leading-order response is again $O(\varepsilon^{1/4})$ and we are effectively "away from resonance".

(c) $\gamma_{w1} = 0$, $\gamma_{w2} = 0$, $\gamma_{w3} \neq 0$, $\gamma_{w4} \neq 0$. In this case we see that a solution of the form

$$f_{n,m} = \begin{cases} A_1 \sin t, & (n,m) = (1,0), \\ A_2 \sin t + A_3 \sin 2t, & (n,m) = (0,1), \\ 0, & \text{otherwise}, \end{cases}$$

is feasible and a very longwinded calculation, that we will not present here, yields complicated formulae for the A_i in terms of λ and the γ_{wn}. The reason for this three mode response is that, because $\gamma_{w3} \neq 0$, $\gamma_{w4} \neq 0$, we have $a_{2,0} = a_{0,3} = a_{0,4} = 0$ (together with the corresponding $b_{n,m}$'s) from (6.2), so that there is no interaction (through the quadratic nonlinearity at third order) between the first two longitudinal modes or the first/second transverse modes with the third/fourth transverse modes and hence no way to excite the third longitudinal mode or the fifth to eighth transverse modes. The disappearance of the second longitudinal mode and the third and fourth transverse modes provides a "shielding" effect, stopping the other modes being excited. However, as in the one-dimensional case (Ockendon *et al* [57]), there is a narrow detuning range where the denominator in the A_i's reaches zero. This is similar to the situation we found in Section 5.1.2 for the limit $\lambda, \nu_w \to \infty$ where the leading-order response was invalid close to the spectral lines (5.25). Likewise, we expect higher-order terms to grow and balance with the leading-order solution when we are in this detuning range and the solution will again contain an infinite number of modes.

We can understand this situation by considering the perturbations to the natural frequencies caused by the wall geometry. In general, we find

$$\omega_{n,m} = \frac{g}{L}\lambda_{n,m}\left[1+\nu_{w0}\left\{\begin{array}{c}\omega^{+}_{(n,m)1}(\gamma_{wi})\\ \omega^{-}_{(n,m)1}(\gamma_{wi})\end{array}\right\}+\nu_{w0}^{2}\left\{\begin{array}{c}\omega^{+}_{(n,m)2}(\gamma_{wi})\\ \omega^{-}_{(n,m)2}(\gamma_{wi})\end{array}\right\}+O(\nu_{w0}^{3})\right] \quad (6.3)$$

where $\lambda^2_{n,m} = n^2 + m^2$ equals the square of an integer, $\pm$ denotes the split in the natural frequencies due to the degeneracy and $\omega^{\pm}_{(n,m)j}$ are functions of the Fourier coefficients γ_{wi}. For the choice of γ_{wn} considered here, $\omega^{\pm}_{(1,0)1} = \omega^{\pm}_{(0,1)1} = 0$ and the detuning may balance with the $\nu^2_{w0}\omega^{\pm}_{(1,0)2}$ and $\nu^2_{w0}\omega^{\pm}_{(0,1)2}$ terms and this corresponds to the A_i growing large. However, the other $\omega^{\pm}_{(n,m)1}$ are non-zero and hence the other modes are not resonant.

Using this particular case we are guided to the following general statement:

(d) $\gamma_{w1} = 0, \ldots, \gamma_{wi} = 0; \gamma_{w(i+1)} \neq 0, \ldots, \gamma_{w2i} \neq 0$. In general we expect the shielding process to force the solution to contain just a finite number of modes as in (c). If we assume that the leading-order solution contains just the $f_{1,0}$ and $f_{0,1}$ wavetrains, then (6.2) holds for all p and we can extend the argument of (c) to see that, for the first i of the γ_{wi}'s vanishing and the next i non-vanishing, the solution will comprise i longitudinal modes and $(i+1)$ transverse modes (and this corresponds to $\omega^{\pm}_{(n,0)1} = \omega^{\pm}_{(0,n)1} = 0$ for $n = 1, \ldots, i$). In general, including all the wavetrains, we expect a similar shielding effect to be possible whereby each wavetrain will contain just a few modes, the number associated with the (n,m)-wavetrain diminishing as $\lambda_{n,m}$ increases. However, it has not been possible to find a general hypothesis about which of the γ_{wi}'s should be zero/non-zero due to the complicated nature of the relations (6.1) for all (n,m).

For stronger variations, $\nu_{w0} \gg \varepsilon^{1/4}$, this classification becomes more complex. For instance, when $\nu_{w0} \sim O(\varepsilon^{1/6})$, we will have to expand $\bar{\phi}$ and $\bar{\eta}$ in powers of $\varepsilon^{1/6}$ and not only will (6.1) need to hold but a further set of restrictions will emerge at third order (as the forcing and nonlinearity now come in at fourth order). Clearly, with more restrictions on the γ_{wn}, $a_{n,m}$ and $b_{n,m}$, we will find it increasingly difficult to find any special cases where the solution is non-trivial. In general, for $\nu_{w0} \sim O(1)$, we expect a single mode response where the forcing frequency is changed by an $O(1)$ amount so that we are still close to a natural frequency.

6.2 Spectra with other degeneracies

We now consider the possibility of having only a few degenerate modes. This arises if we choose the geometry of the resonator in Figure 2.2 so that $a_b(x,y) = a_b(y)$, $\nu_{b0} \sim O(1)$ (so $h_0/L \ll \varepsilon^{1/2}$) and $\nu_{w0} = \varepsilon^{1/2}\nu_w \sim O(\varepsilon^{1/2})$. We will also use the Fourier series representation for the wall geometry $a_w(x)$, namely $a_w(x) = \sum_{n=0}^{\infty} \gamma_{wn} \cos nx$. Then, expanding φ as $\varphi = \varphi_0 + \varepsilon^{1/2}\varphi_1 + \cdots$, we have, from (2.56)–(2.61),

$$\left.\begin{array}{c} \varphi_{0xx} + \varphi_{0yy} + \dfrac{\nu_{b0} a_b'(y)}{1+\nu_{b0}a_b(y)}\varphi_{0y} = \varphi_{0tt}, \\ \varphi_{0x} = 0 \quad \text{on} \quad x = 0,\pi \quad , \quad \varphi_{0y} = 0 \quad \text{on} \quad y = 0,\pi, \end{array}\right\} \tag{6.4}$$

to $O(1)$ and

$$\begin{aligned} \varphi_{1xx} + \varphi_{1yy} + \frac{\nu_{b0} a_b'(y)}{1+\nu_{b0}a_b(y)}\varphi_{1y} &= \varphi_{1tt} + \lambda\varphi_{0tt} + 2\varphi_{0x}\varphi_{0xt} + 2\varphi_{0y}\varphi_{0yt} \\ &\quad +(\gamma-1)\varphi_{0t}\varphi_{0tt}, \end{aligned} \tag{6.5}$$

$$\varphi_{1x} = 0 \quad \text{on} \quad x = 0, \tag{6.6}$$

$$\varphi_{1x} = \sin t \quad \text{on} \quad x = \pi, \tag{6.7}$$

$$\varphi_{1y} = 0 \quad \text{on} \quad y = 0, \tag{6.8}$$

$$\varphi_{1y} = \nu_w \pi[\varphi_{0x}a_w'(x) - \varphi_{0yy}a_w(x)] \quad \text{on} \quad y = \pi, \tag{6.9}$$

to $O(\varepsilon^{1/2})$ where φ_0 and φ_1 are 2π-periodic in time. Then (6.4) has the general solution

$$\varphi_0 = g_{1,0}(t \pm x) + \sum_{n=0}^{\infty}\sum_{m=1}^{\infty} g_{n,m}(y)\cos nx(c_{n,m}\sin\omega_{n,m}t + d_{n,m}\cos\omega_{n,m}t), \tag{6.10}$$

where, as usual,

$$g_{1,0}(\tau) = \tfrac{1}{2}\sum_n (a_{n,0}\cos n\tau + b_{n,0}\sin n\tau),$$

and $g_{n,m}$ satisfies

$$\frac{\mathrm{d}}{\mathrm{d}y}\left([1+\nu_{b0}a_b(y)]\frac{\mathrm{d}g_{n,m}}{\mathrm{d}y}\right) + [1+\nu_{b0}a_b(y)](\omega_{n,m}^2 - n^2)g_{n,m} = 0 \tag{6.11}$$

$$g_{n,m}' = 0 \quad \text{on} \quad y = 0,\pi. \tag{6.12}$$

Now let us suppose we can select an $a_b(y)$ such that $\omega_{0,1} = 1$ and no other $\omega_{n,m}$ ($n \neq 0$) is commensurate with it.[1] Hence the only 2π-time-periodic eigenfunctions

[1] Using a numerical method (NAGD02KAF [53]) we found that

$$1 + \nu_{b0}a_b(y) = [\cos(1.04y + 3)]^{-1}$$

are for $m = 0$ and $(n, m) = (0, 1)$ and so

$$\varphi_0 = g_{1,0}(t \pm x) + (c_{0,1} \cos t + d_{0,1} \sin t) g_{0,1}(y).$$

and, applying the Fredholm Alternative to (6.5)–(6.9) gives

$$\begin{aligned} \lambda g''_{1,0} + (\gamma + 1) g'_{1,0} g''_{1,0} &= -\frac{\sin t}{\pi} - \frac{\pi g_1 g''_{0,1}(\pi) \gamma_{w1} \nu_w}{2} (c_{1,0} \cos t + d_{1,0} \sin t) \\ &+ \frac{g_1 \nu_w}{2} \int_0^\pi g'_{1,0}(2x + t)[a'_w(x) - a'_w(\pi - x)] \mathrm{d}x, \quad (6.13) \\ \left\{ \begin{array}{c} c_{0,1} \\ d_{0,1} \end{array} \right\} &= -\frac{\pi \nu_w \gamma_{w1} g_2}{2\left(\lambda - g_2 g''_{0,1}(\pi) \pi \gamma_{w0} \nu_w\right)} \left\{ \begin{array}{c} a_{1,0} \\ b_{1,0} \end{array} \right\}, \quad (6.14) \end{aligned}$$

where

$$g_1 = \frac{1 + \nu_{b0} a_b(\pi)}{\displaystyle\int_0^\pi [1 + \nu_{b0} a_b(y)] \mathrm{d}y} \quad , \quad g_2 = \frac{g_{0,1}(\pi)[1 + \nu_{b0} a_b(\pi)]}{\displaystyle\int_0^\pi g_{0,1}^2(y)[1 + \nu_{b0} a_b(y)] \mathrm{d}y}.$$

We can only easily see what happens in the anti-symmetric case $a'(x) = a'(\pi - x)$ and we also consider $\gamma_{w0} = 0$, leaving a discussion of the behaviour when $\gamma_{w0} \neq 0$ until later. In this case (6.13) has discontinuous solutions for

$$\lambda^2 \leq \frac{16(\gamma + 1)}{\pi^3} \left[-\frac{\pi^3 \gamma_{w1}^2 g_1 g_2 g''_{0,1}(\pi) \nu_w^2}{6(\gamma + 1)} \pm 1 \right], \quad (6.15)$$

and we plot the shock regime in the (λ, ν_w)-plane in Figure 6.1.

We note there are three different classes of behaviour depending on the size of ν_w^2/λ. Firstly, when $\nu_w^2 \ll \lambda$, the rear wall geometry is weak and $c_{0,1}$ and $d_{0,1}$ are negligible and we return to the one-dimensional response. When $\nu_w^2 \sim \lambda$, both the longitudinal and transverse solutions are of the same order. However, for $\nu_w^2 \gg \lambda$, we find a new possibility because, from (6.13) and (6.14), we find, regardless of whether we are in the shock or no-shock region, that

$$a_{1,0} \sim 0 \quad , \quad b_{1,0} \sim -\frac{\lambda}{\nu_w^2} \quad , \quad c_{0,1} \sim 0 \quad , \quad d_{0,1} \sim -\frac{1}{\nu_w},$$

so that, as $\lambda \to 0$, the wavetrain $g_{1,0}$ is of $O(\lambda/\nu_w)$ smaller that the lowest order transverse mode. This dominating single mode transverse response is due to the amplification of the small longitudinal wavetrain due to the wall variation $a_w(x)$.

yields $\omega_{n,m} = 1$ for the case $n = 0$ with the next few $\omega_{n,m}$ being non-commensurate and hence a function of this general shape may be a suitable example.

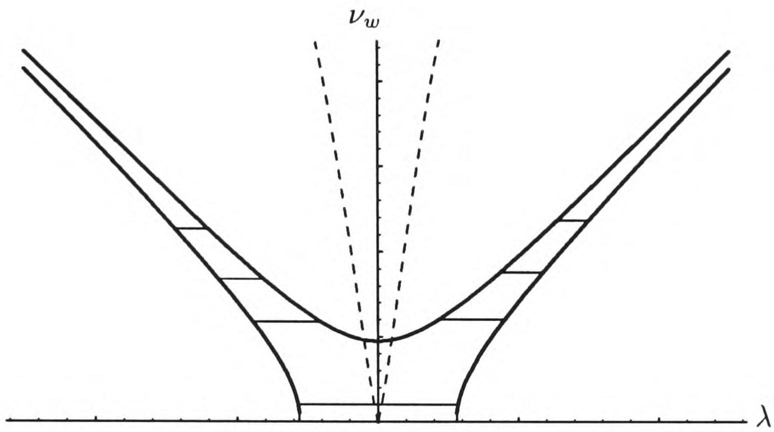

Figure 6.1: Shock region for the special case of one transverse mode. The region between the dashed lines is where the transverse mode dominates.

Thus, although there are some superficial similarities with the "fingers" of Figures 4.2, 4.3 and 5.5(a), the behaviour with zero detuning is very different from the case where all the longitudinal frequencies are degenerate.

Let us now remark on the effect of γ_{w0} being taken to be non-zero. In this case, we find that the transverse mode dominates close to the line $\lambda = g_2 g''_{0,1}(\pi)\pi\gamma_{w0}\nu_w$ instead of $\lambda = 0$. Hence the transverse mode no longer causes the shock region near $\lambda = 0$ to disappear but instead yields a picture similar to Figure 6.2 with a shock region near $\lambda = 0$ and a region near $\lambda = g_2 g''_{0,1}(\pi)\pi\gamma_{w0}\nu_w$ where the transverse mode dominates. It is the possibility of removing shocks near $\lambda = 0$ that makes the case $\gamma_{w0} = 0$ of especial interest.

For any other eigenvalue being degenerate (say $(n, m) = (0, m_1)$ instead of $(0, 1)$), we find a similar response to (6.13) and (6.14) except that, when $\lambda \to 0$, we find $a_{m_1,0}, b_{m_1,0} \to 0$. However, the other $a_{n,0}$ and $b_{n,0}$ remain $O(1)$ and the shock locations in the (λ, ν_w)-plane will be reminiscent of the purely one-dimensional case.

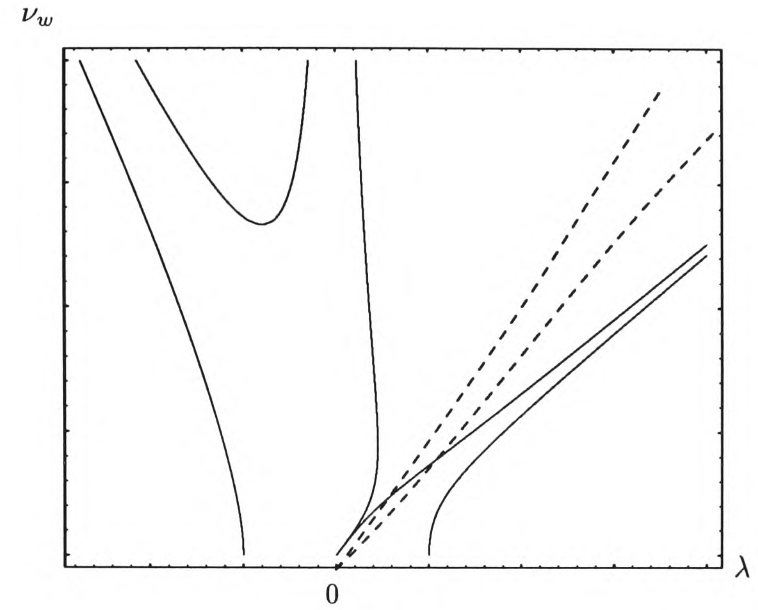

Figure 6.2: Shock region for $\gamma_{w0} \neq 0$. Shocks are found in between the solid lines and the transverse mode dominates in between the dashed lines.

Finally, for acoustic oscillations, all the remarks in this chapter could be extended to three-dimensional oscillations. In particular, we expect shocks parallel to all the sides of an oscillated cube (with slowly varying sides) to be simultaneously possible.

Chapter 7

Conclusions

In this thesis we have tried to analyse and unify a wide range of resonance problems. Beginning with the simplest single-mode response, we have developed theories and solutions for more complicated and intricate scenarios. The results have been illustrated using both sloshing in tanks of fluid and acoustic oscillations and, where appropriate, we have related the two problems.

This thesis has been presented in stages of increasing complexity. To summarise our findings, we first note that the geometry of the tank or resonator is crucial in determining the type of resonant response we find. This is because the spectrum of the tank or resonator is dictated by its shape and two properties of this spectrum are important.

(i) The commensurability of the spectrum. We have seen that the response to forcing near the fundamental depends critically upon whether or not any of the natural frequencies are integer multiples of the fundamental. When there are no commensurate frequencies then the solution is a single-mode; for n commensurate frequencies the solution may contain between 1 and n modes depending on which modes are commensurate and if the whole spectrum is commensurate then the solution contains all the modes.

(ii) The degeneracy of the spectrum. The occurrence of two-dimensional sloshing solutions (where the free surface varies in *two* spatial dimensions, and the velocity potential in three) and two-dimensional acoustic solutions has been shown to result from small geometric variations in situations where there is more than one independent mode associated with a particular natural frequency. The change from one- to two-dimensional solutions as the spectrum becomes degenerate has been one of the central issues of this work.

In general, the determination of the response relies on a consideration of (i) and (ii) simultaneously.

Throughout our discussions we have concentrated on the effects of the small geometrical variations, nonlinearity and dispersion. In reality, dissipation will also play an important role and we have noted at the ends of Chapters 3 and 4 that viscosity will round off large amplitude branches in the response diagrams.

7.1 Summary of results and conclusions

The two physical problems under consideration were formally introduced in Chapter 2. Horizontal oscillations of a nearly cuboid tank of liquid (see Figure 2.1) close to its fundamental frequency were first considered under the assumption that the liquid is inviscid and the motion irrotational. The natural frequencies are

$$\omega_{n,m}^2 = \frac{g}{L}\lambda_{n,m}\tanh(\lambda_{n,m}h), \tag{7.1}$$

$$\sim \frac{g}{L}\lambda_{n,m}^2 h \quad h \ll 1, \tag{7.2}$$

where $\lambda_{n,m}^2 = n^2 + m^2/b^2$. The difference between "deep" and "shallow" water can automatically be seen with reference to (i) above. Equation (7.1) suggests that only high frequency modes could ever be commensurate with the fundamental and in this case damping will prevent these modes from being excited. In stark contrast to this, as the depth becomes small, (7.2) shows that an infinite subset of the spectrum is commensurate and this property is in common with the other physical problem we have considered, namely acoustic oscillations in a two-dimensional resonator (see Figure 2.2 with $\nu_{b0} = 0$).

In Chapter 3 we concentrated on the deep water case and there are a variety of scenarios which we summarised in Table 3.1. The different cases represent our first step in understanding the roles of (i) and (ii) above.

(a) The simplest case is when the breadth is not an integer multiple of the length ($b \neq l$) and (7.1) shows that the lowest frequency is *not* degenerate and the solution is just a single mode whose amplitude satisfies a cubic equation, (3.39), similar to a Duffing-type response, and this result is stable to small variations in geometry.

(b) The solution becomes more interesting when the breadth approaches an integer multiple of the length. We focussed on the case $b = 1$, with small back wall variations, in Sections 3.1.2 and 3.2.2, where the response consists of one longitudinal mode and one transverse mode. Due to the degeneracy of the spectrum, the linear resonant frequency changes from $\lambda_0 = 0$ to two distinct values of λ_0 as the amplitude of the geometric variation (ν_{w0}) increases. The responses (3.37) and (3.38) show that the amplitudes of the two modes satisfy coupled cubic equations. A Duffing-type branch is associated with each resonant frequency so that this case is distinguished by the *two* branches of Figure 3.5 and these branches can be identified with the two "spectral lines".

(c) Although, in general, the motion in the deep water case contains only one longitudinal mode (with, maybe, one transverse mode, as above) there are certain special cases where this is not true. We saw this possibility emerge in Section 3.4 when surface tension was introduced and we concentrated on issue (i) alone by considering a perfectly rectangular tank. Although surface tension is likely to be negligible in most physically realistic cases and the boundary conditions (B.3) are controversial, from a theoretical point of view cases in which the second or third modes are commensurate are interesting. In Section 3.4 we saw that two critical balances between surface tension and the depth were possible where $\omega_{2,0} = 2\omega_{1,0}$ or $\omega_{3,0} = 3\omega_{1,0}$. In the first case, with $\lambda_0 \sim O(\varepsilon^{1/2})$, we initially found that quadratic nonlinearity was enough to couple the first and second modes (of amplitude $O(\varepsilon^{1/2})$). However as $\lambda_0 \to O(\varepsilon^{4/5})$ we found that the second mode dominated with the primary longitudinal mode being relegated to a lower order. This situation, also studied by Peake [58], is characterised by the second mode, and only the second mode, being commensurate with the fundamental.

When the third mode is commensurate, we found the two modes still satisfy coupled cubic equations but, in contrast to the previous case, the solution does not break down as $\lambda_0 \to 0$.

In Chapter 3 we also studied the problem where the simple case of (a) is seen to break down near a critical depth when the response changes from "hard" to "soft" spring behaviour as the nonlinearity bends the response curve back on itself. This forced us to go to fifth order in the detuning range $\lambda_0 \sim O(\varepsilon^{4/5})$ with ϕ growing to $O(\varepsilon^{1/5})$.

There is one omission in our analysis of deep water sloshing: we have not mentioned the possibility of so-called "cross-waves". When a rectangular tank has a wavemaker oscillating at twice a transverse frequency an instability causes this transverse mode to be excited. This parametric resonance has been considered by Garrett [30], Miles [47] and Tsai *et al* [73] and is reminiscent of vertical oscillations of a tank (Faraday [28]; Ockendon & Ockendon [54]; Miles [45]). The effects of geometric variations in such a situation have not been considered and this presents an interesting avenue for future work.

Following on from these "dispersion-dominated" cases, we considered, in Chapter 4, the shallow water limit of this problem and its analogies with acoustic oscillations. As noted above, the spectrum is now found to contain an infinite number of commensurate eigenvalues which all become degenerate when the breadth approaches a rational multiple of the length. In fact, we found that the leading-order solution satisfies the two-dimensional wave equation with Neumann boundary data and is determined by a solvability condition on an inhomogeneous wave equation (rather that the inhomogeneous ordinary differential equations that were encountered in Chapter 3). The solution was only easily found when there are no transverse disturbances and we drew together the various aspects of the one-dimensional solution in this chapter by taking a tank with a flat back wall and a slowly varying base. In this case we found $\phi_0 = f(t+x) + f(t-x)$ where

$$\frac{\kappa^2}{3} f^{(iv)}(t) + \left(\frac{\kappa^2}{3} - \lambda\right) f''(t) - 3f''(t)f'(t) = \frac{2}{\pi}\sin t$$
$$-\frac{\nu_b}{4\pi}\int_0^\pi f'(2s+t)[a_b'(s) - a_b'(\pi - s)]\mathrm{d}s. \tag{7.3}$$

This includes the basic Chester solution ($\nu_b = \kappa = 0$) which shows the emergence of a shock for $|\lambda| < \lambda^*$, and we have given a review of the effects of dispersion and dissipation on this solution. Our main area of interest, however, was in the effects of the integral term in (7.3) and we concentrated on the dispersion-free case which also describes quasi-one-dimensional acoustic oscillations (cf. (4.50)). In Section 4.4.2, we took the first three even Fourier coefficients of $a_b(x)$ to be non-zero. This confirmed the work of Ockendon *et al* [57] and illustrated how the higher-order terms in the Fourier series for $a_b(x)$ have a diminishing effect on the form of the solution (see Figure 4.3). We saw that each even Fourier term in the expression for $a_b(x)$ introduced a new "finger" into the shock pictures of Figures 4.2 and 4.3.

An interesting class of problems arises when the amplitude of the area variation in the tank or resonator is taken to be of the *same order* as the depth of the liquid or the breadth of the resonator respectively. The leading-order problem now satisfies a modified wave equation, (4.65) or (4.72), as we found in Section 4.5 and, as shown there, the leading-order fluid and acoustic problems are no longer the same. In general, the spectrum is non-commensurate and there is a single mode response as in the deep water work. However, we found that there do exist special geometries where the spectrum is commensurate as found from solving inverse eigenvalue problems in Section 4.5. These special geometries are also seen to emerge from an increasing number of restrictions as the amplitude of the area variation increases in the range $0 \ll \nu_{b0} \ll 1$.

The most complex scenario was then confronted in Chapter 5. When the tank breadth is a rational multiple of the length, the spectrum (7.2) contains not only an infinite number of commensurate modes but also an infinite number of degenerate modes and we concentrated on the case $b = 1$. The key to understanding how this doubly-infinite set of modes interact was the observation that the different wavetrains (infinite sets of modes propagating in the same direction) do not interact through the quadratic nonlinearity. This means that in a perfectly square tank or resonator we can single out individual wavetrains with a suitable forcing. We presented two examples of this; firstly, by oscillating such a tank or resonator at an angle, the wavetrains $f_{1,0}$ and $f_{0,1}$ are both excited, satisfying uncoupled higher-order Chester equations; secondly, by forcing the motion with a suitably designed wavemaker oscillating near a higher frequency, we were able to pick out the wavetrain $f_{N,M}$ and again this satisfies a higher-order Chester equation, so shocks propagating in the $(\pm N, \pm M)$ direction are possible (Figures 5.9 and 5.10).

A more interesting consequence of the absence of nonlinear coupling between the wavetrains is that we can also simplify the analysis of oscillations in a square tank with small variations in the back wall. Indeed we found that the solution consists of an infinite set of wavetrains, $f_{n,m}$, where each $f_{n,m}$ satisfies an equation similar to (7.3); however, the forcing only enters the equation for $f_{1,0}$ and the integral term is replaced by a term coupling the wall variation, $a_w(x)$, with *all* the $f_{n,m}$. The problem is thus reduced to an infinite set of coupled integro-differential equations. Our asymptotic analysis and study of this set of equations led to the following conclusions in the dispersion-free case.

- As $\nu_w \to 0$, we retrieve the one-dimensional solution for $f_{1,0}$ and this is changed by a shift in both the strength and location of the shock as ν_w increases and supplemented by the emergence of cross wavetrains that depend on two different parameter regimes for λ. When $\lambda \sim O(1)$ the wavetrains $f_{n,m}$ $((n,m) \neq (1,0))$ are of $O(\nu_w)$ and satisfy a linear equation. More interestingly, for $\lambda \sim O(\sqrt{\nu_w})$ the wavetrains grow to $O(\sqrt{\nu_w})$ and shocks occur in very narrow detuning bands. In both cases the amplitudes of the wavetrains decrease as $\lambda_{n,m}$ increases.

- As $\nu_w \to \infty$ (with $\lambda \sim \nu_w$), the $f_{n,m}$-wavetrain has amplitude $O(\nu_w^{1-2(n^2+m^2)^{\frac{1}{2}}})$ except in narrow detuning ranges (lying close to lines $\lambda/\nu_w = $ const.) that represent the growth of a single mode within the expressions for the $f_{n,m}$. However, this growth only reaches the same size as the leading-order term ($O(1/\nu_w)$ from $f_{1,0}$ and $f_{0,1}$) for the cases of the first *three* modes of $f_{1,0}$ and $f_{0,1}$ as discussed on page 88. Hence, for all λ, ν_w large, these primary wavetrains dominate the solution. Close to these lines of growth, the other modes grow to balance with the leading-order term and shocks are possible. Hence we will see shock fingers in the (λ, ν_w)-plane close to these resonant lines.

Based on these limits we proposed an iteration scheme for $\nu_w \sim O(1)$ using the initial approximation $A(x,y,t) = f_{1,0}^{(0)}(t \pm x) + f_{0,1}^{(0)}(t \pm y)$. This led to a solution such as

Figure 5.5 which agrees well with the above asymptotic solutions. The solution, as ν_w and λ increase, is a finite mode Duffing-type response purely in the longitudinal and transverse directions, except in narrow fingers where shocks occur in either of these directions. The existence of an infinite number of degenerate eigenmodes thus leads to the possibility of two-dimensional shock solutions. Finally, in this chapter, we saw how this shallow water solution matched with the shallow water limit of the deep water solution of Section 3.2 when we re-introduced dispersion.

To complete the picture we considered some generalisations in Chapter 6. In Section 6.1, we saw that, as the amplitude of the wall variation, ν_{w0}, increased, the solution moved away from the infinite mode responses of Chapter 5 and a finite mode response emerged. More interesting is the possibility of an infinite number of commensurate eigenvalues but just a finite number of degenerate eigenvalues. We considered this in Section 6.2 where we saw the solution is a Chester-type equation coupled to a finite mode transverse motion. When the fundamental is degenerate and the average of the wall variation, $a_w(x)$, is zero, this transverse motion dominates in a certain detuning range and removes the possibility of shocks near $\lambda = 0$.

We have encountered a wide variety of resonant responses characterised by the commensurability and degeneracy of the spectrum. The number of different scenarios is, of course, vast but we have tried to highlight the most interesting and important cases here. We hope our general theories can now be used to predict the resonant response within any bounded container and extended to three-dimensional acoustic oscillations (for example, in a cube where geometric imperfections will allow for shocks parallel to each wall of the cube).

Notation

Fluid		Gas	
$\boldsymbol{u}$	Dimensional velocity	$\boldsymbol{u}$	Dimensional velocity
τ/t	Dimensional/non-dimensional time	τ/t	Dimensional/non-dimensional time
p	Pressure	p	Pressure
ρ	Density	ρ	Density
g	Gravity	γ	Ratio of specific heats
Φ/ϕ	Dimensional/non-dimensional velocity potential	Φ/φ	Dimensional/non-dimensional velocity potential
$\boldsymbol{X}/\boldsymbol{x}$	Unscaled/scaled coordinates	$\boldsymbol{X}/\boldsymbol{x}$	Unscaled/scaled coordinates
ξ/η	Dimensional/non-dimensional free surface height	πL	Length and average breadth of resonator
Γ/γ	Dimensional/non-dimensional surface tension coefficient	h	Average height of resonator
σ	Scaled version of γ given by $\gamma = \sigma/(1-\sigma)$	$a_b(x,y)$	Variation in top geometry of resonator
πL	Length of tank	$a_w(x)$	Variation in back geometry of resonator
$b\pi L$	Average breadth of tank	ν_{b0}	Strength of variation in top
hL	Depth of tank	ν_{w0}	Strength of variation in back
λ_0	Detuning	ν_b	Scaled version of ν_{b0} for weak variations
λ_d, λ	Different detuning regimes	ν_w	Scaled version of ν_{w0} for weak variations
a	Amplitude of forcing	ω	Fundamental frequency
ε	a/L	λ	Detuning
$a_w(x)$	Variation in wall of tank	εL	Amplitude of forcing
ν_{w0}	Strength of variation in wall		
$a_b(x)$	Variation in base geometry of tank	$g(\cdot)$	Functional representation for one-dimensional problem

Fluid	
ν_{b0}	Strength of variation in base
ν_{wd}, ν_w	Different geometry parameter regimes
ν_b	Scaled version of ν_{b0} for weak variations
$\omega_{n,m}$	Natural frequencies of oscillation where n is mode number in x-direction and m is mode number in y-direction
b_0, b_d	Perturbation from tank of breadth π
ϕ_i	$(i-1)^{th}$ order term in expansion for ϕ
η_i	$(i-1)^{th}$ order term in expansion for η
γ_{wi}	Coefficients of Fourier series for $a_w(x)$
γ_{bi}	Coefficients of Fourier series for $a_b(x)$
$A, B, C, \ldots$	Amplitudes of deep water modes
σ_s	Scaled version of σ in shallow water problem
κ	Scaled shallow water depth
$f(\cdot)$	Function determining response in one-dimensional shallow water problem
A_n, α_n	Amplitude/phase of shallow water modes for one-dimensional solutions
$A_{n,m}$	'Packet' of modes in (n, m)-direction
$f_{n,m}$	Functional representation of $A_{n,m}$

Table 7.1: Notation.

Appendix A

A.1 Shock considerations

A.1.1 Continuity of entropy

Consider the one-dimensional gas flow equations,

$$\rho_t + (\rho u)_x = 0, \tag{A.1}$$

$$\rho(u_t + uu_x) + \frac{p_x}{\gamma} = 0, \tag{A.2}$$

$$\frac{\mathrm{d}}{\mathrm{d}t}\left(\frac{p}{\rho^\gamma}\right) = 0, \tag{A.3}$$

where we have non-dimensionalised velocity, pressure, density, time and the spatial variations with $a_0 L$, p_a, ρ_a, $1/a_0$ and L respectively. Here L is a typical length-scale, p_a and ρ_a are the values of pressure and density in the equilibrium state and $a_0^2 = \gamma p_a/\rho_a$. The last two of these equations can be written in conservation form as

$$\begin{aligned}(\rho u)_t + \left(\rho u^2 + \frac{p}{\gamma}\right)_x &= 0,\\ \left(\frac{1}{2}\rho u^2 + \frac{c_v}{R}\frac{p}{\gamma}\right)_t + \left(u\left\{\frac{1}{2}\rho u^2 + \left(\frac{c_v + R}{R}\right)\frac{p}{\gamma}\right\}\right)_x &= 0,\end{aligned}$$

where R is the gas constant, c_v is the specific heat at constant volume and $\gamma = (c_v + R)/R$. Hence we find the jump conditions

$$V[\rho] = [\rho u], \tag{A.4}$$

$$V[\rho u] = \left[\rho u^2 + \frac{p}{\gamma}\right], \tag{A.5}$$

$$V\left[\frac{1}{2}\rho u^2 + \frac{c_v}{R}\frac{p}{\gamma}\right] = \left[u\left\{\frac{1}{2}\rho u^2 + \left(\frac{c_v + R}{R}\right)\frac{p}{\gamma}\right\}\right], \tag{A.6}$$

for a shock at $x = Vt$ where $[f]$ denotes the change in f across the shock. We now expand the variables, in accordance with the other expansions employed on the acoustic problems in the thesis, as

$$\begin{aligned} u &= \varepsilon^{1/2}u_0 + \varepsilon u_1 + \cdots, \\ p &= 1 + \varepsilon^{1/2}p_0 + \varepsilon p_1 + \cdots, \\ \rho &= 1 + \varepsilon^{1/2}\rho_0 + \varepsilon \rho_1 + \cdots, \\ V &= 1 + \varepsilon^{1/2}V_0 + \cdots. \end{aligned}$$

Then (A.4)–(A.6) give

$$[\rho_0] = [u_0] = \frac{1}{\gamma}[p_0], \tag{A.7}$$

to $O(1)$ and

$$\begin{aligned} [\rho_1 + V_0\rho_0] &= [u_1 + \rho_0 u_0], && \text{(A.8)} \\ [u_1 + V_0 u_0 + \rho_0 u_0] &= \left[u_0^2 + \frac{p_1}{\gamma}\right], && \text{(A.9)} \\ \left[\frac{(\gamma-1)}{2}u_0^2 + \frac{1}{\gamma}(p_1 + V_0 p_0)\right] &= [u_1 + u_0 p_0], && \text{(A.10)} \end{aligned}$$

to $O(\varepsilon^{1/2})$. Elimination of u_1 and p_1 between (A.9) and (A.10) then gives

$$V_0 = \frac{1}{2}(\bar{p}_0 - \bar{\rho}_0) + \bar{u}_0, \tag{A.11}$$

where the bar denotes the average of the quantity across the shock. Now consider the quantity p/ρ^γ which can be expanded to give

$$\frac{p}{\rho^\gamma} = 1 + \varepsilon^{1/2}(p_0 - \gamma\rho_0) + \varepsilon\left(p_1 - \gamma p_0\rho_0 - \gamma\rho_1 + \frac{\gamma(\gamma+1)}{2}\rho_0^2\right), \tag{A.12}$$

and, from (A.7), (A.8) and (A.10), we find $[p/\rho^\gamma] = 0$ to $O(\varepsilon)$ and hence entropy is continuous across the shock to $O(\varepsilon)$.

A.1.2 Stability of shock

To show that the shocks we encounter are ones of compression we consider a perturbation to a shock at $x = \hat{V}t$. First we re-write (A.3) as $p_t + up_x + \gamma p u_x = 0$ and then write $\xi = x - \hat{V}t$ so that the governing equations are now

$$\rho_t - \hat{V}\rho_\xi + (\rho u)_\xi = 0, \tag{A.13}$$

$$\rho[u_t + (u - \hat{V})u_\xi] + \frac{p_\xi}{\gamma} = 0, \tag{A.14}$$

$$p_t + (u - \hat{V})p_\xi + \gamma p u_\xi = 0. \tag{A.15}$$

We now perturb about the solution $(u, p, \rho) = (\hat{u}, \hat{p}, \hat{\rho})$ by writing

$$\begin{aligned} p &= \hat{p} + \delta c_1 e^{\sigma t + k\xi}, \\ \rho &= \hat{\rho} + \delta c_2 e^{\sigma t + k\xi}, \\ u &= \hat{u} + \delta c_3 e^{\sigma t + k\xi}, \end{aligned}$$

where $\delta \ll 1$ and the shock position is now at $\xi = \delta e^{\sigma t}$. Using these expressions in (A.13)–(A.15) yields that solutions are only possible if

$$\sigma = k\left\{\hat{V} - \hat{u} \pm \left(\frac{\hat{p}}{\hat{\rho}}\right)^{\frac{1}{2}}\right\}, \tag{A.16}$$

where we choose the positive/negative value in (A.16) so that $\sigma = 0$ when there is no change in $\hat{p}, \hat{\rho}, \hat{u}$ across the shock (i.e. $\sigma \to 0$ as $\varepsilon \to 0$ in what follows). Now we consider the situation shown in Figure A.1 so that, from (A.11), $\hat{V} = \mathrm{sgn}(\varepsilon) + \varepsilon(\gamma + 1)/4$ and hence, to the left of the shock, $\sigma = \varepsilon k(\gamma + 1)/4$. Hence, for decaying solutions, $\sigma < 0, k > 0$ we require $\varepsilon < 0$. Likewise, to the right of the shock, $\sigma = -\varepsilon k(\gamma + 1)/4$ and for $\sigma < 0, k < 0$ we need $\varepsilon < 0$. So, in both regions, we require $\varepsilon < 0$ for stable solutions, i.e. shocks must be compressive.

$\hat{u} = 0$	$\hat{u} = \varepsilon$
$\hat{p} = 1$	$\hat{p} = 1 + \gamma\lvert\varepsilon\rvert$
$\hat{\rho} = 1$	$\hat{\rho} = 1 + \lvert\varepsilon\rvert$

$x = \hat{V}t$

Figure A.1: Basic states before perturbing shock.

Appendix B

B.1 Surface tension effects

In Section 3.4 we introduce surface tension effects into the two-dimensional problem ($\nu_{w0} = 0$, so the solution is independent of y). The dynamic condition (2.5) now becomes (see, for example, Batchelor [3])

$$g\xi + \Phi_\tau + \frac{1}{2}(\nabla\Phi)^2 = \frac{\Gamma}{\rho}\frac{\xi_{XX}}{(1+\xi_X^2)^{3/2}} \quad \text{on} \quad Z = \xi,$$

and the linearised natural frequencies are now

$$\omega_{n,m}^2 = \frac{g}{L}\lambda_{n,m}\tanh(\lambda_{n,m}h)\left(1 + \frac{\Gamma}{\rho g L^2}\lambda_{n,m}^2\right). \tag{B.1}$$

Non-dimensionalising with the scaling suggested by Concus [19], $\Gamma = \rho g L^2\sigma/(1-\sigma)$ ($0 \le \sigma < 1$), then gives

$$(1-\sigma)\eta + (1+\lambda_0)\tanh h\left[\phi_t + \frac{1}{2}\left({\phi_x}^2 + {\phi_z}^2\right)\right] = \sigma\frac{\eta_{xx}}{(1+\eta_x^2)^{3/2}}, \tag{B.2}$$

on $z = 0$, instead of (2.23).

In general σ will be small compared to the effects of gravity, but we consider the case $\sigma \sim O(1)$ so we can study the possibility of the second or third modes being commensurate. The pursuit of the nonlinear response when $\sigma \neq 0$ reveals how the single mode solution breaks down when one of these modes is commensurate. Hence we solve the nonlinear model (2.31)–(2.38) and (B.2) rescaled with (2.29), and we assume that the free surface makes an angle $\pi/2$ with the walls $x = 0, \pi$, so that

$$(\eta_d)_x = 0 \quad \text{on} \quad x = 0, \pi. \tag{B.3}$$

(In reality, this boundary condition is likely to be much more complicated as discussed in Hocking [31]. However, we use this simplified model to study the importance of commensurability.) Hence, using expansions (3.25) and (3.26) we find

$$\phi_0 = A\cos x\cosh(z+h)\sin(t+\alpha_1), \quad , \quad \eta_0 = -A\cos x\sinh h\cos(t+\alpha_1),$$

where $A > 0$, and the $O(\varepsilon^{2/3})$ terms are

$$\begin{aligned}
&\nabla^2\phi_1 = 0 \quad , \quad \phi_{1x} = 0 \quad \text{on} \quad x = 0,\pi \quad , \quad \phi_{1z} = 0 \quad \text{on} \quad z = -h, \\
&\eta_{1x} = 0 \quad \text{on} \quad x = 0,\pi \quad , \quad \phi_{1z} = \eta_{1t} + \eta_{0x}\phi_{0x} - \eta_0\phi_{0zz} \quad \text{on} \quad z = 0, \\
&(1-\sigma)\eta_1 + \tanh h(\phi_{1t} + \eta_0\phi_{0tz} + \tfrac{1}{2}(\phi_{0x}^2 + \phi_{0z}^2)) = \sigma\eta_{1xx} \quad \text{on} \quad z = 0, \\
&\int_0^\pi \eta_1 \mathrm{d}x = 0 \quad , \quad \nabla\phi_1(x,z,t+2\pi) = \nabla\phi_1(x,z,t),
\end{aligned} \tag{B.4}$$

which have solution

$$\begin{aligned}
\phi_1 &= \beta_0 t + B\cos x\cosh(z+h)\sin(t+\alpha_1) \\
&\quad + [A_1 + A_2\cos 2x\cosh 2(z+h)]\sin 2(t+\alpha_1), \\
\eta_1 &= -B\cos x\sinh h\cos(t+\alpha_1) - A_2\cos 2x\sinh 2h\cos 2(t+\alpha_1) \\
&\quad + C\cos 2x + \frac{A^2}{4}\sinh h\cosh h\cos 2x\cos 2(t+\alpha_1),
\end{aligned}$$

where

$$A_1 = \frac{A^2}{16}(4\sinh^2 h + 1) \quad , \quad A_2 = \frac{3A^2(1 + 2\sigma\cosh^2 h)}{16(3\sigma\cosh^2 h - \sinh^2 h)},$$
$$C = \frac{A^2\tanh h}{8(1+3\sigma)}(2\sinh^2 h + 1) \quad , \quad \beta_0 = -\frac{A^2}{8}.$$

Going to the third order leads to the problem

$$\begin{aligned}
&\nabla^2\phi_2 = 0 \quad , \quad \phi_{2x} = \sin t \quad \text{on} \quad x = 0,\pi \quad , \quad \phi_{2z} = 0 \quad \text{on} \quad z = -h, \\
&\eta_{2x} = 0 \quad \text{on} \quad x = 0,\pi \quad , \quad \phi_{2z} = \eta_{2t} + F_1(x,t) \quad \text{on} \quad z = 0, \\
&(1-\sigma)\eta_2 - \sigma\eta_{2xx} + \tanh h\phi_{2t} = F_2(x,t) - \frac{3\sigma}{2}\eta_{0xx}\eta_{0x}^2 \\
&\qquad\qquad -\lambda_d\tanh h\phi_{0t} \quad \text{on} \quad z = 0, \\
&\nabla\phi_2(x,z,t+2\pi) = \nabla\phi_2(x,z,t),
\end{aligned}$$

where

$$\begin{aligned}
F_1(x,t) &= (\eta_0\eta_{0x}\phi_{0xz} + \phi_{1x}\eta_{0x} + \phi_{0x}\eta_{1x} - \eta_0\phi_{1zz} - \eta_1\phi_0 - \tfrac{1}{2}\eta_0^2\phi_{0z})|_{z=0}, \\
F_2(x,t) &= -\tanh h\left(\eta_1\phi_{0tz} + \tfrac{1}{2}\eta_0^2\phi_{0t} + \eta_0\phi_{1tz} + \eta_0\phi_{0x}\phi_{0xz} + \phi_{0x}\phi_{1x}\right. \\
&\quad \left. + \eta_0\phi_{0z}\phi_0 + \phi_{0z}\phi_{1z}\right)|_{z=0}.
\end{aligned}$$

We can now employ the Fredholm Alternative on this problem to arrive at the solvability conditions

$$\lambda_d A \sinh h + \mathcal{H}(\sigma, h) A^3 = \frac{4}{\pi} \tanh h \cos \alpha_1, \tag{B.5}$$

and $\sin \alpha_1 = 0$, where

$$\mathcal{H}(\sigma, h) = \Big[2 - 9\cosh^2 h(1 + 3\sigma^2) + \cosh^4 h(24 + 18\sigma + 27\sigma^2 - 81\sigma^3) + \cosh^6 h(-8 + 27\sigma + 36\sigma^2 + 81\sigma^3)\Big] / [32 \sinh h \cosh^2 h(3\sigma \coth^2 h - 1)(3\sigma + 1)]. \tag{B.6}$$

Clearly for $\sigma = 0$, $\mathcal{H} = H$, and we return to equation (3.40). For $\sigma \neq 0$ this result agrees with Concus [19] who considered the problem of standing waves in a tank when surface tension effects were included. The response is again similar to that of the Duffing equation but now the hard/soft spring behaviour depends of whereabouts in the (h, σ)-plane we are. Figure B.1 summarises the situation, showing regions I where $\mathcal{H} > 0$ (soft spring) and regions II where $\mathcal{H} < 0$ (hard spring), and is the same as Concus' Figure 1. Firstly, $\mathcal{H}$ changes sign when the numerator of (B.6) passes through zero and this is shown by the solid line in Figure B.1, and the solution close to this line was found in Section 3.3 for $\sigma = 0$. The second change is due to the denominator passing through zero (as can also be seen in the coefficient A_2) which corresponds to

$$\sigma = \frac{1}{3} \tanh^2 h, \tag{B.7}$$

and is shown by the dashed line. Also, if we proceed to solve the ϕ_2 problem we find that there is a term in ϕ_2 of the form $b_{33} \cos 3x \cosh 3(z + h) \sin 2t$ where b_{33} is proportional to $[1 - \sigma(1 + 3\coth^2 h)]^{-1}$ so when

$$\sigma = \frac{1}{1 + 3\coth^2 h}, \tag{B.8}$$

there is one other place in the (h, σ)-plane where the solution breaks down. This is shown in Figure B.1 by the dotted line. The solution breaks down when we are close to or on any of these lines.

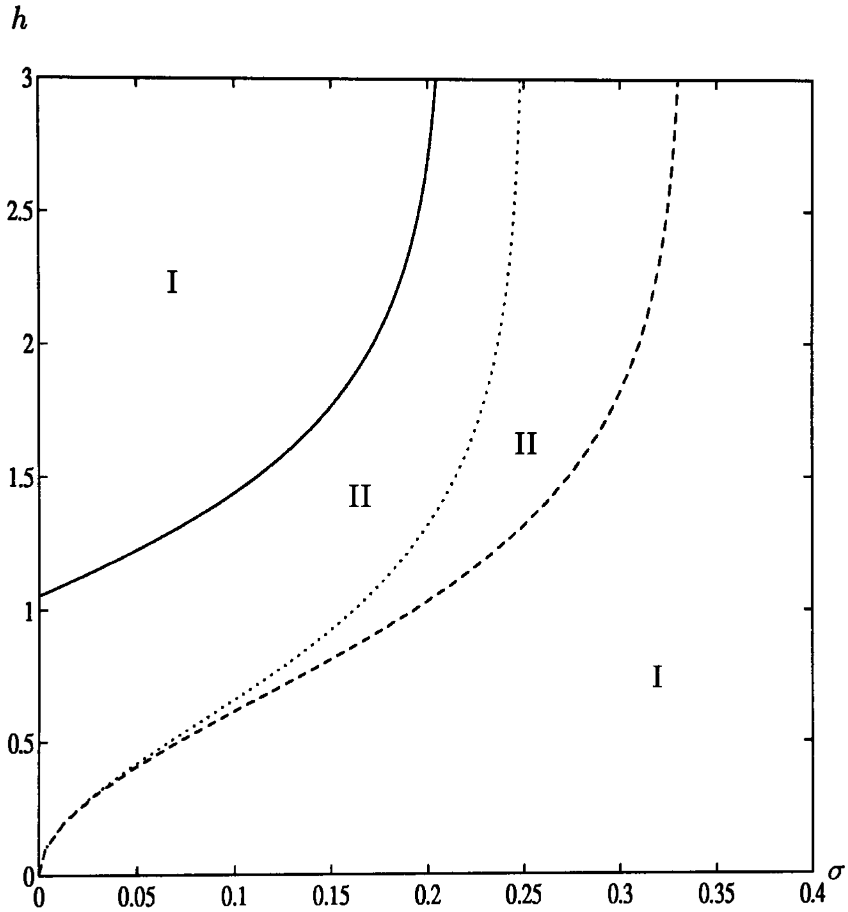

Figure B.1: Plot showing how the solution (B.5) breaks down. The solid line corresponds to $\mathcal{H}(\sigma, h) = 0$ whereas the other two lines show a resonance of higher modes. Also the response is like a soft spring in regions I and a hard spring in regions II.

Appendix C

C.1 Other aspects of one-dimensional resonant sloshing and acoustics

In this appendix we discuss two other aspects of the problems considered in Chapter 4 that are of interest, but that do not tie in with the general themes of this thesis.

C.1.1 Forcing near a higher frequency

We can study oscillations generated when the forcing is close to a natural frequency other than the fundamental, i.e. when the ends of the tank are at $-\varepsilon \cos kt$ and $\pi - \varepsilon \cos kt$, by repeating the analysis of Sections 4.1 and 4.3 to give, in the absence of dispersion and geometric effects,

$$\lambda f'' + 3f'f'' = -\frac{2k}{\pi} \sin kt,$$

where k must be even for the tank (due to the forcing on *both* ends, see (2.15)) but could be any natural number for the acoustic problem. As a point in case, we consider $k = 3$. Once again continuous solutions can be found for $c \geq 0$ and are

$$f' + \frac{\lambda}{3} = \pm \left(\frac{8}{3\pi}\right)^{1/2} \left(\cos^2 \frac{3t}{2} + c\right)^{\frac{1}{2}},$$

and these have period $2\pi/3$, the same period as the forcing. However in the shock region we can construct not only solutions with period $2\pi/3$ which contain three shocks in an interval 2π, but also solutions with just one shock in a period 2π. Figure C.1 illustrates the two possibilities. The point to note is that the Fourier series of the three shock solutions contains only $\cos 3nt$ ($n = 1, 2, \ldots$) modes and

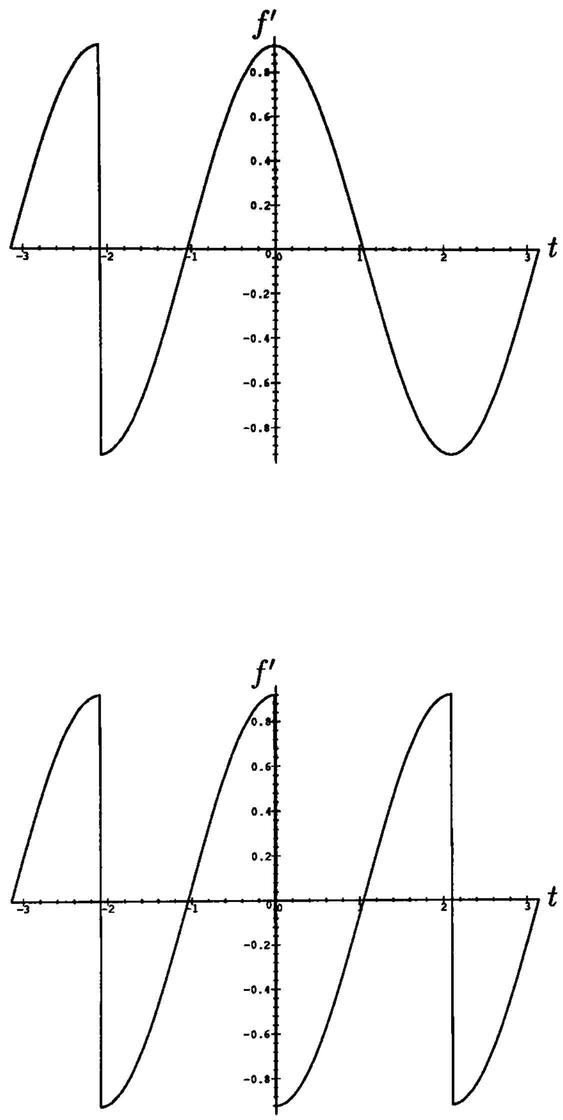

Figure C.1: One-shock and three-shock solutions at $\lambda = 0$ when the forcing is proportional to $\sin 3t$.

thus a subset of the spectrum only is excited. In the case of one shock, however, all modes are excited and the response contains terms which are subharmonic with respect to the forcing.

For oscillations at a higher frequency we must exhibit some caution and restrict ourselves to relatively small values of k because as k gets large and time derivatives grow large, our asymptotic analysis will eventually break down. Seymour & Mortell [63] have presented a method for solving the *acoustic problem* when the forcing frequency is close to any natural frequency. To show how (4.49) and (4.2) arise from their theory for low values of the forcing frequency we present an outline of their ideas, changing the scalings slightly to agree with our configuration.

Defining Lagrangian variables (ξ, T) by

$$x = x(\xi, T) \quad , \quad t = T,$$

where $\xi = x(0)$, then (2.40)–(2.42) become (for one-dimensional motion)

$$\left.\begin{aligned} [(1+e)^{-1}]_T - u_\xi &= 0, \\ u_T + p_\xi &= 0, \\ \gamma p &= (1+e)^\gamma - 1, \end{aligned}\right\} \tag{C.1}$$

after scaling velocity with a_0, pressure with $\rho_0 a_0^2$, density with ρ_0, length with L and time with L/a_0, where $a_0^2 = \gamma p_0/\rho_0$ and $e = \rho - 1 \ll 1$. As in Section 2.2 we take the ends of the resonator to be at $x = 0$ and $x = \pi - \varepsilon \cos \omega t$ so that

$$\left.\begin{aligned} u = 0 \quad &\text{on} \quad \xi = 0, \\ u = \varepsilon\omega \sin \omega T \quad &\text{on} \quad \xi = \pi. \end{aligned}\right\} \tag{C.2}$$

We now define $c(e)$ by

$$c(e) = \int_0^e \frac{a(s)}{(1+s)^2} \mathrm{d}s = e + O(e^2),$$

where

$$a(e) = (1+e)^2 \frac{\mathrm{d}p}{\mathrm{d}e} = (1+e)^{\gamma+1} = 1 + Me + O(e^2),$$

and $M = (\gamma+1)/2$, and this is the correct definition of $c(e)$ as opposed to Seymour & Mortell's who had $a(s)/(1+s)$ as the integrand, although the final results are the same. Equations (C.1) can now be rewritten as

$$\left(\frac{\partial}{\partial T} \pm a(e) \frac{\partial}{\partial \xi}\right)(u \pm c(e)) = 0,$$

so that

$$u - c = 2f_1(\beta) \quad \text{on} \quad \left.\frac{\mathrm{d}\xi}{\mathrm{d}T}\right|_\beta = -a(e), \tag{C.3}$$

$$u + c = -2f_2(\alpha) \quad \text{on} \quad \left.\frac{\mathrm{d}\xi}{\mathrm{d}T}\right|_\alpha = a(e), \tag{C.4}$$

where f_1 and f_2 are arbitrary functions. Integrating these characteristics is the subtlest part of the calculation. An intuitive way of proceeding is to concentrate on either the α-wave or the β-wave and hence consider the solution as a simple wave. Hence we might solve just (C.3) for a signal propagating along the α-characteristic to give

$$u - c = 2f_1(\beta) \quad \text{on} \quad T + \xi + M\xi f_1(\beta) = f_{10}(\beta),$$

or solve just (C.4) in the same way to give

$$u + c = -2f_2(\alpha) \quad \text{on} \quad T - \xi - M\xi f_2(\alpha) = f_{20}(\alpha),$$

where f_{10} and f_{20} are arbitrary functions. In general, of course, the two signals pass through each other and interact. However, Mortell & Varley [52] and Mortell & Seymour [50] have shown that this interaction is negligible for small amplitude motions and we hence persist with the above formulae and parameterise the characteristics by $\alpha = \omega T$ on $\xi = 0$ and $\beta = \omega T$ on $\xi = \pi$ to give

$$u = f_1(\beta) - f_2(\alpha), \tag{C.5}$$

$$\frac{\alpha}{\omega} = T + \xi + M\xi f_2(\alpha) \quad , \quad \frac{\beta}{\omega} = T + \xi - \pi + M(\xi - \pi) f_1(\beta). \tag{C.6}$$

We can now apply the boundary conditions (C.2) to give

$$\left.\begin{aligned} f_1(\eta) - f_2(s) &= \varepsilon\omega \sin\eta, \\ \eta &= s + 2\omega\pi + 2\omega M\pi f_1(s), \end{aligned}\right\} \tag{C.7}$$

and

$$f_2(\psi + \omega\pi + \omega M\pi f(\psi)) = f_1(\psi). \tag{C.8}$$

If we now look near resonance so $\omega \simeq n$ by writing

$$\omega = n(1 + \lambda_0)$$

and define

$$F(y) = f_1(y) + \frac{\lambda_0}{M(1+\lambda_0)},$$

then (C.7) become

$$\left.\begin{array}{rcl} F(\eta) - F(s) & = & \varepsilon n(1+\lambda_0)\sin\eta, \\ \eta & = & s + 2n\pi + 2nM\pi(1+\lambda_0)F(s), \end{array}\right\} \tag{C.9}$$

This is essentially the functional equation derived by Seymour & Mortell and is often referred to as the "standard mapping". Its solutions have been thoroughly analysed by Seymour & Mortell in [49]–[51] and [63]–[65]. We just note than in the so-called "small-rate" limit where we assume[1] $|2nM\pi F'| \ll 1$ then (C.9) can be expanded to give

$$F(s) = F(\eta) - 2n\pi(1+\lambda_0)MF(\eta)F'(\eta)[1 + O(2nM\pi F')],$$

(bearing in mind that $F(\eta - 2n\pi) = F(\eta)$), and hence we find

$$2\pi MF(\eta)F'(\eta) = \varepsilon\sin\eta. \tag{C.10}$$

Now note that, in this limit, $x = \xi$ and (C.5), (C.6) and (C.8) give

$$u = f_1(t + x - \pi) - f_1(t - x - \pi).$$

Hence, putting $\lambda_0 = \frac{1}{2}\lambda\varepsilon^{1/2}$ (in agreement with (2.52)), $f_1(t-\pi) = \dfrac{\varepsilon^{1/2}}{1+\delta}g'(t)$ so that

$$\varphi = \frac{\varepsilon^{1/2}}{1+\lambda_0}(g(t+x) + g(t-x)),$$

(so that $u = \dfrac{\partial\varphi}{\partial x}$) in agreement with (4.49) and the scaling for φ in (2.53), we see from (C.10) that g satisfies

$$\lambda g'' + (\gamma+1)g'g'' = -\frac{1}{\pi}\sin t,$$

i.e. we return to (4.2) — Chester's equation.

---

[1]Note this restriction is equivalent to saying

$$2\pi M\varepsilon n^2 \ll 1,$$

as can be seen by writing $F = \tilde{F}/2n\pi M$ to give

$$\begin{array}{rcl} \tilde{F}(\eta) - \tilde{F}(s) & = & 2\varepsilon n^2\pi M(1+\lambda_0)\sin\eta, \\ \eta & = & s + 2n\pi + (1+\lambda_0)\tilde{F}(s), \end{array}$$

and then $2\pi M\varepsilon n^2 \ll 1$ implies that $|\tilde{F}'| \ll 1$ and hence $|2nM\pi F'| \ll 1$.

C.1.2 Evolution to a periodic response

Throughout Chapter 4 we must bear in mind the issue of whether or not a periodic motion evolves from an initial state of rest. This was first considered by Cox & Mortell [21] (for the acoustic problem) and [22] (for the fluid problem). We can arrive at a similar result by introducing a long timescale over which either a non-periodic or periodic response may develop. The necessary timescale in this case is $\tau = \varepsilon^{1/2}t$ and using the method of multiple timescales we can rework the calculations of Section 4.1 to find that $\phi_0 = f(t+x;\tau)+f(t-x;\tau)$ where $G(t;\tau) = \partial f(t;\tau)/\partial t$ satisfies

$$-\frac{\kappa^2}{3}\frac{\partial^3 G}{\partial t^3} + \left(\lambda - \frac{\kappa^2}{3}\right)\frac{\partial G}{\partial t} + 3G\frac{\partial G}{\partial t} + 2\frac{\partial G}{\partial \tau} = -\frac{2}{\pi}\sin t,$$

and $G(t+2\pi;\tau) = G(t;\tau)$ and G has has zero mean over the interval $0 < t < 2\pi$. This is just a forced Korteweg-de Vries equation which is the same as (4.48) when G is independent of τ (periodic motion). Cox & Mortell [22] considered this as an initial value problem to see whether periodic motion arose and using numerical techniques reached the conclusion that *no* periodic response was possible unless a damping term similar to that in Section 4.7 was included. However, in the absence of dispersion, Cox & Mortell [21] discovered, by finding an analytical solution (using the method of characteristics), that the solution does tend to a periodic state, even in the absence of damping. Hence we see that the inclusion of dispersion causes an instability in the evolution process and this may be related to the non-uniqueness of the solution in this case (see Section 4.6). It seems likely that the solution moves between the different possible solution branches as the motion evolves. Also, the inclusion of dissipation reduces the number of possible solutions for a fixed detuning and hence reduces the chance of instability, so a periodic motion can evolve.

References

[1] ACHESON, D., Elementary Fluid Dynamics *Oxford University Press* (1990).

[2] BARCILON, V., Explicit Solutions Of The Inverse Problem For A Vibrating String *Math. Anal.* **93** 222–234 (1983).

[3] BATCHELOR, G. K., An Introduction To Fluid Dynamics *Cambridge University Press* (1967).

[4] BAUER, H. F. & EIDEL, W., Non-Linear Liquid Oscillations In Paraboloid Containers *Z. Flugwiss. Weltraumforsch.* **12** 246–252 (1988).

[5] BECKER, E., Gas Dynamics *Academic Press* (1968).

[6] BETCHOV, R., Nonlinear Oscillations Of A Column Of Gas *Phys. Fluids* **1** 205–212 (1958).

[7] BOUSSINESQ, J., Théorie des ondes et des remous qui se propagent le long d'un canal rectangulaire horizontal, en communiquant au liquide contenu dans ce canal des vitesses sensiblement pareilles de la surface au fond *J. Math. Pures Appl.* **17** 55–108 (1872).

[8] BRIDGES, T. J., Cnoidal Standing Waves And The Transition To The Travelling Hydraulic Jump *Phys. Fluids* **29** 2819–2828 (1986).

[9] BRIDGES, T. J., On The Secondary Bifurcation Of Three-Dimensional Standing Waves *SIAM J. Appl. Math.* **47/1** 40–59 (1987).

[10] BRIDGES, T. J., Secondary Bifurcation And Change Of Type For Three Dimensional Standing Waves In Finite Depth *J. Fluid Mech.* **179** 137–153 (1987).

[11] BYATT-SMITH, J. G., Resonant Oscillations In Shallow Water With Small Mean-Square Disturbances *J. Fluid Mech.* **193** 369–390 (1988).

[12] BYRD, P. F. & FRIEDMAN, M. D., Handbook Of Elliptic Integrals For Engineers and Scientists *Springer* (1971).

[13] CAN, N. & ASKAR, A., Nonlinear Elastic Surface Gravity Waves: Continuous And Discontinuous Solutions *Wave Motion* **12** 485–495 (1990).

[14] CHESTER, W., Resonant Oscillations In Closed Tubes *J. Fluid Mech.* **18**, 44–65 (1964).

[15] CHESTER, W., Resonant Oscillations Of Water Waves *Proc. Roy. Soc. A* **306**, 5–22 (1968).

[16] CHESTER, W. & BONES, J. A., Resonant Oscillations Of Water Waves II: Experiment *Proc. Roy. Soc. A* **306**, 23–39 (1968).

[17] CHESTER, W., Acoustic Resonance In Spherically Symmetric Waves *Proc. Roy. Soc. A* **434** 459–463 (1991).

[18] CHESTER, W., Nonlinear Resonant Oscillations Of A Gas In A Tube Of Varying Cross-Section *Proc. Roy. Soc. A* **444** 591–604 (1994).

[19] CONCUS, P., Standing Capillary-Gravity Waves Of Finite Amplitude *J. Fluid Mech.* **14** 568–576 (1962).

[20] CONCUS, P., Standing Capillary-Gravity Waves Of Finite Amplitude: Corrigendum *J. Fluid Mech.* **19** 264–266 (1964).

[21] COX, E. A. & MORTELL, M. P., The Evolution Of Resonant Oscillations In Closed Tubes *Z. A. M. P.* **34** 845–866 (1983).

[22] COX, E. A. & MORTELL, M. P., The Evolution Of Resonant Water-Wave Oscillations *J. Fluid Mech.* **162** 99–116 (1986).

[23] DIAS, F. & BRIDGES, T. J., The Third Harmonic Resonance For Capillary-Gravity Waves With $O(2)$ Symmetry *Stud. Appl. Maths* **82** 13–35 (1990).

[24] DUFFING, G., Erzwungene Schwingungen Bei Veränderlicher Eigenfrequenz *F. Vieweg u. Sohn, Braunschweig* (1918).

[25] ELLERMEIER, W., Nonlinear Acoustics In Non-Uniform Infinite And Finite Layers *J. Fluid Mech.* **257** 183–200 (1993).

[26] ELLERMEIER, W., Acoustic Resonance Of Cylindrically Symmetric Waves *Proc. Roy. Soc. Lond. A* **445** 181–191 (1994).

[27] EVANS, D. V. & LINTON, C. M., Sloshing Frequencies *Q. J. Mech. Appl. Math.* **46/1** 71–87 (1993).

[28] FARADAY, M., On A Peculiar Class Of Acoustical Figures; And On Certain Forms Assumed By Groups Of Particles Upon Vibrating Elastic Surfaces *Phil. Trans. R. Soc. Lond.* **121** 299–340 (1831).

[29] FULTZ, D., An Experimental Note On Finite-Amplitude Standing Gravity Waves *J. Fluid Mech.* **13** 193–212 (1962).

[30] GARRETT, C. J. R., On Cross-Waves *J. Fluid Mech.* **41** 837–849 (1970).

[31] HOCKING, L. M., The Damping Of Capillary-Gravity Waves At A Rigid Boundary *J. Fluid Mech.* **179** 253–266 (1987).

[32] ILLINGWORTH, C. R., Modern Developments In Fluid Dynamics — High Speed Flow (Shock Waves) Vol. I (ed. Howarth, L.) *Oxford University Press* (1953).

[33] JOHNSON, A. D., D. Phil Thesis *Oxford University, Oxford, England* (1986).

[34] JORDAN, D. W. & SMITH, P., Nonlinear Ordinary Differential Equations *Oxford University Press* (1977).

[35] KELLER, J. J., Resonant Oscillations In Closed Tubes: The Solution Of Chester's Equation *J. Fluid Mech.* **77** 279–304 (1976).

[36] KELLER, J. J., Nonlinear Acoustic Resonance In Shock Tubes With Varying Cross-Sectional Area *Z. A. M. P.* **28** 107–122 (1977).

[37] KORTEWEG, D. G. & DE VRIES, G., On The Change Of Form Of Long Waves Advancing In A Rectangular Canal, And On A New Type Of Stationary Wave *London, Dublin & Edinburgh Phil. Magazine* **5/39**, 422–443 (1895).

[38] LIEPMANN, H. W. & ROSHKO, A., Elements Of Gas Dynamics *Galcit Aeronautical Series* (1957).

[39] LIGHTHILL, M. J., Introduction To Fourier Series And Generalised Functions, *Cambridge University Press* (1958).

[40] LIGHTHILL, M. J., Waves In Fluids, *Cambridge University Press* (1978).

[41] MARCHENKO, V. A., Stürm-Liouville Operators And Applications *Birkhäuser* (1986).

[42] MCIVER, P., Sloshing Frequencies For Cylindrical And Spherical Containers Filled To An Arbitrary Depth *J. Fluid Mech.* **201** 243–257 (1989).

[43] MILES, J. W., Nonlinear Surface Waves In Closed Basins *J. Fluid Mech.* **75** 419–448 (1976).

[44] MILES, J. W., The Korteweg-de Vries Equation: A Historical Essay *J. Fluid Mech.* **106** 131–147 (1981).

[45] MILES, J. W., Nonlinear Faraday Resonance *J. Fluid Mech.* **146** 285–302 (1984).

[46] MILES, J. W., Resonantly Forced, Nonlinear Gravity Waves In A Shallow Rectangular Tank *Wave Motion* **7** 291–297 (1985).

[47] MILES, J. W., Parametrically Excited, Standing Cross-Waves *J. Fluid Mech.* **186** 119–127 (1988).

[48] MOISEYEV, N. N., On The Theory Of Nonlinear Vibrations Of A Liquid *Prikl. Mat. Mech.* **22** 612–621 (1958).

[49] MORTELL, M. P. & SEYMOUR, B. R., Exact Solutions Of A Functional Equation Arising In Nonlinear Wave Propogation *SIAM J. Appl. Math.* **30** 587–596 (1976).

[50] MORTELL, M. P. & SEYMOUR, B. R., Nonlinear Forced Oscillations In A Closed Tube: Continuous Solutions Of A Functional Equation *Proc. Roy. Soc. Lond. A* **367** 253–270 (1979).

[51] MORTELL, M. P. & SEYMOUR, B. R., The Calculation Of Resonance Separatices For The Near-Integrable Case Of The Standard Mapping *Z. A. M. P.* **39** 861–873 (1988).

[52] MORTELL, M. P. & VARLEY, E., Finite Amplitude Waves In Bounded Media: Nonlinear Free Vibrations Of An Elastic Panel *Proc. Roy. Soc. Lond. A* **318** 169–196 (1970).

[53] NAG02KAF, NAG Fortran Library Manual Mark 14, Chapter D02 (1990).

[54] OCKENDON, J. R. & OCKENDON, H., Resonant Surface Waves *J. Fluid Mech.* **59**, 397–413 (1973).

[55] OCKENDON, H. & TAYLER, A. B., Inviscid Fluid Flows *Springer* (1983).

[56] OCKENDON, J. R., OCKENDON, H. & JOHNSON, A. D., Resonant Sloshing In Shallow Water *J. Fluid Mech.* **167**, 465–479 (1986).

[57] OCKENDON, H., OCKENDON, J. R., CHESTER, W. & PEAKE, M. R., Geometric Effects In Resonant Gas Oscillations *J. Fluid Mech.* **257**, 201–217 (1993).

[58] PEAKE, M. R., D.Phil Thesis *Oxford University, Oxford, England* (1993).

[59] PENNY, W. G. & PRICE, A. T., Some Gravity Wave Problems In The Motion Of Perfect Liquids. Part II. Finite Periodic Stationary Gravity Waves In A Perfect Liquid *Phil. Trans. A* **244** 254–284 (1952).

[60] PÖSCHEL, J. & TRUBOWITZ, E., Inverse Spectral Theory *Academic Press* (1987).

[61] REYNOLDS, D. W. & COX, E. A., Periodic Solutions Of An Integro-Differential Equation Modelling Resonant Sloshing *IMA J. Appl. Maths* **38** 243–253 (1987).

[62] RUSSELL, S., Report On Waves *Brit. Ass. Adv. Sci. Rep. On 14th Meeting* 311–350 (1844).

[63] SEYMOUR, B. R. & MORTELL, M. P., Resonant Acoustic Oscillations With Damping: Small Rate Theory *J. Fluid Mech.* **58** 353–373 (1973).

[64] SEYMOUR, B. R. & MORTELL, M. P., A Finite-Rate Theory Of Resonance In A Closed Tube: Discontinuous Solutions Of A Functional Equation *J. Fluid Mech.* **99** 365–382 (1980).

[65] SEYMOUR, B. R. & MORTELL, M. P., The Evolution Of A Finite Rate Periodic Oscillation *Wave Motion* **7** 399–409 (1985).

[66] STOKER, J. J., Nonlinear Vibrations In Mechanical And Electrical Systems *Interscience* (1950).

[67] STOKER, J. J., Water Waves *Interscience* (1958).

[68] STOKES, G. G., Collected Papers *Cambridge University Press* (1880).

[69] STURTEVANT, B., Nonlinear Gas Oscillations In Pipes. Part 2. Experiment *J. Fluid Mech.* **63** 97–120 (1973).

[70] TADJBAKHSH, I. & KELLER, J. B., Standing Surface Waves Of Finite Amplitude *J. Fluid Mech.* **8** 442–451 (1960).

[71] TAYLOR, G. I., An Experimental Study Of Standing Waves *Proc. Roy. Soc. A* **218** 44–59 (1953).

[72] TITCHMARSH, E. C., Eigenfunction Expansions I, *Oxford University Press* (1962).

[73] TSAI, W. T., YUE, D. K. P. & YIP, M. K., Resonantly Excited Regular And Chaotic Motions In A Rectangular Wave Tank *J. Fluid Mech.* **216** 343–380 (1990).

[74] VANDEN-BROECK, J., Nonlinear Gravity-Capillary Waves In Water Of Arbitrary Uniform Depth *J. Fluid Mech.* **139** 97–104 (1984).

[75] VERMA, G. R. & KELLER, J. B., Three Dimensional Standing Surface Waves Of Finite Amplitude *Phys. Fluids* **5** 52–56 (1962).

[76] WATERHOUSE, D. D., M.Sc Dissertation *Oxford University, Oxford, England* (1993).

[77] WATERHOUSE, D. D., Resonant Sloshing Near A Critical Depth *J. Fluid Mech.* **281** 313–318 (1994).

[78] WILTON, J. R., On Ripples *Phil. Mag.* **29** 688–700 (1915).

[79] WHITHAM, G. B., Linear And Nonlinear Waves *Interscience* (1974).